Synthesis and Gas Transport Properties of Graphene Oxide Membranes

by

Amr Fatehy Muhammad Ibrahim

A Dissertation Presented in Partial Fulfillment

of the Requirements for the Degree

Doctor of Philosophy

Approved November 2017 by the
Graduate Supervisory Committee:

Jerry Lin, Chair
Bin Mu
Mary Laura Lind
Matthew Green
Qing Hua Wang

ARIZONA STATE UNIVERSITY

May 2018

ABSTRACT

Graphene oxide membranes have shown promising gas separation characteristics specially for hydrogen that make them of interest for industrial applications. However, the gas transport mechanism for these membranes is unclear due to inconsistent permeation and separation results reported in literature. Graphene oxide membranes made by filtration, the most common synthesis method, contain wrinkles affecting their gas separation characteristics and the method itself is difficult to scale up. Moreover, the production of graphene oxide membranes with fine-tuned interlayer spacing for improved molecular separation is still a challenge. These unsolved issues will affect their potential impact on industrial gas separation applications.

In this study, high quality graphene oxide membranes are synthesized on polyester track etch substrates by different deposition methods and characterized by XRD, SEM, AFM as well as single gas permeation and binary (H_2/CO_2) separation experiments. Membranes are made from large graphene oxide sheets of different sizes (33 and 17 μm) using vacuum filtration to shed more light on their transport mechanism. Membranes are made from dilute graphene oxide suspension by easily scalable spray coating technique to minimize extrinsic wrinkle formation. Finally, Brodie's derived graphene oxide sheets were used to prepare membranes with narrow interlayer spacing to improve their (H_2/CO_2) separation performance.

An inter-sheet and inner-sheet two-pathway model is proposed to explain the permeation and separation results of graphene oxide membranes obtained in this study. At room temperature, large gas molecules (CH_4, N_2, and CO_2) permeate through inter-sheet

pathway of the membranes, exhibiting Knudsen like diffusion characteristics, with the permeance for the small sheet membrane about twice that for the large sheet membrane. The small gases (H_2 and He) exhibit much higher permeance, showing significant flow through an inner-sheet pathway, in addition to the flow through the inter-sheet pathway. Membranes prepared by spray coating offer gas characteristics similar to those made by filtration, however using dilute graphene oxide suspension in spray coating will help reduce the formation of extrinsic wrinkles which result in reduction in the porosity of the inter-sheet pathway where the transport of large gas molecules dominates. Brodie's derived graphene oxide membranes showed overall low permeability and significant improvement in in H_2/CO_2 selectivity compared to membranes made using Hummers' derived sheets due to smaller interlayer space height of Brodie's sheets (~3 Å).

Dedicated to my family

for their endless love, support and encouragement

ACKNOWLEDGMENTS

I would like to express my sincere gratitude and appreciation for my advisor, Prof. Jerry Lin for his support and guidance directing my research towards success. I am very grateful for his insightful advices on different aspects beside research. Everything I learned from him is extremely beneficial to both my future career and life. I would like to express my deepest appreciation to Dr. Bin Mu, Dr. Mary Laura Lind, Dr. Matthew Green and Dr. Qing Hua Wang, for their time and efforts in their roles as committee members. I really appreciate their invaluable inputs and suggestions to my research and dissertation.

I would like to acknowledge all the current and former members in Prof. Lin's group that I have had the pleasure to work with: Dr. Xueliang Dong, Dr. Yang Liu, Dr. Xiaoli Ma, Dr. Nick Linneen, Dr. Alex Kasik, Dr. Lie Meng, Dr. Sainan Liu, Dr. Judith Ramirez Moreno, Dr. Liang-Chih Ma, Dr. Joshua James, Suzanne Williams, Fateme Banihashemi, Jiansong Miao, Kishen Rafiz, Gaurav Sharma, Paul Mcafee, and Narayan kanhere. I would also like to thank Mr. Fred Pena for his assistance in building gas separation set up and lab equipment repairs.

Finally, I would like to extend my appreciation to the National Science Foundation for the financial support of this work and to the PhD scholarship provided by the Egyptian Government through the Cultural Affairs and Missions Sector.

TABLE OF CONTENTS

Page

Chapter Page

Appendix Page

LIST OF TABLES

LIST OF FIGURES

Figure Page

Figure Page

Figure Page

CHAPTER 1

INTRODUCTION AND LITERATURE REVIEW

1.1 General Introduction

In the past several decades, membrane gas separation has gone from a laboratory curiosity to commercial reality. The gas separation membrane market has grown significantly since its beginnings in the 1970s. According to the forecast made in 2002 (Baker, 2002) the total market of membrane gas separation in 2010 would be 350 million USD. However, the rate of its growth was faster than expected, and it amounted to about 500 million USD in 2010 (Yampolskii, 2012).

Different from conventional gas separation unit operations (e.g., cryogenic distillation, pressure swing adsorption and chemical absorption processes), membrane gas separation is considered to be the most promising because of low energy consumption, possibility for continuous operation, and ultimately cost effectiveness. In addition, the small environmental footprint and the absence of moving parts make membrane gas separation systems particularly suited for use in remote locations such as offshore gas-processing platforms (Spillman, 1989). Continued growth in membrane separation is expected in different applications such as purification of natural gas, air separation, carbon dioxide capture and hydrogen recovery provided that membrane performance is further improved (Sanders et al., 2013).

Substantial progress has been made in improving the performance of state-of-the-art membranes, membrane configuration, and preparation routes. Some of these developments have had a significant effect on the economics of certain membrane processes, others have led to new applications and markets (Bernardo et al., 2009). Today, much of the research

work is being addressed to the investigation of new materials and the development of new membrane structures that exhibit both higher selectivity and permeability to specific gases. In this dissertation, we address the current status of graphene oxide gas separation membranes and provide more understanding of their gas transport mechanism, scaling up potential and approaches to enhance their molecular sieving characteristics. The obtained results will be important to applying these membranes to industrial gas separation processes.

In this chapter we introduce membrane gas separation concepts and fundamentals, major membrane gas transport mechanisms and examples of conventional polymeric and inorganic membranes. A separate section will introduce emerging two-dimensional materials as promising building blocks for membrane synthesis. Finally, a detailed review on graphene oxide gas separation membranes and their permeation and separation characteristics, synthesis methods and transport mechanism will be presented, followed by the objectives of this work.

1.2 Membrane Gas Separation

1.2.1 Fundamental Concepts

In the broadest sense, a gas separation membrane is simply a permeable or semi-permeable medium which selectively allows certain gas molecules to permeate across it while excluding or retarding the permeation of the other gases as shown in Figure 1.1. The driving force for the mass transport is the pressure or concentration gradient for each species across the membrane. The high gas pressure side of a membrane is referred to as the feed or up streamside whilst the other side is known as the permeate or downstream side. The

retentate is that part of the feed that does not pass through the membrane, while the permeate is that part of the feed that does pass through the membrane.

The most commonly reported and compared performance characteristics of gas separation membranes are the permeability, P, or permeance, F, and the selectivity, α, (Robeson, 1999). The permeation rate or permeation flux J, [$mol.m^{-2}.s^{-1}$], is the amount of gas which permeates through the membrane per unit time and unit surface area of the membrane. The permeation flux is usually normalized per unit of pressure, [$mol.m^{-2}.s^{-1}.Pa^{-1}$], and called the permeance, or is further normalized per unit of thickness, [$mol.m.m^{-2}.s^{-1}.Pa^{-1}$], and called the permeability, if the thickness of the separation layer is known. The ability of a membrane to separate two gas species in a mixture as shown in Figure 1.1 is expressed as selectivity or separation factor. Selectivity, is the ratio of the permeability of the two gases in the binary gas pair, (P_A/P_B), where P_A is the permeability of the more permeable gas and P_B is the permeability of the less permeable gas. The separation factor can be defined in terms of molar concentrations of component A to component B in the permeate and retentate as in Equation 1.1. Membranes with both high permeability and selectivity are desirable. Higher permeability decreases the amount of membrane area required to treat a given amount of gas, thereby decreasing the capital cost of membrane units. Higher selectivity results in higher purity product gas.

$$S_{AB} = \frac{[X_A/X_B]\,permeate}{[Y_A/Y_B]\,retentate} \qquad \text{Equation 1.1}$$

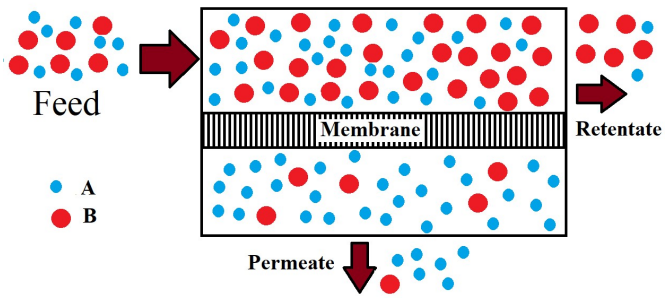

Figure 1.1 Simplified concept schematic for membrane gas separation.

Membranes used today in various applications consist of solid dense or porous polymer, ceramic or metal films with symmetric or asymmetric structures. The membrane material determines the membrane mechanical, chemical, and thermal stability fouling tendency and compatibility with the operation environment. Membranes are manufactured as flat sheets, hollow fibers, or tubes. For practical applications membranes are installed in a suitable device, which is referred to as membrane module. The most commonly used devices are pleated cartridges, tubular membrane modules, spiral-wound modules, and hollow-fiber modules. The key properties of efficient membrane modules are high packing density, good control of concentration polarization and membrane fouling, low operating and maintenance costs, and cost-efficient production (Strathmann, 2001).

1.2.2 Gas-Transport Mechanisms

As a fundamental expression for transport in membranes, the molar flux of species i, J_i, [mol.m^{-2}.s^{-1}], is related to the driving force for mass transport through the membrane as presented in Equations 1.2 and 1.3 (Sotirchos &Burganos, 1999).

$$J_i = -D_i . F_i \qquad \text{Equation 1.2}$$

$$J_i = \frac{\varepsilon}{\tau} D_{e,i} . F_i \qquad \text{Equation 1.3}$$

Where D_i is the ordinary molecular diffusivity, [$m^2.s^{-1}$]. In the case of membranes an effective diffusivity, $D_{e,i}$, is used as in Equation 1.3, where the porosity, ε and tortuosity, τ of the membrane are included. The tortuosity is a factor that accounts for the increased length of a pore by the presence of twists and turns. In general, porous media, and especially porous membranes, are anisotropic structures, and therefore, $D_{e,i}$ is a tensor quantity. However, for transport in one direction only, as is the case in most membrane applications, the tensorial character for $D_{e,i}$ can be ignored. The local driving force (pressure, concentration gradient, … etc.) for mass transport, F_i is usually expressed in terms of the partial pressure difference of species i, imposed across the two faces of the membrane.

As given in Figure 1.2 gas transport and separation mechanisms in membranes can be divided into gas phase transport (viscous flow and Knudsen diffusion) and transport through interaction with the solid (surface diffusion, multilayer diffusion and capillary condensation). When the pore size of the medium is of molecular dimensions, the transport mechanism is molecular sieving or micropore diffusion. In nonporous membranes the transport is by solution of the (gas) molecules in the membrane, followed by diffusion of the species through the membrane and finally dissolution, which is known as solution diffusion (Uhlhorn &Burggraaf, 1991). The contributions of these different mechanism depend on the properties of both the membrane and the gas under the operating temperature and pressure.

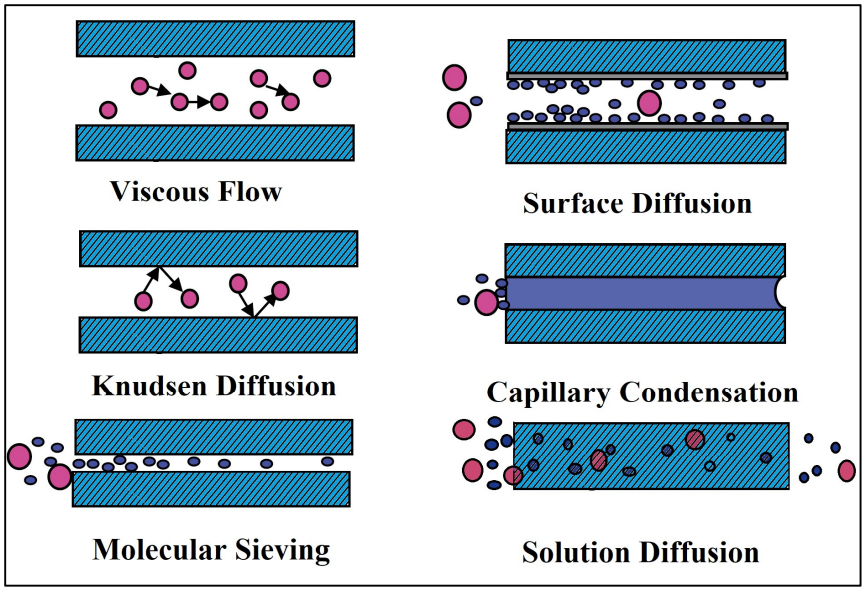

Figure 1.2 Schematic representation of major gas-transport mechanisms in membranes. Adapted from (Tan &Li, 2014).

When the sizes of the pores are much larger than the mean free path (the average distance covered by a molecule between molecular collisions) of permeating gas molecules, and the driving force for transport through the porous structure is the total pressure gradient, the mechanism follows viscous flow. In this case the molecules "see" each other much more than they see the pore wall and collisions between gas molecules govern the flow. The flux through the membrane under viscous flow can be described by the Hagen-Pouisselle equation (Tan &Li, 2014):

$$J_V = -\frac{\varepsilon}{\tau}\frac{d_p^2}{32\mu}\frac{p}{RT}\frac{dp}{dx} \qquad \text{Equation 1.4}$$

Where dp is the pore diameter, [m], μ, is the dynamic viscosity, [Pa.s], R the gas constant, T the absolute temperature, [K], and dp/dx represent the pressure gradient. Based on Equation 1.4 permeability due to viscous flow can be expressed as:

$$P_V = \frac{\varepsilon}{\tau}\frac{d_p^2}{32}\frac{p_m}{RT} \qquad \text{Equation 1.5}$$

Where P_m is the average pressure of the downstream and upstream pressure. If two kinds of molecules are present, there is a continual transfer of momentum from the lighter, faster molecules to the heavier, slower molecules with the result that both kinds of molecules travel with the common drift velocity and the flow is non- separative (Sotirchos &Burganos, 1999).

When the pore diameter is smaller than the mean free path of propping gas molecules, the molecules see the pore wall much more than they see each other, and a molecule traveling through the pore has very little chance of colliding with another molecule in the pore. The Knudsen diffusivity is obtained from the gas kinetic velocity and geometric parameters associated with the membrane. The flux can be described by Knudsen equation (Tan &Li, 2014):

$$J_k = -\frac{\varepsilon}{\tau}\frac{d_p}{3}\sqrt{\frac{8RT}{\pi M}}\quad\frac{1}{RT}\frac{dp}{dx} \qquad \text{Equation 1.6}$$

Where M is the molecular weight of the diffusing gas, [kg/mol]. Permeability according to Knudsen diffusion can be expressed as:

$$P_k = -\frac{\varepsilon}{\tau}\frac{d_p}{3}\sqrt{\frac{8}{\pi MRT}} \qquad \text{Equation 1.7}$$

The collisions between gas molecules and the walls of the pores are elastic, so there is no tendency for the molecules to interact with the surface. For pure gases, a good indication of which mechanism is dominant, Knudsen diffusion or viscous flow, is given by the Knudsen number, K_N, which is the ratio of the molecular mean free path and the pore diameter. Poiseuille flow through a porous medium occurs for $K_N << 1$, while Knudsen diffusion dominates for $K_N >> 1$ (Uhlhorn &Burggraaf, 1991). For $K_N \sim 1$ and for pure gases, Poiseuille flow and Knudsen diffusion are assumed to be additive(Lin &Burggraaf,

1993). As can be seen from Equations 1.5 and 1.7, Poiseuille flow is non separative, while gas separation by Knudsen diffusion can separate gases according to their molecular mass. For gas mixtures, description of transport becomes more difficult. If only Knudsen diffusion occurs, the molecules do not see each other and for binary mixtures Equation 1.7 is valid. In the case of combined viscous flow and Knudsen diffusion, several models were Developed to describe diffusion through porous media. For example, Watson and coworkers (1961) developed the so-called dusty-gas model. In this model, the porous medium is depicted as huge gas molecules fixed in time and space. This model, although fairly complicated, is commonly used to predict fluxes through porous media (Veldsink et al., 1995).

A third mechanism encountered in gas permeation is surface diffusion. Gas molecules, having strong affinity with the material that makes up the walls of the pores, adsorb on the membrane walls and diffuse along the pore surface by moving from one adsorption site to another and desorb at the pore exit. This mechanism is likely to be dominant for condensable gases at high pressures and low temperatures. This mechanism becomes important with relatively small pores because of the relatively high proportion of surface area compared to pore volume. The gradient in surface diffusion is a surface concentration gradient (Sotirchos &Burganos, 1999). The flux due to surface diffusion is generally described by a Fick's law type of expression (Tan &Li, 2014):

$$J_s = -\frac{\varepsilon}{\tau}\,\rho_{mem}\,D_s\frac{dq}{dx} \qquad \text{Equation 1.8}$$

ρ_{mem} is the density of the porous membrane, [$kg.m^{-3}$], D_s, is the surface diffusion coefficient [$m^2.s^{-1}$], and q, is the adsorption capacity [$mol.Kg^{-1}$], dq/dx is the gradient in surface occupation. Equation 1.8 can be rewritten in terms of pressure and the relationship

between adsorption capacity ,q and pressure can be expressed by an adsorption isotherm such as a Langmuir equation as (Tan &Li, 2014):

$$J_s = -\frac{\varepsilon}{\tau}\ \rho_{mem}\ D_s \frac{dq}{dp}.\frac{dp}{dx} \qquad \text{Equation 1.9}$$

The surface diffusion coefficient has been the subject of many investigations. In most cases it is assumed that molecules jump from one site to another which is an activated process. Thus, the relationships for *D*, *S*, and *P* as a function of temperature can be expressed in the form of Arrhenius type equation(Oyama et al., 2011):

$$D = D_o\ exp\left(-\frac{E_d}{RT}\right) \qquad \text{Equation 1.10}$$

$$S = S_o\ exp\left(-\frac{\nabla H_S}{RT}\right) \qquad \text{Equation 1.11}$$

$$P = P_o\ exp\left(-\frac{E_P}{RT}\right) \qquad \text{Equation 1.12}$$

Where E_d is the activation energy of diffusion, ∇H_S is the heat of sorption and E_P ($E_d + \nabla H_S$) is the activation gas energy of permeation. D_o, S_o and P_o are the diffusivity, solubility and permeability respectively at infinite temperature.

Activated, configurational, or micropore diffusion may be viewed as surface diffusion at the limit at which the pore size becomes comparable to the molecular size. With the gradient of the fluid concentration in the pores (adsorbate) as the driving force. Because of the many similarities between surface diffusion and activated diffusion, many of the methods employed to study the former and the relationships developed for the surface-diffusion coefficient also apply to the latter. Activated (micropore) diffusion and Knudsen diffusion are the main two transport mechanisms of interest for selective membranes. For Knudsen diffusion, the selectivity is determined by the ratio of the molecular weights, but in the case of activated diffusion, the diffusion coefficients of the two gases are strong

functions of the molecular shape and size, the pore size, and the strength of the interactions between pore walls and molecules (Sotirchos &Burganos, 1999).

The gas translational mechanism was used to explain gas permeation results that occurs with small pore such as zeolite membranes sizes (Xiao &Wei, 1992),where the movement of molecules form site to site become restricted and must overcome the energy barrier imposed by the channels. Therfore, the molecules requires an amount of energy that is equal or greater than the activation energy by thermeal interacton with its surroundings to climb out of the well and move over the barrier to enter a new a equilibrium position. Considering this, a mechanism which is a combination of the Knudsen diffusion model and the surface diffusion model has been proposed. The following permeation equation, which is referred to as the gas-translation model or activated Knudsen, was derived for diffusion through microporous inorganic membranes based on Knudsen equation using probability, ρ, which indicates the probability of diffusion through the micropore (Shelekhin et al., 1995).

$$P_T = \frac{\varepsilon}{\tau} d_p \rho \sqrt{\frac{8}{\pi MRT}} \qquad \text{Equation 1.13}$$

This probability, ρ, consists of a pre-exponential, ρ_o, and the kinetic energy, E_d, to overcome the diffusion barrier (Shelekhin et al., 1995), and thus, the permeability in Equation 1.13 can be expressed in Equation 1.15

$$\rho = \rho_o exp\left(-\frac{E_d}{RT}\right) \qquad \text{Equation 1.14}$$

$$P_T = \frac{\varepsilon}{\tau} d_p \rho_o \sqrt{\frac{8}{\pi MRT}}\ exp\left(-\frac{E_d}{RT}\right) \qquad \text{Equation 1.15}$$

According to gas translation model, Equation1.15 covers the activated diffusion ($E_d > 0$), surface diffusion ($E_d < 0$) and Knudsen diffusion ($E_d = 0$). The activation energy can be determined by the interactions between permeating molecules and the pore wall, based on the Lennard-Jones potential using the size (membrane pore size, molecular size of permeating molecules) and the interaction parameters(Xiao &Wei, 1992).

Capillary condensation occurs when the pores are small enough and the gas is a condensable vapor so that the whole pore is filled with liquid. Owing to the capillary condensation, gas-phase diffusion through the pores can be blocked, leading to reduced permeation flux but improved selectivity (Tan &Li, 2014). Solid-state diffusion or solution diffusion mechanism occurs with further decrease in the pore size, or when no pore space is available for diffusion. The gas molecule interacts strongly with the membrane material and its solubility needs to be considered. Under the driving force of a pressure difference across a membrane or concentration gradient, penetrant molecules dissolve in the upstream (or high pressure) face of a membrane, diffuse across the membrane, and desorb from the downstream (or low pressure) face of the membrane. In this case permeability is the product of solubility and diffusivity. Permeability is typically quite low, in comparison to that in porous membranes, primarily due to the low values of diffusion coefficients in the solid membrane phase. There are three cases that belong to this class of transport mechanism, permeation through glassy membranes, metallic membranes, and polymeric membranes (Oyama et al., 2011).

1.2.3 Polymeric Membranes

Over the past three decades, polymeric gas separation membranes have become widely used for a variety of industrial gas separations applications. Despite the large

number of polymeric materials investigated and developed for gas separation applications, the number of polymers used in commercial systems is still limited (Bernardo et al., 2009). In 1979, Permea (now a division of Air Products) launched its hydrogen-separating membrane marked as Prism® (basic membrane material: polysulfone hollow-fiber) to mine hydrogen from the ammonia purge gas and recycle it to the process. This was the first large industrial application of gas separation membranes (Baker, 2002). Prism® membranes are also used for syngas ratio adjustment (H_2:CO) and refinery off gas purification (Air-Products, 2017).

By far, the largest market for membrane-based air separation is for nitrogen enrichment applications. Membranes are often the most economical option, especially if required N_2 purity is between about 95 and 99% (Baker, 2002). By the mid-1980s, Generon introduced a membrane system to separate nitrogen from air. These first air separation systems were based on poly(4-methyl-1-pentene) (TPX) membranes with an oxygen/nitrogen selectivity of about 4. These membranes were only competitive in a few niche areas requiring 95% nitrogen (Baker, 2002). Research into new membrane materials and design quickly improved air separation performance, and by the early 1990s, several new hollow fiber membranes were brought to market, including tetrahalogenated bisphenol based polycarbonates by Generon, polyimides by Praxair, and polyimide and polyaramide membranes by Medal, now part of Air Liquide, (Sanders et al., 2013).

Removal of CO_2 and H_2S (*i.e.*, acid gases) from natural gas is a growing area for membrane technology to prevent natural gas pipeline corrosion as well as adjust the heating value. The first membranes for natural gas purification were developed in the early to mid-1980s. Separex (now part of UOP) developed spiral-wound membranes, and Cynara (now

part of Natco) developed hollow-fiber membranes based on cellulose acetate. These cellulose acetate membranes are still widely used today, but polyimides and other materials have gained some attraction in this field over the past 15–20 years (Baker &Lokhandwala, 2008).

An important feature for polymer membranes is its processability into hollow fiber membranes ("spinnability"). Hollow fiber modules (each module contains thousands of fibers) are of interest for large-scale industrial applications, due to the high membrane area to module volume ratio which results in high productivity per volume unit and cost efficient production (Strathmann, 2001). On the other hand, polymers cannot withstand high temperatures and aggressive chemical environments; moreover, when applied in petrochemical plants, refineries, and natural gas treatment, heavy hydrocarbons in feed gas streams can be a problem, particularly in hollow fiber modules. Many polymers can be swollen or plasticized when exposed to hydrocarbons or CO_2 with high partial pressure, even in low concentrations: their separation capabilities can be dramatically reduced, or the membranes gets damaged. Therefore, pretreatment selection and condensate handling are critical decision factors for a proper operation of polymer gas separation modules (Bernardo et al., 2009).

Moreover, polymeric membranes generally undergo a trade-off limitation between permeability and selectivity: (Robeson, 1991) as selectivity increases, permeability decreases, and vice versa. Unless significant enhancement in solubility selectivity could be achieved, the upper bound would represent the asymptotic end point in the performance of polymeric membranes whose separation properties are related to solution-diffusion

transport mechanism. To achieve higher selectivity/permeability combinations, materials that do not obey these simple rules would be required.

1.2.4 Inorganic Membranes

The development of inorganic membranes is particularly interesting because they can withstand aggressive chemicals and high temperature in addition to their, well-defined stable pore structure, and chemical inertness (Lin, 2001). One of the extensively studied inorganic membranes is zeolite membranes. Zeolite membranes in principle might separate continuous mixtures on the basis of differences in the molecular size and shape but also on the basis of different adsorption properties (Yu et al., 2011). The presence of intercrystalline gabs in the zeolite layer limit their gas separation quality.eg A H_2/N_2 separation factor of ~24 was reported for the small-pore zeolite A (Xu et al., 2000). Post-synthesis modification to decrease the pore size and gabs was reported to increase the separation quality of zeolite membranes. A MFI membrane with a H_2/N_2 separation factor of 1.4-4.5 reached values of 90-140 after silane catalytic cracking (Masuda et al., 2001). The first commercial application is that of LTA zeolite membranes for solvent dehydration by pervaporation (Morigami et al., 2001). However, zeolite membranes exhibit somewhat lower diffusion-controlled selectivity for gas mixtures or unstable separation characteristics due to adsorption induced microstructural changes. These problems together with high membrane costs and modest defect free reproducibility have hindered industrial applications of zeolite membranes for gas separations (Lin &Duke, 2013).

Dense inorganic membranes based on palladium and palladium alloys have been used for many years for the selective transport of hydrogen. These membranes have practically infinite selectivity for hydrogen. However, their large-scale industrial applications are

limited due to the high price of the metal and low hydrogen permeability (Al-Mufachi et al., 2015). Dense ceramic membranes based on perovskites exhibit high mixed electronic and oxygen ion conductivitiy, and for this reason they are widely studied for applications in solid oxide fuel cells, oxygen sensors, and membrane reactors. A substantial disadvantage for the large-scale production of oxygen with perovskite membranes is their low oxygen permeability at room temperature. To obtain reasonable oxygen fluxes, these membranes must be used at temperatures in excess of 600 ^{o}C which makes sealing a difficult task (Kharton et al., 1999).

Carbon molecular sieve (CMS) membranes show excellent intrinsic performance for gas separation applications. These materials are obtained through the pyrolysis (at high temperature in an inert atmosphere) of polymeric precursors already processed in the form of membranes (Saufi &Ismail, 2004). Carbon membranes are believed to contain slit-shaped pores among planar aromatic moieties. The mechanism of separation in carbon membranes depends on the pore size and molecular sieving is dominant when the effective pore diameters are on the molecular scale (3-5 Å). Major disadvantage that hinders their commercialization is their brittleness, making them require careful handling and pore blocking by higher organics. Their cost compared to polymeric membranes may be justified only when they achieve a much better performance than polymeric membranes (Ockwig &Nenoff, 2007). Carbon nanotube membranes (CNTs) showed high permeation flux but, they are limited to theoretical studies because of several technical challenges such as relatively high cost of CNTs, complex process of obtaining high density aligned CNTs, and difficulties in achieving large-scale production (Bernardo et al., 2009).

1.3 Two-Dimensional Membrane Materials

The isolation of graphene in 2004 from graphite by Novoselov and Geim (2004) was a defining moment for the "birth" of a field: two-dimensional (2D) materials. Each layered material, when thinned to its physical limits, exhibits novel properties different from its bulk counterpart. The true potential of these layered materials may emerge from the ability to stack them, layer-by-layer in any desired sequence, to create novel three-dimensional (3D) architectures with entirely new functions. These two-dimensional materials are very attractive subjects for membrane research because they are expected to function as ideal gas separation membrane materials. Current research trends are focusing on graphene and its derivatives, together with other emerging ones, such as, molybdenum disulfide, boron nitride, zeolite nanosheet membranes, … etc. to considerably improve performance of membrane technologies.

1.3.1 Graphene

Graphene, in its pristine form, is the name given to a single layer of sp^2-bonded carbon atoms arranged in densely packed benzene-ring structure (Novoselov et al., 2004). It is naturally found as the building block of graphite, where π-stacking of graphene sheets holds the lamellar graphite structure strongly in place, with an interlayer spacing of 3.34 Å between the sheets. The carbon–carbon bond, the strongest chemical bond in the world, has a high bonding energy of 4.9 eV, resulting in extraordinarily high mechanical strength (42 N/m) and Young's modulus (1TPa) (Bunch et al., 2008). Graphene and its derivatives offer a wide range of opportunities for membrane applications because of their unique one-atom-thick nanostructure, flexibility, mechanical strength and chemical inertness (Huang et al., 2014b; Huang et al., 2015; Xu et al., 2015).

Graphite can be exfoliated to generate single layers of graphene. This was initially demonstrated by micromechanical exfoliation, the sequential cleavage of graphite to graphene using adhesive tape (Novoselov et al., 2004). Micromechanical exfoliation generates very high-quality graphene, ideal for research purposes. Micromechanical exfoliation, however, is labor-intensive and not scalable for large-scale use of graphene. Graphene can be exfoliated from graphite by ultrasonication of graphite in organic solvents; however, this approach was found to generate relatively low yields (Zhu et al., 2010). Chemical vapor deposition, CVD, of hydrocarbons or alcohols has been widely used for growing graphene membranes with mono- and few-layers on metal catalyst surfaces (Ni, Pd, Ru, Ir, Cu). A carbon-containing gas, such as CH_4 or C_3H_8, decomposes at high temperature, and is converted into graphene on the catalytic metal surface (Li et al., 2009).

The perfect graphene nanosheet is impermeable to all liquids, vapors, and gases as small as helium (Bunch et al., 2008) as the localized electron density of its hexagonal rings will repel the atoms and molecules trying to pass through them (Berry, 2013). Therefore, theoretical and experimental studies were reported on graphene membranes with nanopores : nanoporous graphene membranes (Zhang et al., 2014). The selective passage of ions through nanoporous graphene is determined by pore sizes and the electrostatic interaction between the ions and the pores (Sint et al., 2008). Molecular dynamics (MD) simulations have predicted that monolayer graphene with subnanometer pores could act as a highly selective and permeable separation membrane with much higher efficiencies than those of state-of the art polymeric filtration membranes. (Cohen-Tanugi &Grossman, 2012; Du et al., 2011; Lee &Aluru, 2013). In MD simulations, nanopores with a high number density and predefined sizes can be ideally introduced into a monolayer graphene membrane.

Unfortunately, precisely controlling pore sizes and achieving high pore density on a large-area graphene are technically challenging. Nevertheless, extensive efforts have been devoted to reaching this aim. The advantages and limitations of different perforation methods are summarized in Table 1.1.

Table 1.1

Advantages and Limitations of Different Perforation Methods for Nanopore Formation in Graphene (Perreault et al., 2015)

Method	Pore size (nm)	Advantages	limitations
Focused electron beam irradiation	3.5, 0.7	Controlled pore size	Small area
Low-energy ion beam and unfocused electron beam irradiations	0.45–2.2	Controlled pore size	Small area
Nitrogen-assisted electron beam irradiation	5.9 ± 0.4	Controlled pore	Small area
Block copolymer lithography and plasma etching	>5±2	Large area and controlled pore size	Pores too large for salt rejection
UV oxidative etching	0.4–10	Large area	Wide pore size distribution
High temperature O_2 etching	20–250	Large area	Pore size range of <1 nm
Low energy ion beam and chemical oxidation	0.4 ±0.2	Controlled pore size	

So far, the most commonly used technique to fabricate large-area monolayer graphene is CVD (Bae et al., 2010). However, the successful transferring of CVD graphene membrane from Cu foil to the target porous substrate is extremely difficult. Wrinkles and cracks are easily induced, especially for large-area membranes (Li et al., 2009). Regardless of the excellent predicted separation performance, these membranes and methods are not scalable for industrial separation applications and thus films made by stacking graphene oxide nanosheets is an interesting candidate (Huang et al., 2014b; Huang et al., 2015; Xu

et al., 2015). When the graphene oxide nanosheets are stacked, small liquid and gas molecules can go through the well-ordered 2D nano-channels between the nanosheets (Nair et al., 2012). Since graphene oxide membranes is the main focus of this dissertation, more details about the graphene oxide synthesis methods and staking into membranes as well as their gas separation characteristics will be presented later.

1.3.2 Materials Beyond Graphene

Two-dimensional hexagonal boron nitride (BN) nanosheets, also called 'white graphene' or 'non-carbon graphene', consist of a few layers of alternating boron and nitrogen atoms in a hexagonal arrangement. This structure resembles graphene with a similar lattice constant and shows the excellent impermeability to O atoms and moisture. BN has outstanding thermal and electrical properties, excellent chemical stability, good resistance to corrosion, low density, and a high melting point (Li et al., 2014). The methods for fabricating BN nanosheets are quite similar to those of graphene fabrication, which can also be classified into mechanical exfoliation, chemical exfoliation, and CVD (Pakdel et al., 2014). The holes in BN can be drilled via either electron beam punching or chemical etching techniques, as employed in graphene. Simulation studies also confirmed the potential of porous born nitride with appropriate pore size for gas separation (Darvish Ganji &Dodangeh, 2017; Zhang et al., 2015b). Manufacturing of membranes from boron nitride is much more difficult than from graphene or graphene oxides because of the poor dispersibility of BN in water, which limits its exfoliation and preparation of colloidal solutions (Lei et al., 2015).

Molybdenum Disulfide layered material, MoS_2 possesses good chemical and thermal stability and is mechanically strong. In addition, the current preparation technique for single-layered MoS_2 nanosheets in massive quantity via chemical exfoliation is becoming more and more mature, like that for GO. Park and coworkers(Wang et al., 2015a) reported for the first time the use of single-layered molybdenum disulfide (MoS_2) nanosheets as building blocks for constructing laminate-stacked ultrathin membranes for high-permeance H_2 separation. 17-60 nm thick membrane was prepared by vacuum-filtering an aqueous dispersion of single-layered MoS_2 nanosheets onto anodic aluminum oxide. The membranes showed high permeance but the obtained H_2/CO_2 selectivity of ~3 due to large interlayer spacing between stacked sheets of 1.1 nm. Subsequent studies show that the MoS_2 membranes were found to be thermally stable up to 160 °C. The mechanism of gas permeation through the MoS_2 membranes was found to be through interbundle spaces instead of interlayer spaces of individual MoS_2 sheets (Achari et al., 2016).

Membranes based on stacking of 2-D materials such as graphene oxide usually suffer from long travelled tortuous distance of gas molecules and selective sheet defects are randomly distributed. Therefore, the hydrogen permeance reported for ultrathin graphene oxide membranes with thickness as low as 1.8 nm is ~$1x10^{-7}$ [$mol/m^2.s.Pa$] gas permeation units (Li et al., 2013), still at the same level as conventional microporous membranes. Therefore, some researchers give more attention to porous material with a layered structure that can be exfoliated to give nanometer-thick molecular sieves. Tsapatsis and coworkers (2011), demonstrated the fabrication of molecular sieve membranes based on exfoliated zeolite nanosheets with thickness at the unit cell level (~3 nm). Layered metal-organic frameworks would be a diverse source of crystalline sheets with nanometer thickness for

molecular sieving if they could be exfoliated. Peng and coworkers (2014) reported the preparation of 1nm-thick sheets with large lateral area and high crystallinity from layered MOFs. These sheets were used as building blocks for ultrathin molecular sieve membranes, which achieved hydrogen gas (H_2) permeance of up to several thousand gas permeation units with H_2/CO_2 selectivity greater than 200. These results suggest that ultrathin membranes constructed by stacking nanosheets in a proper manner have great potential for achieving excellent gas separation performance beyond expectations.

1.4 Graphene Oxide Characteristics

Graphene oxide (GO) sheets are the oxidative exfoliation product of graphite with atomic layer thickness and oxygen-containing functional groups attached to their edges and basal planes (Lerf et al., 1998). Among various graphene derivatives, GO is very cheap and can be mass-produced by oxidizing graphite (Sun &Fugetsu, 2013). The oxidation product from graphite consists of several stacked graphene layers with enlarged interlayer spacing (from 0.34 nm to 0.95 nm) depending on the degree of oxidation (Marcano et al., 2010). When GO is subsequently exfoliated by mechanical stirring or ultrasonication, it yields GO single sheets of ~1 nm and lateral dimensions varies between a few nanometers and several microns (Marcano et al., 2010).

Despite its close relation to graphene, GO has its own scientific importance as a unique form of oxidized carbon. The presence of various oxygen-containing functional groups renders the material hydrophilic and dispersible in many solvents, particularly water. This hydrophilic nature, combined with its high surface area and functional group density, allows for a wide variety of chemical functionalization to be performed on GO sheets

(Dreyer et al., 2010). GO is therefore widely considered as a building block for novel graphene-based materials (Compton &Nguyen, 2010).

1.4.1 Synthesis Methods

Graphite the starting material for preparing GO is extremely inert and hard to be attacked/reacted by most oxidizing agents. Therefore, only harsh chemical methods can covalently functionalize/oxidize the graphene basal planes. Benjamin C. Brodie, a British chemist, is believed to be the one who first synthesized graphene oxide in 1859. He mixed potassium chlorate ($KClO_3$) with graphite in the presence of fuming nitric acid (HNO_3) at 60 °C for three to four days. He found that the substance formed, by this treatment when washed free from the salts produced in the reaction, and dried at 100 °C, and again oxidized, it gradually underwent a change in appearance, until, after the fourth repetition of the process, the whole of the graphite was converted into tiny transparent and brilliant plates of a light-yellow color. According to his elemental analysis of the final product, The C:H:O composition was determined to be 61.04:1.85:37.11; a net molecular formula of $C_{11}H_4O_5$. Brodie's results and conclusions were largely limited by the theories and characterization techniques at that time (Dreyer et al., 2010) However, his exploratory study has begun a new era of research for graphene and its derivatives and provided today's researchers all over the world an endless space to further explore.

In 1898, Staudenmaier improved Brodie's method by adding the sodium chlorate ($NaClO_3$) in multiple aliquots during the reaction rather than in a single addition as Brodie had done. He also added concentrated H_2SO_4 to the mixture to increase the acidity of the reaction mixture. Staudenmaier's method resulted in an overall extent of oxidation similar to Brodie's multiple oxidation approach (C:O ~2:1). However, Staudenmaier's method is

more straightforward, and it can be performed more practically in a single reaction vessel (Dreyer et al., 2010).

In 1958, Hummers and Offeman reported an alternative method for the synthesis of graphene oxide by using potassium permanganate ($KMnO_4$) and sodium nitrate ($NaNO_3$) in concentrated H_2SO_4. Since then, different modifications to Hummers' methods were proposed to increase the yield such as using expanded graphite as a starting material (Sun &Fugetsu, 2013) and using a pre-expansion step of graphite where graphite is first treated with a mixture of concentrated sulfuric acid (H_2SO_4), potassium persulfate ($K_2S_2O_8$) and phosphorus pentoxide (P_2O_5) at 80 °C for several hours (Kovtyukhova et al., 1999). Tour and coworkers (2010) excluded sodium nitrate as an additive due to its negligible role in graphite oxidation. A mixture of H_2SO_4/H_3PO_4 (9:1 volume ratio) instead of only H_2SO_4 resulted in increased hydrophilic and oxidized GO without the emission of toxic nitric gases.

Though others have developed slightly modified versions, these three methods comprise the primary routes for GO synthesis. For dry samples, GO powder produced by Brodie's method shows the smallest interlayer distance and largest carbon content: Brodie(1859) (carbon content 62 wt %, layer distance 5.5−5.9 Å), Staudenmaier (1898) (52 wt %, 6.3−6.5 Å) and Hummers (1958) (57 wt %, 6.7−6.9 Å). Improving the GO yield using hummers' method by increasing the amount of oxidant will result in increased spacing between the sheets eg. adding twice the amount of $KMNO_4$ resulted in d- spacing of 9 Å (Marcano et al., 2010). Moreover, despite an extensive washing process, using H_2SO_4 in Hummers's and Staudenmaier's methods unavoidably results in contaminants which are very difficult to remove completely. For example, impurity of sulfur in GO

prepared by the Hummers' method was reported to affect ammonia adsorption on GO powder (Petit et al., 2009). Moreover, significant differences with respect to hydration, solvation and exfoliation properties was reported for GO powders synthesized by Brodie's and Hummers' methods (You et al., 2013).

1.4.2 Structure Models

knowledge of the surface chemistry of GO is necessary to explain the GO's physical and chemical properties observed in experiments and to exploit this substance efficiently. The precise chemical structure of GO has been the subject of considerable debate over the years and different structure models of GO were proposed based on experimental and theoretical studies. The earliest model was proposed in 1939. Hofmann and Holst proposed a structural model of GO with only epoxy groups on the basal planes with sp^2 hybridization and net molecular form C_2O. In 1947, Ruess proposed a variation of this model considering the presence of hydrogen in GO species by introducing hydroxyl moieties in the basal plane of graphite. With this modification, this model acquired a sp^3 character and is formed by a repeat unit where 1/4 of cyclohexanes with epoxide groups localized in the 1, 3 positions and hydroxilated in 4 position. Scholz and Boehm (1969) have substituted the epoxide in Hofmann and Holst model by quinoidal species in a corrugated backbone. All these early models of GO are generally based on the chemical formula and elemental analysis without the support from the spectral information and GO is treated as a material built up by repetitive units.

Lerf and co-workers (1998) based on expert NMR studies, depicts a GO layer as a random distribution of flat aromatic regions with unoxidized benzene rings and wrinkled regions with aliphatic six-membered rings bearing C=O, C-OH and the sheets of GO

terminate with C-OH and COOH groups. This model is based on GO produced using Hummer's method. Ultra-high-resolution transmission electron microscopy studies showed that the GO nanosheet consists of three types of regions: holes (defects), pristine graphite regions, and oxidized regions with areal percentages of approximately 2%, 16%, and 82%, respectively (Erickson et al., 2010). The oxidized regions form a continuous network across a GO sheet and pristine graphitic regions form isolated islands (Erickson et al., 2010; Pacilé et al., 2011) and thus, the pristine graphitic regions are unlikely to form a continuous network across a GO sheet.

Besides the interpretation of experimental data to elucidate the GO structure, theoretical studies were carried out approaching towards the full understanding of this material. Paci and coworkers (2007) explored the formation of GO structure by means of Monte Carlo method. They showed that epoxide and hydroxyl functional groups dominate and are randomly distributed on both sides of the graphene plane. They found a set of hydroxyl-hydroxyl and hydroxyl-epoxide hydrogen-bonding interactions and, occasionally, defects made by small holes. Lim and coworkers (2016) looked into the oxidative process of graphene at edges using density-functional theory calculations. Their results showed that the oxidation is more favorable along the edges comparing with the central part of the graphene basal plane.

Although much effort has been done theoretically and experimentally in an attempt to understand this material much remains to be learned about its structural details. Variations in the degree of oxidation caused by differences in starting materials (principally the graphite source) or oxidation protocol can cause substantial variation in the structure

and properties of the material, rendering the term "graphite oxide" subject to misinterpretation.

1.4.3 Gas Separation Membranes

Since the pioneering work of Geim and coworkers (Nair et al., 2012), there has been a growing interest in the synthesis of graphene oxide membranes for water purification, desalination (Hegab &Zou, 2015) and gas separation applications (Huang et al., 2015). However, the number of reports of pure GO membranes focusing on gas separation is still very limited. Table 1.2 highlights studies on GO membranes with interesting gas transport and separation characteristics. GO membranes show a promising potential for hydrogen separation. Yu and coworkers (2013) presented an extraordinarily high H_2/CO_2 selectivity of 3400 in a 9-nm thick GO membrane, which is the highest record of all the membranes reported so far. Park and coworkers (2013) reported few-layered GO membrane exhibiting CO_2-selective and permeable behaviors under wet conditions, which is suitable for post-combustion CO_2 capture.

The GO membranes listed in Table 1.2 show very different gas permeability and separation characteristics among themselves. It appears that synthesis method, substrate structure and characteristics of GO sheets (size or defects) affect the permeability and separation characteristics of these membranes. Yu and coworkers (2013) found that the permeance of small gasses such as H_2 and He decreases exponentially as the membrane thickness increases from 1.8 to 180 nm, which could explain why the ~1 μm thick GO membrane prepared by Geim and coworkers (2012) was impermeable to He. The application of a transmembrane pressure can help overcome the energy barriers of molecules entering and diffusing within GO nanochannels and could enhance the

permeability of GO membranes to gases (Kim et al., 2013). Gases could permeate through even thick GO membranes at elevated transmembrane pressure (Kim et al., 2013; Romanos et al., 2015).

Table 1.2

GO Gas Separation Membrane Studies and Proposed Transport Mechanisms

Method (substrate)	Membrane thickness	GO sheet size	Gas study	H_2 permeability, Barrer	Gas selectivity	Transport channels	Ref.
Spi n coating (copper foil)	~1000 nm	~1 µm	permeable to water but completely impermeable to vapors, gases and other liquids			2D capillaries formed by closely spaced graphene sheets	(Nair et al., 2012)
spin coating (PES-100 nm)	~ 5 nm	300 - 500 nm	CO_2 and N_2	~0.12	~20* dry feed	edge- to -edge openings and adsorption induced separation are dominant over interlayer galleries	(Kim et al., 2013)
dip and spin coating (PES-100 nm)			H_2 and CO_2	~0.17	~30* dry feed		(Kim et al., 2013)
spray coating (Al_2O_3- 100 nm)	1 µm	~ 1 µm	H_2/CO_2	80.6	20.9		(Guan et al., 2017)
filtration-spin **(Al_2O_3- 100 nm)	1 µm	~ 1 µm	H_2/CO_2	1000	~ 30	finely tuned edge- to -edge openings and interlayer-galleries	(Shen et al., 2016)
filtration (AAO-20nm)	9 nm	300-700 nm	H_2/CO_2	2.69	~ 3400	selective structural defects on GO sheets	(Li et al., 2013)
			H_2/N_2		~ 900		
filtration (AAO-20nm)	~ 20 nm	13 µm	H_2/CO_2	31.04	51		(Chi et al., 2016)
spin coating (AAO-20nm)			H_2/CO_2	20.42	240		
self-standing by filtration (MCE, 450nm)	20 µm	N/A	H_2, CH_4 C_2H_4, and C_4H_{10}	47.46	twice Knudsen relative to H_2*	inter-GO stack space was dominant over interlayer space	(Romanos et al., 2015)

* permselectivity, ** alternatively depositing GO and polyethylenimine, PES: polyether sulphone, AAO: anodic aluminum oxide, MCE: mixed cellulose ester. 1 barrer = 1×10^{-10} cm^3 $cm/cm^2 \cdot sec \cdot cm$ Hg at STP.

The GO sheets used in the studies listed in Table 1 were mostly of small lateral dimensions because they were prepared from exfoliation of GO powder by sonication in water. This sonication method usually results in fragmentation of GO nanosheets into

smaller pieces with a wide distribution of sheet sizes (Ogino et al., 2014). The effect of GO sheet size on the permeability and selectivity of GO membranes is not clear from the studies listed in Table 1. GO membranes made by sheet sizes ~2 μm show less permeance, but with same mixture H_2/CO_2 separation factor compared to the GO membranes made by sheet size of 1 μm (Guan et al., 2017). The gas permeance decreases and ideal selectivity increases with increasing GO sheet size from 300 to 1000 nm for 4~6 μm thick GO membranes made by filtration on anodic alumina substrates (Kim et al., 2013). Using one type of commercially available GO, Yu and coworkers (2013) focused on the effect of the centrifugation time and dilution of the GO suspension used in the filtration, emphasizing on the importance to get rid of GO aggregates and large GO sheets through centrifugation at 10000 rpm in order to develop membranes of enhanced gas separation performance. GO powders from commercial resources were prepared by a mild freeze thaw exfoliation method as reported by Zhao's group (2016) to produce large GO nanosheets (13 μm) for membrane synthesis. They noticed that very small GO particles mixed with the large exfoliated sheets lower the membrane performance and thus purification of exfoliated GO nanosheets through pH adjustment was necessary to produce high quality GO membranes.

1.4.4 Membrane Synthesis

The 2D nature of GO sheets (single-atom-thick with lateral dimensions as high as tens of micrometers) allows disordered sheets in suspension to be uniformly deposited onto various types of substrates in the form of thin films using a prober assembly method. Synthesis of GO membranes has been accomplished by filtration and film coating techniques such as dip coating, spin coating, and drop casting (Huang et al., 2014b). The common point of these methods is to obtain GO dispersion first and then introduce solvent

evaporation or filtration to eventually form GO membrane. Filtration is the most commonly used method to prepare stacked GO membranes with good control over membrane thickness. Yu and coworkers (2013) reported ultrathin GO membranes with a thickness down to 1.8 nm. Filtration under vacuum is a time-consuming method specially for preparation of thick GO membranes and the decrease in the vacuum rate as the filter cake thickness grows with time, causes the GO layers near the substrate to become compact, but those away from it become loose (Tsou et al., 2015). It was also demonstrated that the GO porosity strongly depends on the filtration rate and a very slow filtration resulted in more ordered structures (Romanos et al., 2015).

Park and coworkers (Kim et al., 2013) used interface contact and spin casting rather than filtration to prepare very thin GO membranes (3-10 nm) on microporous polyethersulfone substrates. They focused on testing the relative importance of electrostatic repulsion and capillary force on the GO stacking structure. GO sheet edges are negatively charged in alkaline aqueous solutions. When the substrate surface contacts the GO solution in a dip coating process, the primarily GO sheets attached to the substrate surface are governed by the repulsive GO sheet edge-to-edge interactions, which leads to an island-like assembly of GO sheets on the substrate surface. This method leads to a relatively heterogeneous GO deposition. In contrast, when GO solution-substrate contact occurs only during spin casting, the initial deposition is governed more by capillary interactions between the GO sheet faces and not the electrostatic interaction between the GO edges resulting in considerably denser GO deposition. Zhao and coworkers (2016) also used spin coating to prepare 20 nm thick GO membranes that showed H_2/CO_2 separation factor of 240. Using the same GO suspension, the GO membranes prepared by filtration

show H_2/CO_2 selectivity of 51. The decrease of the quality of the membrane was attributed to the formation of extrinsic wrinkles in the membranes made by filtration.

Spray-coating techniques such as air-brushing have been used to produce graphene or GO films on various dense substrates (Gilje et al., 2007; Li et al., 2008; Pham et al., 2010). These studies focused on the production of transparent conductive films to carry out electrical measurements and not for separation applications. Recently, Jin and co-workers (2017) used spray-evaporation induced self-assembly to fabricate GO membranes on alpha-alumina substrates for gas separation. Their study focused on the effect of the evaporation rate on the GO stacking during the whole assembly process by controlling the volume of ethanol to water in GO suspension. They reported H_2/CO_2 separation factor of 20.9 but the hydrogen permeance was low.

Other synthesis methods were cited in literature for GO membranes, but these membranes were not tested for gas separation applications. Drop-casting method is not suitable for large-area homogeneous membrane formation. The deposition of GO membranes by this technique is affected by the upward driving force associated with vaporizing the liquid which result in a heterogeneous GO layer with loop structures (Tsou et al., 2015). They also found that the microstructure of pressure and vacuum filtration greatly varies. XRD results indicated that the GO layer d-spacing varied from 8.3 Å to 9.7 Å for pressure and vacuum filtration methods respectively. The GO XRD peak shifts to a larger angle when the applied pressure during pressurized filtration increases from 2 to 5 bar and then slightly decreases when further increasing pressure to 20 bar, indicating an evolution of the packing density as a function of the preparation process(Tang et al., 2014).

GO membranes have been synthesized on different types of substrates. The highest quality GO membranes were made on anodic aluminum oxide substrates (AAO) (Chi et al., 2016; Li et al., 2013). These substrates are fragile and very difficult to scale up. Jin and co-workers (2017; 2016) made GO membranes on α- alumina substrates, these substrates are mechanically strong but still difficult to scale up and relatively expensive. GO membranes were fabricated on polymer substrates for liquid applications such as polyacrylonitrile (Zhao et al., 2015), and cellulose acetate(Hung et al., 2014) for ethanol dehydration, and polysulfone (Hu &Mi, 2013) and nylon (Akbari et al., 2016) for water purification. However, very limited studies were reported for GO membranes on polymer substrates for gas separation such as polyethersulfone (Kim et al., 2013) and cellulose acetate (Athanasekou et al., 2017). Moreover, Romanos (2015) showed that there is a correlation between the gas separation capacity of the GO membranes and the pore size of the used support. As shown in Table 1.1, the anodic aluminum oxide substrates showing excellent separation characteristics for H_2 is 20 nm in pore diameter. However, this issue of the pore size of the support remains an unexamined topic in the field of GO membranes development.

1.4.5 Gas Transport

The early work reported by Geim and coworkers (2012) and presented in Figure 1.3 demonstrated that ~ 1 μm thick GO membranes are completely impermeable to liquids, vapors and gases including helium. On the contrary, these membranes allow unimpeded permeation of water and are therefore appropriate for water desalination with pressure driven or forward osmosis processes. They explained this phenomenon as follows: a GO sheet is composed of two types of regions: oxidized and pristine graphitic regions. The

oxidized regions act as spacers to keep adjacent GO sheets apart and help water molecules to intercalate between GO sheets. The pristine graphitic regions in GO sheets form a network of capillaries, that open up when GO membrane is immersed in water (d~ 13 Å) and allow nearly frictionless flow of a water, similar to the case of water transport through carbon nanotubes (Nair et al., 2012). The nanocapillaries can block all solutes with hydrated radii larger than 4.5Å (Joshi et al., 2014), which indicates that the interlayer spacing play a significant role in molecular transport in aqueous phase applications. For gas permeation, different transport models were proposed, and these models are not consistent and negate each other.

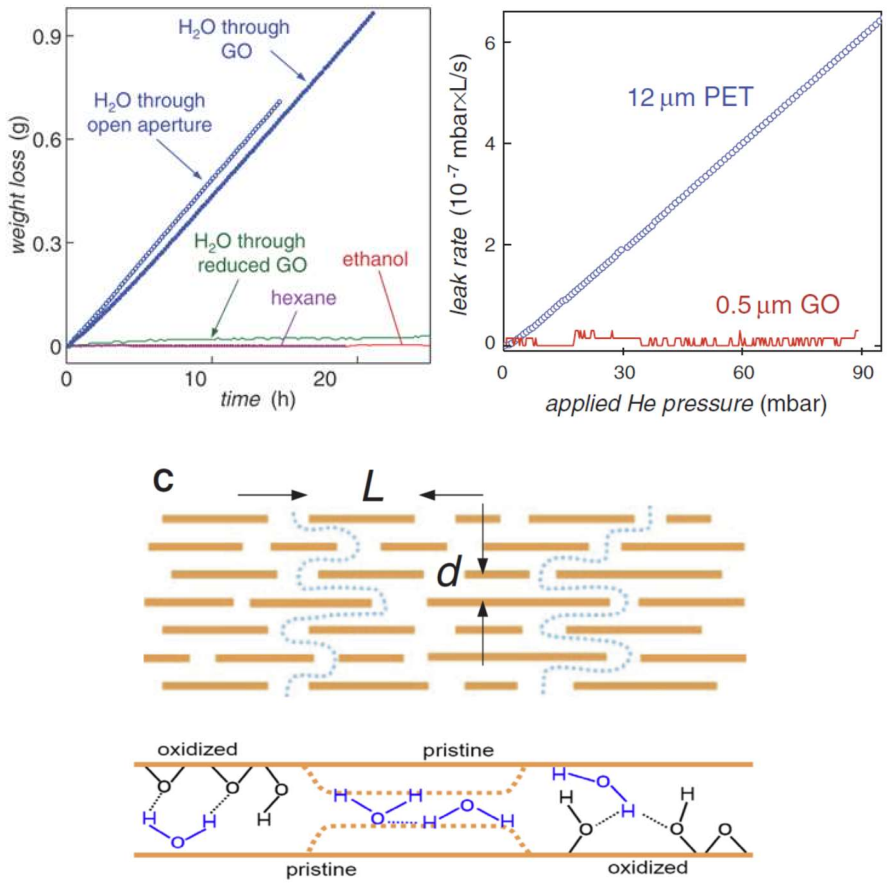

Figure 1.3 GO membrane characteristics and transport mechanism as reported by Geim and coworkers (2012)

For gas applications, in the dry state, with a typical interlayer spacing (d ~9±1 Å), and taking into account that the d-spacing for pristine graphite is about 4 Å, the empty space's width (pore size) can be estimated as 5 ± 1 Å (Nair et al., 2012). In general, the gas transport through such an opening can be explained by the Knudsen transport of gases in nanoporous membranes (Kim et al., 2013). Knudsen diffusion leads to separation of gases with large differences in their molecular weights. Membranes made by contacting the polyethersufone substrate surface to the GO suspension followed by spin coating showed typical H_2, He, CH_4, N_2, and O_2 permeation behavior explained by Knudsen transport in nanoporous membranes (Kim et al., 2013) as shown in Figure 1.4. Also, Spray coated GO membranes showed Knudsen diffusion characteristics for H_2, CH_4, N_2, and O_2 (Guan et al., 2017). The high selectivity for hydrogen through GO membranes reported by Jin's group (2016) (H_2/CO_2:29 and H_2/C_3H_8:260) was attributed to achieving small interlayer spacing of 0.4 nm between stacked GO sheets. Moreover, Geim's group (2014) showed that the chemical reduction of GO laminates with the aid of hydroiodic or ascorbic acids can lead membranes as thin as 30 nm to be highly impermeable to hydrogen and moisture. Both the little structural damage during reduction and the highly decreased interlayer spacing (d=3.6Å) contributes to the exceptional barrier properties.

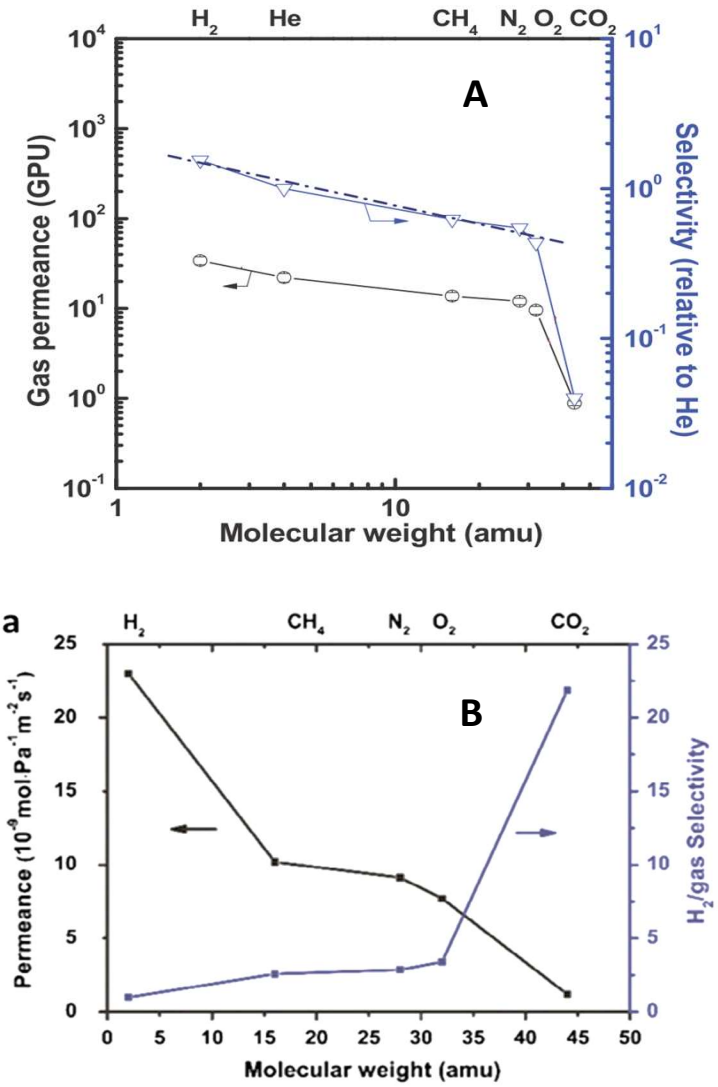

Figure 1.4 Pure gas permeation results showing dominant flow of gasses through interlayer spacing with Knudsen transport characteristics except for CO_2 adapted from : A (Kim et al., 2013), B (Guan et al., 2017).

The results reviewed above confirm the importance of the interlayer spacing in gas transport of GO membranes. However, other research groups suggested that other transport pathways exist and may be dominant over transport through interlayer spacing. Based on XRD characterization and pure gas permeation data for self-standing ~20 μm thick GO

membranes prepared at different filtration rates, Romanos and coworkers (2015) suggested that the gas permeates through interconnected gaps which are located between the deposited GO stacks which is dominant over transport through the interlayer space. The formation of stacks is very liable especially due to concentration polarization in the dead-end filtration system and their concentrated GO suspension (1.5 mg/ml).

As presented above in Figure 1.4, GO membrane by Jin's and Park's groups (2017; 2013) showed Knudsen transport characteristics for H_2, CH_4, N_2, and O_2 while CO_2 was significantly lower and thus high H_2/CO_2 selectivity was achieved. They suggested that the nanopores created by the edges of non-interlocked GO sheets act as traps for CO_2. The polar groups, such as –COOH and –OH, on GO sheets' edges could provide a preferential site for CO_2 adsorption. The adsorbed CO_2 molecules begin to act as barriers to hinder further penetration of CO_2 molecules through the boundaries between nanosheets. Park's group (2013) also found that direct spin-casting of GO solution on the surface of the substrate generates a more compact and uniform, lower permeability GO membranes that show gas molecular sieving characteristics for H_2, He, N_2, and O_2 while the permeance for CO_2 was significantly promoted. These suggest that the in-plane edge to edge spacing became smaller to achieve molecular sieving of permeating gases and the adsorption phenomena of CO_2 at these edges are responsible for its higher permeance. These membranes showed good CO_2/N_2 selectivity (~20) that further increases with increasing the humidity percentage in the gas feed.

The permeance of pure gasses through ultrathin GO membranes prepared by Yu and coworkers (2013) decreases with increasing molecular weight of the permeating gas as presented in Figure 1.5. Gas order follows $H_2 > He \gg CH_4 > N_2 > CO_2$. The ideal selectivity

for hydrogen over N_2 and CO_2 is much higher than the corresponding Knudsen values. The gas permeance of a18 nm GO membrane did not show obvious change after narrowing the spacing between the stacked GO sheets through membrane reduction. Additionally, their adsorption isotherms on GO powder showed much stronger CO_2 adsorption than H_2. Therefore, they suggested that the major transport pathway for gas molecules is selective structural defects within GO sheets, instead of free spacing between stacked GO sheets. Zhao and coworkers (2016) adopted the same gas transport model to explain the molecular sieving behavior of their GO membranes for gas permeation results with the obtained gas permeance in the order He > $H_2 \gg CH_4 > CO_2 > N_2 \gg SF_6$,(Figure 1.5). However, the membranes prepared by filtration give higher permeance and lower selectivity compared to those made by spin coating. They attributed this degradation in the membrane performance to the formation of extrinsic wrinkles in the assembled GO membrane. This model, while suggesting that adsorption property does not have any effect on the permeation of pure gases and gas mixtures through the membrane, does not answer the question why the large CH_4 (3.8 Å) has permeance higher than smaller CO_2 (3.3 Å) and N_2 (3.6 Å)(Chi et al., 2016; Li et al., 2013) or why N_2 permeance is higher than that of CO_2 (Li et al., 2013).

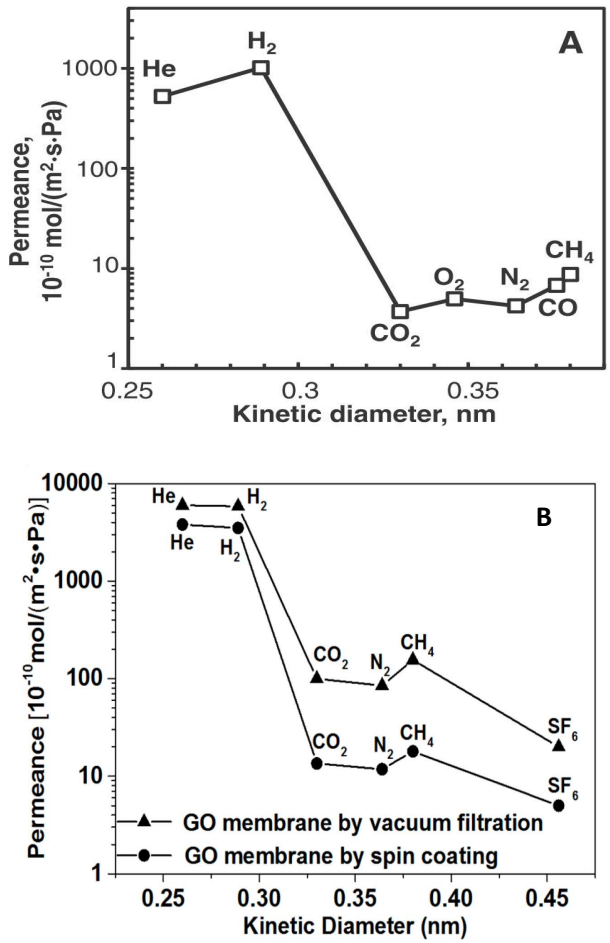

Figure 1.5 Pure gas permeation results through GO membranes prepared by Yu's group(A) and Zhao's group (B) (Chi et al., 2016; Li et al., 2013) .

GO membranes also showed different behavior upon changing the permeation temperature. H_2/CO_2 separation selectivity decreased with increasing temperature, resulting from the faster increase of CO_2 permeance than that of H_2. H_2/CO_2 selectivity decreases from 3400 at room temperature to 150 at 100 ^oC for the 9-nm thick membrane(Li et al., 2013). Zhao's group (2016) also reported a decrease in H_2/CO_2 separation selectivity from 240 at room temperature to 47 at a higher temperature of 120 °C (Figure 1.6). These

results suggested a more activated CO_2 diffusion than that of H_2 through GO membranes, resulting from the tight fit of CO_2 molecules in these GO sheet defects(Li et al., 2013).

Park's densely packed GO membranes (2013) showed a different behavior as a function of temperature as given in Figure 1.6. CO_2 permeance decreases rapidly at 50 °C and the membrane became H_2 selective. CO_2 permeance keeps decreasing slightly up to 150 °C and then start to increase with temperature. Below 130°C, H_2 permeance increased gradually. At ~130° to 140°C, H_2 permeance increased abruptly resulting in high H_2/CO_2 selectivity. These results suggested that thermal annealing made the microstructures of the GO active layers more porous due to irreversible pore formation. Without such structural deformation, the slope of gas permeance versus temperature should be linearly positive (for H_2) or negative (for CO_2) under thermally activated diffusion conditions. However, two distinct slopes were observed, presenting evidence of a more open porous structure.

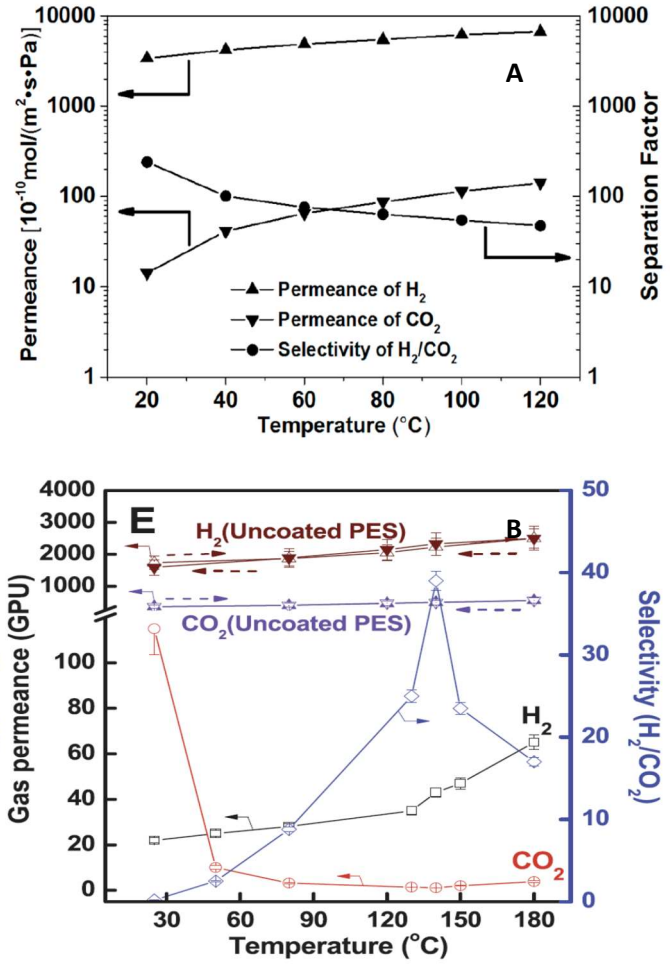

Figure 1.6 Effect of temperature on H_2/CO_2 gas permeation and separation of GO membranes prepared by Zhao's group (A) and Park's group (B):(Chi et al., 2016; Kim et al., 2013)

1.5 Research Objectives and Significance

As reviewed in this chapter, GO membranes have attractive gas separation characteristics showing potential for industrial applications however, several challenges remain unsolved. It appears that synthesis method, substrate structure and characteristics of GO sheets affect the permeability and separation characteristics of these membranes. The gas transport mechanism for GO membranes is still unclear due to inconsistent

permeation and separation results reported in literature. Also, the effect of GO sheet size on the permeability and separation characteristics of these membranes is confusing. In order to meet the requirements for industrial applications GO membrane synthesis method should be simple and suitable for large area cost-effective substrates, while the examined GO membranes were prepared on substrates and/or by synthesis methods that are difficult to scale up. Also, the formation of extrinsic wrinkles in GO membranes prepared by filtration seems to lower their separation performance and has to be controlled through membrane synthesis method and synthesis conditions. To be more significant in membrane industry, the performance of GO membranes must be further improved. One approach to enhance the membrane separation quality is to produce GO membranes with controlled narrow interlayer galleries which is still a challenge. The general objective of this dissertation is to present a systematic study into the synthesis, characterization, and gas permeation properties of GO membranes prepared by different deposition methods on polyester polymer substrates. Results will shed more light on their gas transport and separation mechanism. Different synthesis methods will be compared to find out the optimum conditions for the synthesis of GO membranes with enhanced separation performance. Such data are important to applying these membranes in industrial processes such as hydrogen recovery and CO_2 capture.

The first objective in this study is to provide rich understanding of the gas permeation and separation characteristics of GO membranes and clarify their transport mechanism. To address this objective, different from previous GO membrane studies, we used large size GO sheets to provide better order of stacked GO sheets and obtain reliable gas permeation results that will help elucidate the permeation mechanism of these membranes. Single gas

permeation experiments were conducted on membranes prepared from large GO sheets of different sizes (33 and 17 μm) using vacuum filtration. Single gas permeation and binary H_2/CO_2 mixture separation experiments were conducted both at room temperature and as a function of permeation temperature to understand the transport behavior of these membranes.

The second objective of this work is to prepare GO membranes on the scalable polyester substrate using a scalable deposition technique such as spray coating while controlling the formation of extrinsic wrinkles. GO membranes made by filtration, the most common method for GO membrane synthesis usually suffer from extrinsic wrinkles that affect their gas permeation and separation characteristics. The GO sheets' edge to edge interactions play a dominant role in determining the formation of extrinsic wrinkles. Due to the intimate interplay between GO membrane wrinkles and their gas permeation properties. Fabrication of membranes with less extrinsic wrinkles on the GO membrane is therefore important. In this regard, we focused on minimizing GO sheet's edge-to-edge interactions using GO suspensions of large size (33μm) and dilute concentrations and thus spray coating deposition technique is expected to spread the sheets on the substrate with large edge- to-edge distances and sheets' interactions will be minimized. Results will potentially offer a cost-effective and efficient approach for membrane synthesis for industrial applications.

The third objective of this contribution is to produce GO membranes with narrow interlayer spacing height to improve the molecular sieving characteristics of GO membranes. As discussed in this chapter, GO membrane studies showed that the interlayer galleries, as a prominent characteristic of GO laminates play an important role in selective

gas transport in addition to the flow through GO sheet defects. The defect size and concentration on GO sheets depend on the GO synthesis conditions, and thus it will be difficult to control. Therefore, producing GO membranes with enhanced molecular sieving property requires decreasing the interlayer spacing height to add more restriction to the flow of large gas molecules, which remains a great challenge. To fulfill this objective, GO sheets with small interlayer spacing was prepared using a modification of Brodie's method. Pressure filtration system was also used to enhance the packing density of stacked GO sheets. Permeation of pure gases and separation of equimolar (H_2/CO_2) mixture experiments were conducted and correlated with XRD and SEM characteristics of the membranes.

1.6 Dissertation Structure

This dissertation is divided into five chapters. Chapter 1 aims to provide sufficient background about the principles and fundamental separation mechanisms of membrane gas separation and review the efforts and studies for preparing GO membranes for gas separation applications. The following chapters in this dissertation will serve to accomplish the objectives mentioned above. Chapter 2 addresses objective 1 to study gas permeation and separation characteristics of GO membranes and shed light on their transport mechanism. Chapter 3 addresses objective 2 by introducing spray coating techniques as a simple, scalable approach for membrane synthesis in large area applications. Objective 3 is fulfilled by Chapter 4 where a detailed study on the characteristics of Brodie's derived GO membranes with narrow interlayer spacing height is provided. Chapter 5 summarizes all the work presented in this dissertation with general conclusions and recommendations for future development of GO membranes for gas separation.

CHAPTER 2

GAS PERMEATION AND SEPARATION PROPERTIES OF LARGE-SHEET STACKED GRAPHENE OXIDE MEMBRANES

2.1 Introduction

Graphene is the name given to a single layer of sp^2-bonded carbon atoms arranged in a honeycomb lattice (Novoselov et al., 2004). Among various graphene derivatives, graphene oxide (GO) nanosheets offer an encouraging opportunity to assemble ultrathin, high- flux and energy-efficient molecular sieving membranes (Huang et al., 2014b). Since the pioneering work of Geim and coworkers (2012), there has been a growing interest in the synthesis of graphene oxide membranes for water purification, desalination (Hegab &Zou, 2015) and gas separation applications (Huang et al., 2015). However, the number of reports of GO membranes focusing on gas separation is still very limited. Table 1.2 (Chapter 1) highlights studies on GO membranes with interesting gas transport and separation characteristics specially for hydrogen separation.

Synthesis of GO membranes has been accomplished by filtration and film coating techniques such as dip coating spin coating, and spray-coating (Huang et al., 2014b). Filtration is the most commonly used method to prepare stacked GO membranes with a good control over membrane thickness (Li et al., 2013). However, the GO membranes listed in Table 1.2 show very different gas permeability and separation characteristics among themselves. It appears that synthesis method, substrate structure and characteristics of GO sheets (size or defects) affect the permeability and separation characteristics of these membranes. Yu and coworkers (2013) found that the permeance of small gasses such as H_2 and He decreases exponentially as the membrane thickness increases from 1.8 to 180

nm, which could explain why the ~1 μm thick GO membrane prepared by Geim and coworkers (2012) was impermeable to He. The application of a transmembrane pressure can help overcome the energy barriers of molecules entering and diffusing within GO nanochannels and could enhance the gas permeability of GO membranes (Kim et al., 2013). Gases could permeate through even thick GO membranes at elevated transmembrane pressure (Kim et al., 2013; Romanos et al., 2015). Moreover, the gas transport mechanism through GO membranes is still not clear and proposed models contradict each other.

Park and coworkers (2013) used two methods to prepare very thin GO membranes (3 to 10 nm) on microporous polyethersulfone substrates. They found that contacting the substrate surface to the GO suspension followed by spinning produces relatively heterogeneous GO membranes that show Knudsen transport characteristics for all pure gases except for CO_2 with a significantly retarded permeability. They also found that direct spin-casting a GO solution on the surface of the substrate generates a more compact and uniform, lower permeability GO membranes that show gas molecular sieving characteristics except for CO_2 with significantly promoted permeance. They suggested that gas permeation occur through nanopores created by the edges of non-interlocked GO sheets, where the polar groups, such as –COOH and –OH, on GO sheets could provide a preferential site for CO_2 adsorption. These results indicate that molecular separation performance of a GO membrane depends on the stacking mode of GO sheets. The GO membranes reported by Jin and coworkers (2017) show gas transport behavior similar to those prepared by the GO suspension coating method of Park's group. The permeation experiments conducted by both Jin's and Park's groups were done with transmembrane pressure of 1 bar.

The permeance of pure gasses through ultrathin GO membranes prepared by Yu and coworkers (2013) decreases with increasing molecular weight of the permeating gas. However, the ideal selectivity for hydrogen over N_2 and CO_2 is much higher than the corresponding Knudsen values (the ratio of squared root of molecular weight of diffusing gas species). The gas permeance of a 18 nm GO membrane did not show obvious change after narrowing the spacing between the stacked GO sheets through membrane reduction. Additionally, their adsorption isotherms on GO powder showed much stronger CO_2 adsorption than H_2. Therefore, they suggested that the major transport pathway for gas molecules is selective structural defects within GO sheets, instead of free spacing between stacked GO sheets. Zhao and coworkers (2016) adopted the same gas transport model to explain the molecular sieving behavior of their GO membranes for gas permeation results.

The GO sheets used in the studies listed in Table 1.2 were mostly of small lateral dimensions because they were prepared from exfoliation of GO powder by sonication in water. This sonication method usually results in fragmentation of GO nanosheets into smaller pieces with a wide distribution of sheet sizes (Ogino et al., 2014). GO powders from commercial resources were prepared by a mild freeze thaw exfoliation method producing large GO nanosheets (13 μm) for membrane synthesis (Chi et al., 2016). These GO membranes generally show high quality and high permeability. Their gas permeability tests were conducted without applying a transmembrane pressure, and adsorption of all gases was almost the same. This suggests that increasing the average size of GO sheets may lead to increased gas permeability of the GO membrane. Also, GO membranes assembled from stacked large GO sheets may provide a structure with improved order and lead to more reliable understanding of the gas permeation and separation of these

membranes. Moreover, membrane synthesis with different sheet size fractions could shed more light on their transport mechanism. GO membranes made by sheet sizes ~2 μm show less permeance, but with same mixture H_2/CO_2 separation factor, compared to the GO membranes made by sheet size of 1 μm (Guan et al., 2017). The gas permeance decreases and ideal selectivity increases with increasing GO sheet size from 300 to 1000 nm for 4~6 μm thick GO membranes made by filtration on anodic alumina substrate (Kim et al., 2013). These limited studies show that the effect of GO sheet size on the permeability and selectivity of GO membranes is not clear.

In this chapter, we investigated the permeability and separation characteristics of GO membranes made from large GO sheets of two different sizes (average sizes of 33 and 17 μm) on polyester track etch substrates by vacuum filtration method. Single and binary gas permeation/separation experiments for these GO membranes were studied. The objective of the work is to provide improved understanding of the gas permeation and separation characteristics of GO membranes and to shed more light on their gas transport mechanism.

2.2 Experimental

2.2.1 Synthesis and Characterization of GO Sheets and Membranes

The Hummers' method (Hummers &Offeman, 1958) with some modifications for full conversion of the graphite to GO sheets was applied for the synthesis of GO sheets. Typically, 100 ml of concentrated sulfuric acid (H_2SO_4, EMD Millipore, SX1244, 95.0-98.0%) was charged into a flask equipped with a Teflon mechanical stirrer. The flask was cooled down to 0 °C using an ice bath. 2 g graphite flakes (Sigma-Aldrich, SKU: 332461, ~150 μm flakes) were added to the flask under stirring followed by 1g sodium nitrate ($NaNO_3$, Alfa Aesar, ACS, 99.0%). 5 min later, 12 g of potassium permanganate ($KMnO_4$,

Alfa Aesar, ACS, 99.0%) was slowly added in small doses to the mixture under stirring in a period of 10 min so that the temperature did not exceed 5 °C to prevent strong reaction at local points. The whole mixture was then stirred for 30 min, and the suspension changed in color from black to dark green. Then the ice bath was replaced by tap water bath and the GO suspension was heated to 40 ^{o}C and kept at that temperature for 5 hr while stirring. The dark green suspension gradually became a grey viscous fluid and finally turned into dark brown. After that, 100 ml of deionized water was slowly added to the flask in 10 min, and as result of the hydration heat the temperature increased to 98°C. The mixture was further stirred at this temperature for 15 min with no external heat and subsequently diluted with 300 ml of deionized water and 6 ml of hydrogen peroxide (H_2O_2, Sigma Aldrich, 35 wt. %) to reduce residual permanganate to soluble manganese ions, the color of the solution changes from dark brown to yellow.

The resulting solid material was separated from the solution by centrifugation at a speed of 6000 rpm and washed 2 x 200 ml 10% HCl solution to remove metal ions and then 5 x 200 ml deionized water to remove the remnant acid. Centrifugation was used to collect the solids. Finally, the GO powder was washed with ethanol and later dried under vacuum at room temperature for 24 h. To investigate the effect of average GO size on the gas transport behavior, we first prepared GO suspensions of uniformly large GO sheets. Zhang et al. (2015a) demonstrated that a facile exfoliation and then fractionation of GO into uniformly large sheets ($d > 25$ μm) can be carried out by GO sonication and gravity sedimentation in polar organic solvents. Inspired by this finding, in this work the GO suspension at a concentration of 2 mg/ml was prepared using ethanol as the solvent, and ultrasonicated for variable times to achieve exfoliation of the sheets with two different size

ranges using Cole-Parmer ultrasonic cleaner (model 8890-21-USA,70W, 42 kHz). The suspension was sonicated for 30 min and 4 h to produce fractions of GO sheets of large and small sizes, respectively.

Hydrophilic macroporous polyester track etch (PETE) membranes obtained from commercial resources (Sterlitech, SKU: PET0125100) were used as the substrates for coating GO membranes. The substrates are 10 μm in thickness and 25 mm in diameter, contain cylindrical pores with pore diameter of 0.1μm and pore density of $4x10^8$ pore/cm^2. For membrane fabrication, the prepared GO suspensions (2 mg/ml in ethanol) for the two size fractions were further diluted with water to a concentration of 0.002 mg/ml. GO membranes are synthesized in this study by vacuum filtration of 40 ml of the large and small sheet GO suspensions on the PETE substrates. The produced GO membranes were dried in vacuum to remove the residue water before characterization and permeation tests. GO membranes are named as MEM-Fx-y, where x represents L for large sheets and S for small sheets, and y represent the membrane thickness in nm.

GO nanosheets and membranes prepared in this work were characterized by XRD for phase structure and crystallinity (Bruker D8ADVANCE X-ray diffractometer; Cu Kα radiation λ = 1.542 Å at 40 kV and 40 mA, scan step of 0.05°). Scanning electron microscope (SEM, Amray 1910) was used for imaging membrane surface topology and cross-section as well as the lateral dimension of the GO sheets. Bruker Dimension D3000 atomic force microscopy, AFM, was used to image the produced GO sheets in a taping mode. The thermal properties of GO powder were characterized by thermogravimetric analysis (TGA, SDTQ600). Fourier transform infrared (FT-IR, Thermo Nicolet 6700) was used for identifying surface functional groups of GO nanosheets.

Three characterization tools were suggested to obtain more information about the GO sheet defects: transmission electron microscopy (TEM), nitrogen adsorption and Raman spectroscopy. Some efforts were done for direct imaging of GO sheet defects using high resolution transmission electron microscopy. Yu and coworkers (2013) did not find any conclusive evidence of obvious defects on GO flakes using high transmission electron microscopy, although Raman spectrum suggested the existence of defects on GO. Ultrahigh- resolution transmission electron microscopy images of suspended GO sheets, showed that the GO sheet consists of three major regions: defects, graphitic regions and high contrast disordered regions, indicating areas of high oxidation (Erickson et al., 2010). Defects represented an area of 2% of the GO sheet and were usually less than 5 nm^2.

Though direct imaging of the atomic structure of graphene has been achieved extensively using aberration-corrected transmission electron microscopy, it has proven more challenging to apply similar approaches to GO due to the increased amounts of surface contaminants relative to graphene that mask the atomic structure (Dave et al., 2016). Furthermore, these surface contaminants react with the high energy of the electron beam, leading to structural changes that do not represent the intrinsic GO material and could lead to misinterpreted results (Dave et al., 2016). In addition, Methods such as baking in air or vacuum reliably clean graphene for direct observation using microscopy, but none of these methods are effective in cleaning GO. Plitzko and coworkers (2010) showed that partial reduction by baking GO sample at 200 ^oC, was necessary to partially restore conductivity for TEM imaging, however no defects in GO sheets could be found. The rapid degradation of GO sample under electron beam irradiation at 80 kV at room temperature

showed that care must be taken when analyzing GO samples by TEM, and detecting defects or nanopores that are intrinsic to the material is extremely challenging (Dave et al., 2016).

Gas adsorption is of major importance for the characterization of a wide range of porous material. Dekany and coworkers(2006) reported un realistic BET specific surface area (26-43 m^2/g) of freeze-dried GO sheets synthesized by Brodie's method using N_2 adsorption. They suggested that the N_2 molecules cannot penetrate into the interspace of GO powder. Samples for nitrogen adsorption have to be outgassed to reach a well-defined intermediate state by the removal of physiosorbed molecules; and to avoid any drastic change as a result of aging or surface modification. Outgassing is generally performed through the application of vacuum and controlled heating. GO oxide is thermally unstable. Experimental and computational studies show that the oxygen - rich groups, hydroxyl and epoxy, tend to diffuse and cluster gradually on the GO sheet even at low ~50 (Kumar et al., 2014) or moderate temperature ≤ 70 ºC (Zhou &Bongiorno, 2013), forming well-defined graphitic domains and oxidized regions within the sheet. Therefore, to avoid any possible changes in GO structure and to gain information about defects in graphene oxide powder, Raman spectroscopy is an adequate method (Araujo et al., 2012). Raman spectroscopy measurements were performed on a Renishaw InVia Raman microscope with a 488-nm laser for excitation to quantify the defects of GO powder.

2.2.2 Gas Permeation and Separation Experiments

Gas permeation experiments of the prepared GO membranes were conducted on a multicomponent gas permeation/separation system with the schematic shown is Figure A.1. A PETE supported GO membrane was mounted in a stainless-steel membrane cell, with the GO layer facing the feed side, and sealed by silicone O-rings. Pure gases and gas

mixture experiments were performed in the Wicke Kallenbach configuration with atmospheric feed at room temperature, with zero transmembrane pressure difference. The total flow rate of the feed side was controlled using mass flow controllers at 25 ml/min in single gas experiments and 50 ml/min in 50/50 vol.% binary (H_2/CO_2) gas mixtures. The permeate side was swept by 25 ml/min argon. Also, pure and equimolar (H_2/CO_2) mixture permeation experiments were conducted as a function of feed temperature. Permeation temperature was increased from room temperature to 80 ºC so as not affect the GO structure. 30 min were allowed at each temperature before taking samples for composition analysis. Gas permeation data is reported as a mean of three measurements and maximum error of 3%. The composition of the permeate and retentate streams was determined by gas chromatography (Agilent Technologies, 6890 N, Appendix B) The permeance and separation factor are calculated according to equations 2.1 and 2.2.

$$F_i = \frac{Q_p X_i}{A\left(P_f Y_i - P_s X_i\right)} \qquad \text{Equation 2.1}$$

$$S_{ij} = \frac{[X_i/X_j]_{permeate}}{[Y_i/Y_j]_{retentate}} \qquad \text{Equation 2.2}$$

where Q_p is the molar flowrate of the permeate (measured by a bubble flowmeter), A is the membrane area, P_f and P_s is the total pressure in the feed and sweep side (1 atm), X_i and X_j are mole fractions of components i and j in the permeate stream; Y_i and Y_j are mole fractions of components i and j in the retentate stream. The retentate composition is same as the average composition in the feed because the permeation flow was much smaller than the feed flow.

2.3 Results and Discussion

2.3.1 GO Sheets and Membrane Characteristics

XRD patterns for the produced GO powder and the graphite used as a starting material are given in Figure 2.1. The characteristic diffraction peaks of the (002) plane for both graphite and graphene oxide are related to their stacking order. As shown, the graphite has an intensive peak at 2θ of 26.65°, whereas GO has its diffraction peak at 2θ of 10.4°, corresponding to an interlayer distance, d_{002} of 3.34 and 8.5 Å for graphite and GO respectively. The attachment of the oxygen functional groups during the oxidation process increases the distance between graphitic layers depending on the oxidation degree of graphite (Marcano et al., 2010), hence weakening the van der Waals forces and facilitating exfoliation of the GO powder into single sheets.

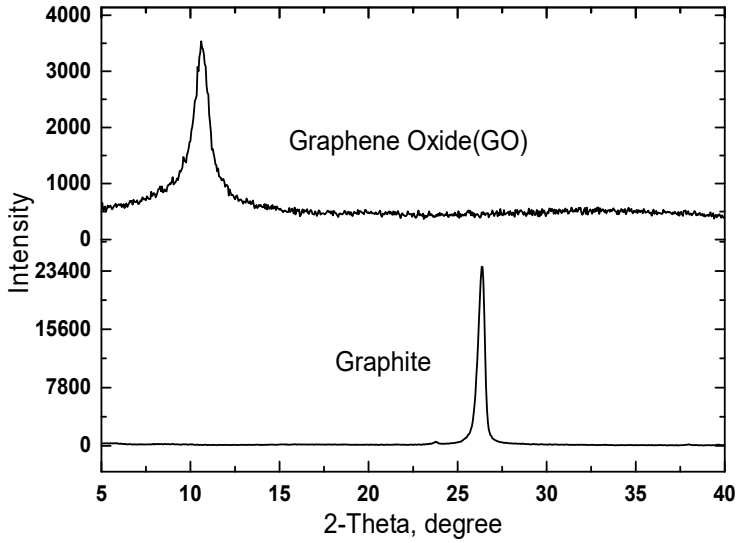

Figure 2.1 XRD patterns of used graphite flakes and produced GO powder.

The FT-IR spectrum for the produced GO powder is given in Figure 2.2. The broad band between 3200 cm^{-1} and 3700 cm^{-1} is attributed to the stretching vibrations of free hydroxyl groups (O-H), due to adsorbed water and structural hydroxyl groups of GO

(Marcano et al., 2010). The band located at 1725 cm^{-1} has been assigned to stretching vibration of carbonyl groups bonded to an aromatic ring or carboxyl groups (C=O) attached to the edges of the GO sheets while the band centered around 1620 cm^{-1} is attributed to the stretching of unoxidized graphitic sp^2 (C=C) bonds (Marcano et al., 2010). Other prominent signals in the GO's spectrum such as those at 1369 cm^{-1}, 1222 cm^{-1}, and 1036 cm^{-1} originate from the (O-H) deformation, the (C-O) epoxy stretching vibration, and the (C-O) alkoxy stretching, respectively (Zhang et al., 2010).

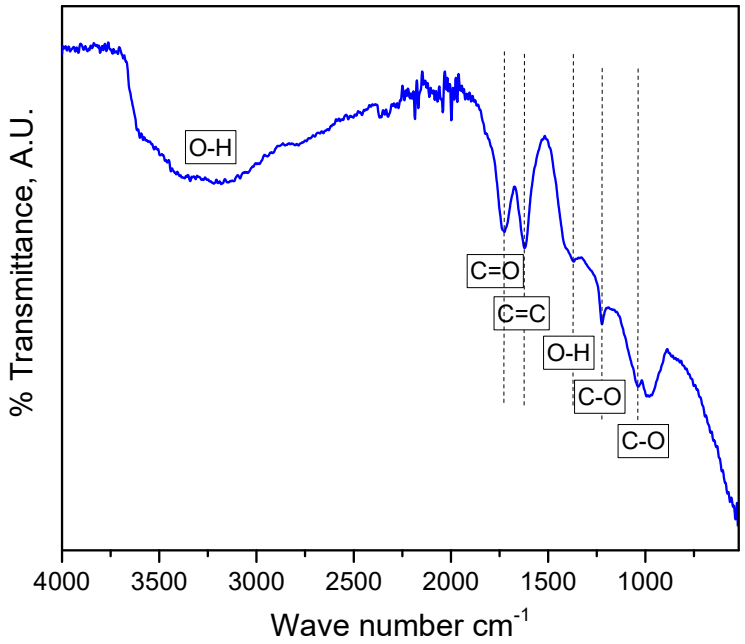

Figure 2.2 FT-IR spectrum of synthesized GO powder.

TGA plot of GO powder in 30 ml/min nitrogen stream upon increasing the temperature from 25 to 1000 ºC is presented in Figure 2.3. The presence of the oxygen functional groups on the basal planes and edges of the sheets makes GO thermally unstable. GO exhibits about 10% weight loss below 150 ºC resulting from the removal of adsorbed water and trapped interlayer water molecules. The notable weight decrease (~30%) between 150 °C and 200 °C is due to decomposition of the less stable oxygen-containing groups to CO_2,

and CO gases and the weight loss with a slower rate at >200 °C is assigned to the removal of more stable oxygen-functional groups (Marcano et al., 2010).

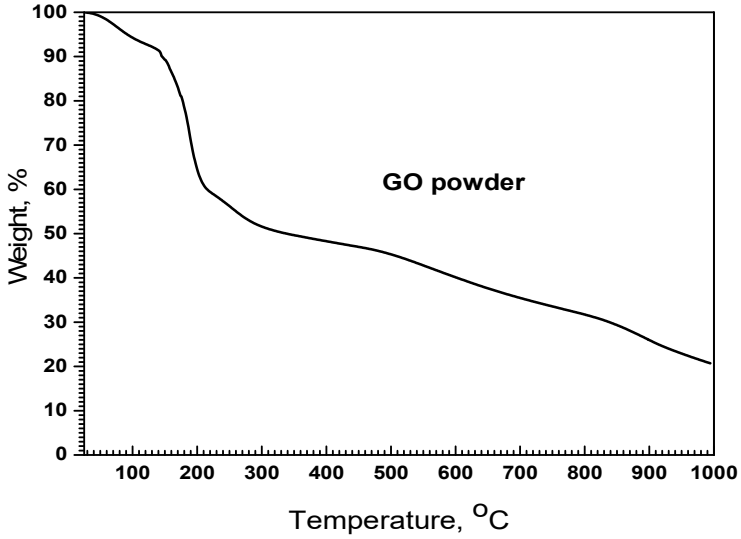

Figure 2.3 TGA plot for produced GO aggregate in nitrogen stream of 30 ml/min at ramping rate of 5 °C/ min.

SEM images of GO sheets used for membrane fabrication as well as the corresponding histograms of the sheet size distributions obtained by measuring the longest lateral dimension of 100 sheets in each sample are indicated in Figure 2.4. Variation of the ultrasonication time of GO powder in ethanol resulted in variation in the GO lateral dimensions. Wrinkles and folds are observed. The large size fraction produced by ultrasonication of GO for 30 min shows an average sheet size of 33 μm and some of the sheets are not fully exfoliated into single sheets. Increasing the sonication time to 4 h resulted in an average sheet size of 17 μm. Figure 2.5-A and B shows AFM height image with section analysis profile of a GO sheet prepared in this work. As shown, the thickness of the produced GO sheet is 0.88 nm, and the thickness at the sheet fold is 1.64 nm which

indicates that the sheets are well exfoliated into single sheets (Marcano et al., 2010). The imaged sheet is about 15x25 µm., falls in the average size range of the large sheets used in this work. Figure 2.5-C shows the phase image of the sheet with consistent composition and no contaminants or large defects. The two different size fractions GO suspensions will help study the effect of sheet size on the single and binary gas permeation through fabricated GO membranes.

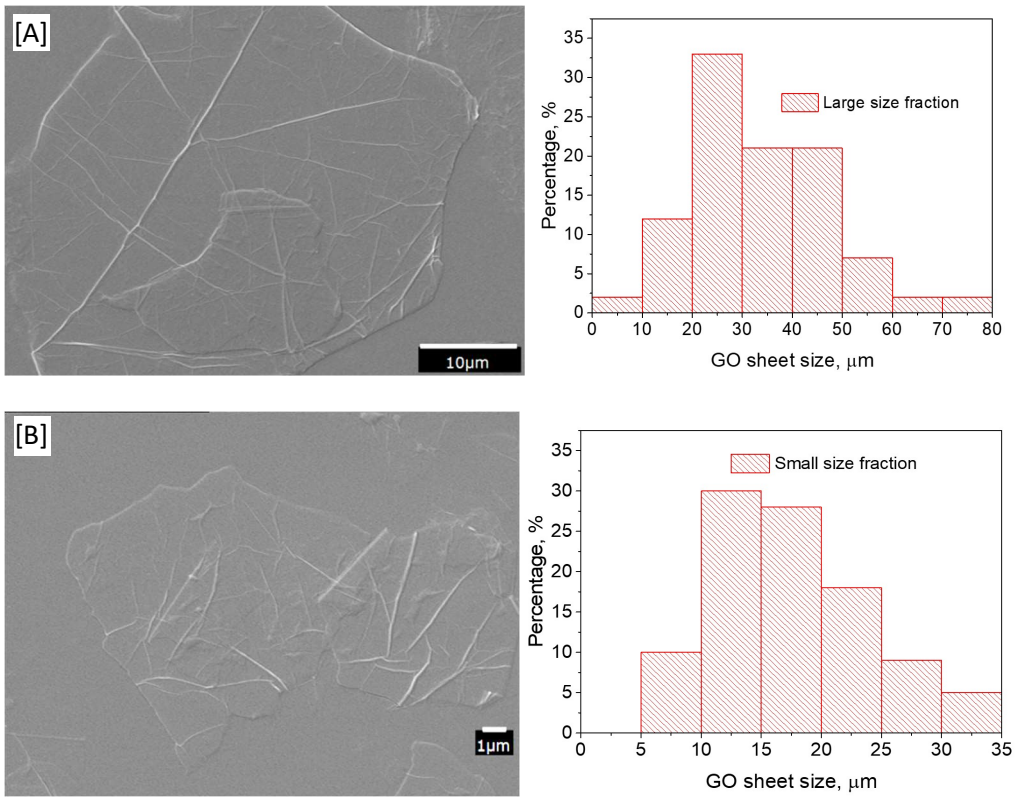

Figure 2.4 SEM images and corresponding histograms of produced GO large, [A] and small, [B] size fractions.

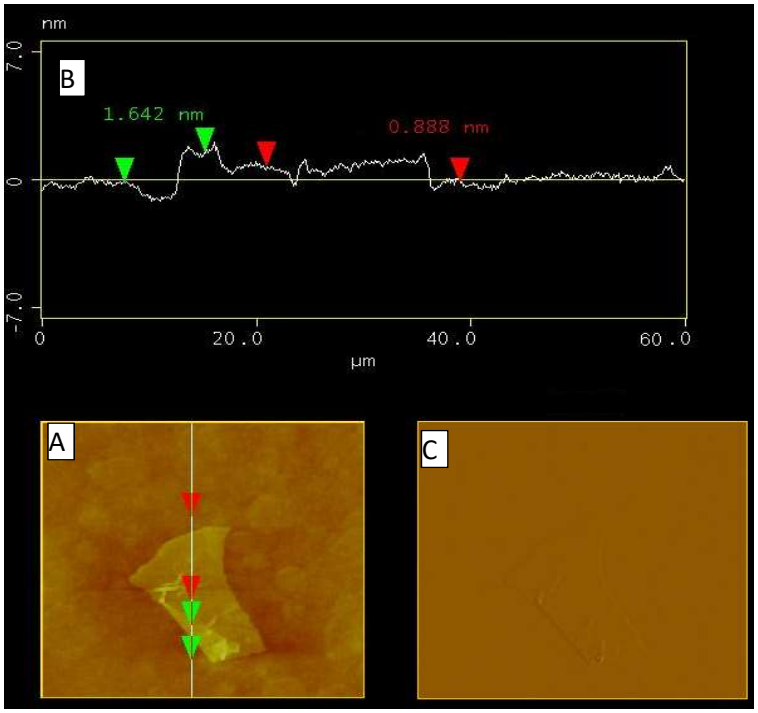

Figure 2.5 60 x 60 µm AFM images GO sheets produced in this study. A and B: height image with section analysis and C: phase image.

The well-known Raman characteristics of carbon materials are the G band at 1580 cm^{-1} and D band 1350 cm^{-1}, which are usually assigned to the graphitized structure and local defects/disorders (Vidano &Fischbach, 1978). Therefore, a smaller peak intensity ratio, (I_D/I_G), can be assigned to lower defects/disorders in the graphitized structure. The Raman spectrum shown in Figure 2.6 displays the G band at 1590 cm^{-1} and the D band at 1355 cm^{-1}. The value of the (I_D/I_G) ratio was also obtained and presented in Figure 2.6. Cançado and coworkers (2011) developed a methodology to correlate the (I_D/I_G) ratio with the distance between point-like defects (L_D) and defect density, n_D on single layer graphene. This dependence of (I_D/I_G) on L_D was be applied to GO and chemical reduced GO (Eigler et al., 2012). According to Cançado and coworkers (2011), it is possible to distinguish between stage 2(L_D<3 nm) and stage 1 (L_D>10 nm) by analyzing Raman

spectra in terms of full width at half maximum (FWHM). This is necessary because an (I_D/I_G) of ratio 0.89 can correlate to a defect distance of 12.3 or 1.4 nm based on equations 2.3 and 2.4(Cançado et al., 2011; Ferrari &Robertson, 2000) weather the material is stage 2 or stage 1(E_L =2.54 eV for the He-Ne (488-nm) laser). The FWHM of the D and G peaks are 196 and 108 cm^{-1} respectively, and thus typical of stage 2 region. For stage 1 a FWHM of about 20 and 14 cm^{-1} would be expected for D and G peaks respectively (Cançado et al., 2011). Based on the distance between two defects, a defect density $n_D(\mu m^{-2}) = 10^8/\pi\, L_D^2$ (Cançado et al., 2011) of 159122 can be calculated.

$$L_D^2(nm^2) = \frac{4.3\ x10^3}{E_L^4}\left(\frac{I_D}{I_G}\right)^{-1} \qquad \text{Equation 2.3}$$

$$L_D^2(nm^2) = 5.4\ x10^{-2} E_L^4\ \left(\frac{I_D}{I_G}\right) \qquad \text{Equation 2.4}$$

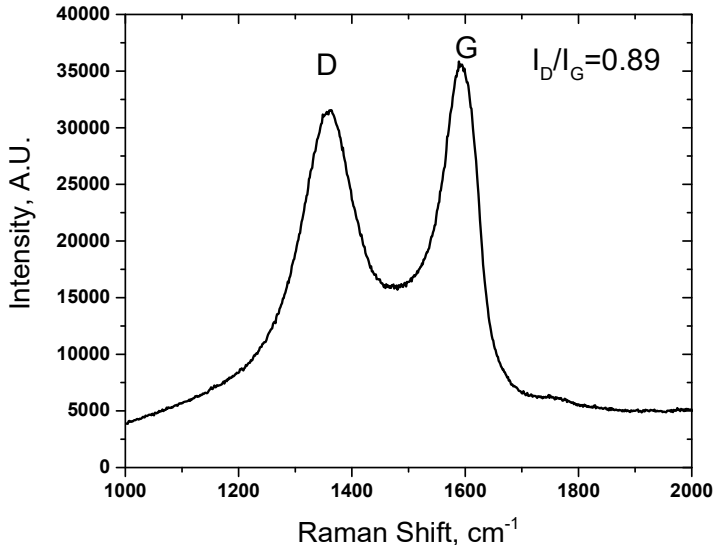

Figure 2.6 Raman spectrum of GO powder produced in this work.

XRD characterization was also carried out to study the stacking behavior of GO membranes. XRD patterns for the membranes MEM-FL200 and MEM-FS200 obtained by vacuum filtration through PETE using GO suspensions of large and small sheet sizes are

given in Figure 2.7. The membranes on PETE sample clearly show one diffraction peak at 2θ of 10.3º and 10.5º for MEM-FL200 and MEM-FS200 respectively. The corresponding interlayer distances using Bragg's law are 8.59 and 8.34 Å. Considering that the electronic clouds around graphene sheets extend over a distance of ~3.34 Å, the above interlayer distances translates into an 'empty' space available for gas molecules to diffuse through of 5.25 and 5.09 Å for membranes MEM-FL200 and MEM-FS200 respectively (Nair et al., 2012).

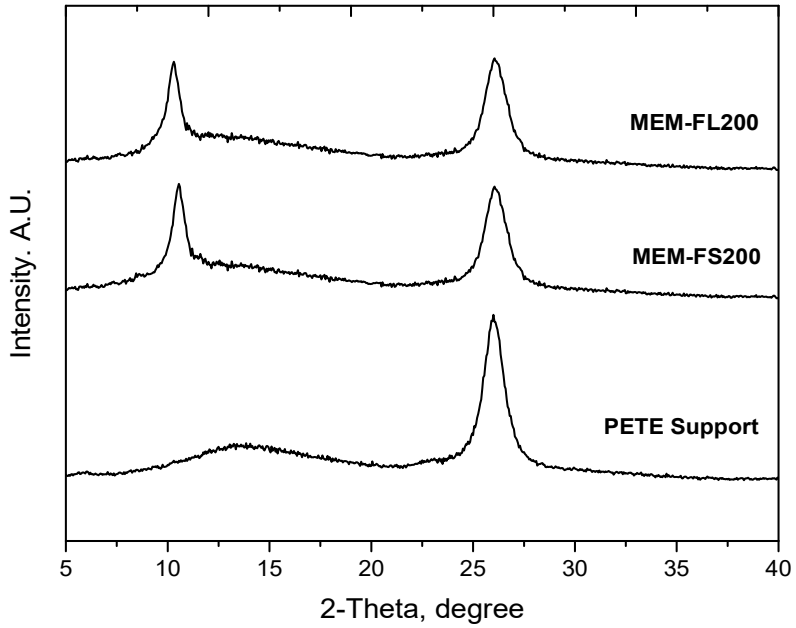

Figure 2.7 XRD spectra of GO membranes MEM-FL200 and MEM-FS200 prepared by vacuum filtration deposition on PETE substrate.

The SEM images of the surface and cross sections of the synthesized GO membranes MEM-FL200 and MEM-FS200 as well as the PETE substrate are given in Figure 2.8. The surface of the substrates is very smooth with 100 nm straight holes, while the surface of the GO membranes is generally corrugated as seen from the low magnification image (Figure 2.8- B) indicating the boundaries of the GO sheets and sheet wrinkles. Zhao and

coworkers (2016) reported similar wrinkles on the surface of GO membranes made by vacuum filtration on AAO substrates. The cross-section images of both membranes show a 200 nm thick GO layer and a good adhesion between the GO film and the PETE substrate.

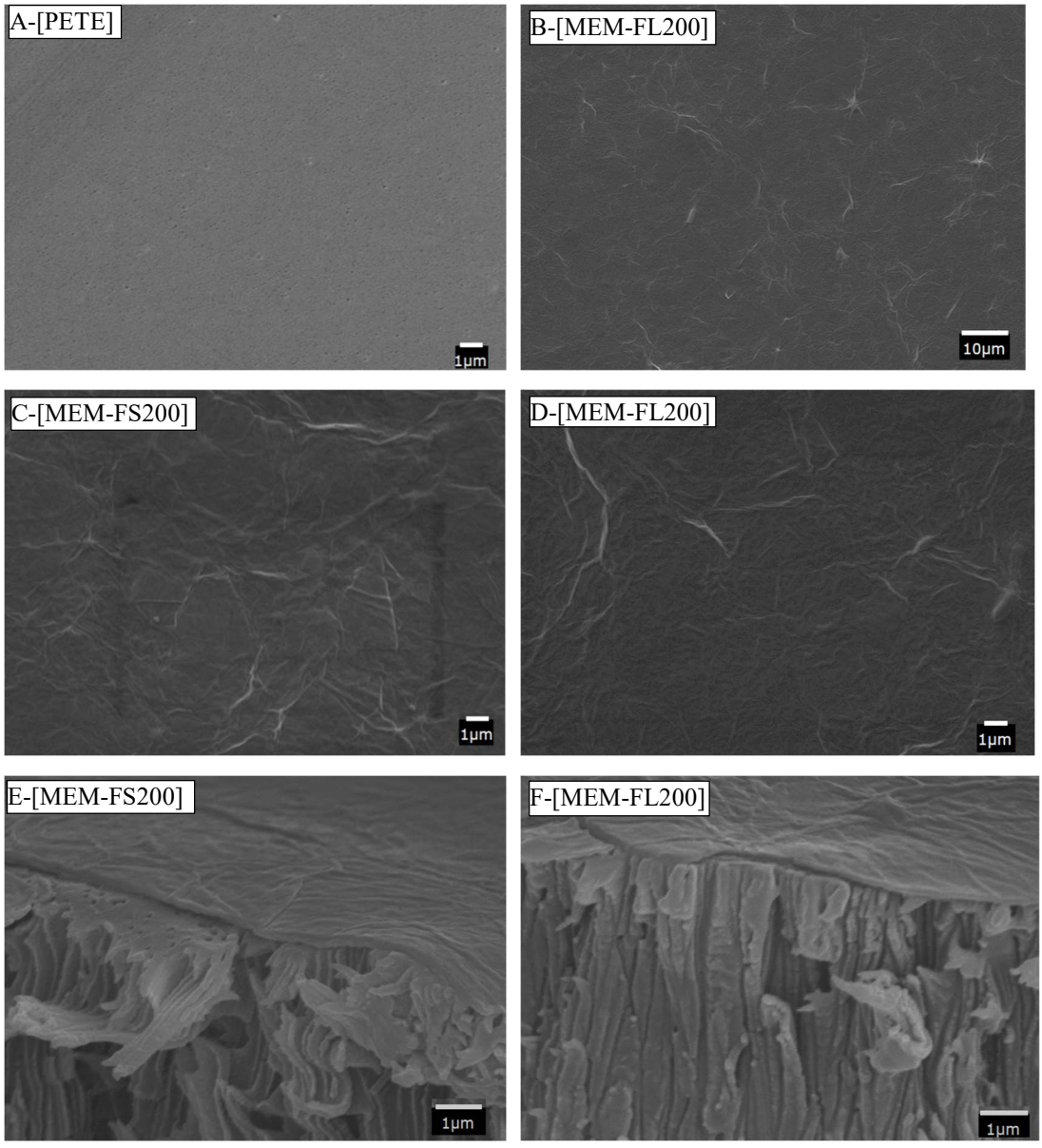

Figure 2.8 SEM images of surface and cross-section of MEM-FL200 and MEM-FS200 GO membranes prepared by vacuum filtration on PETE substrate.

2.3.2 Gas Permeation and Separation Properties.

The permeance of five pure gases, H_2 (kinetic diameter of 2.9Å), He (2.6 Å), CH_4 (3.8Å), N_2 (3.6Å) and CO_2 (3.3Å), through the synthesized membranes is shown in Figure 2.9. Both GO membranes made of either large or small sheets exhibit faster permeance for the smaller gases (He and H_2) but slower permeance of the larger gases (CH_4, N_2, and CO_2). The permeance decreases in the same order as the molecular weight as H_2 > He ≫ CH_4 > N_2 >CO_2. However, for both membranes, the permeance for the three larger molecules CH_4, N_2 and CO_2, can be correlated to the reciprocal of the squared root of molecular weight by straight lines, conforming to the Knudsen diffusion controlled permeation. The permeace for the two smaller molecules, He and H_2, is quite far above the Knudsen straight lines, indicating additional pathway for transport of these two gases. The ratio of the permeance for the small sheet GO membrane to that for the large sheet GO membrane, $F_{MEM\text{-}FS200}/F_{MEM\text{-}FL200}$, is 2.0, 2.5 and 1.8 for CH_4, N_2, and CO_2, respectively, and 1.4 for both H_2 and H_2.

Table 2.1 compares binary mixture H_2 and CO_2 permeance and separation data for the two GO membranes with the pure component data. A control H_2/CO_2 mixture experiment for the PETE support show a H_2/CO_2 separation factor of 3. The GO membranes are perm-selective to H_2 with pure and mixture gas feeds. Figure 2.10 shows permeance and separation factor for MEM-FL200 GO membrane as a function of time. GO membrane exhibits stable operation for at least 36 h, sufficiently long for examining stability of the membrane performance. Gas permeance for H_2 and CO_2 with pure gas and binary mixture feed for MEM-FL200 membrane at different temperatures is presented in Figure 2.11. Permeance for both H_2 and CO_2 increases with temperature, with apparent activation

energy for permeation for H_2 and CO_2 respectively of 3.2 and 8.5 for pure components and 1.6 and 8.1 kJ/mol for the binary mixture. The idea selectivity (pure feed) or separation factor (mixture feed) decreases with increasing temperature due to lower activation energy for H_2.

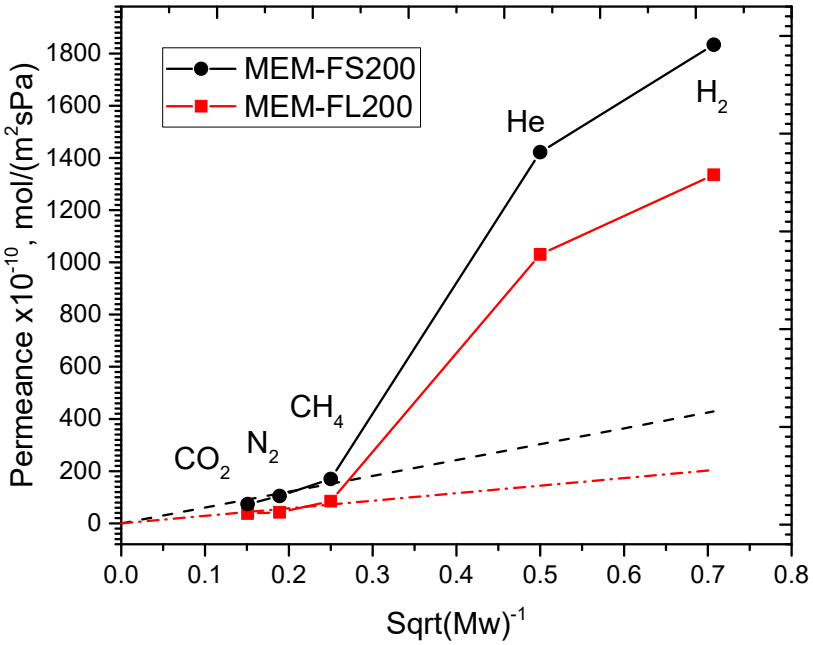

Figure 2.9 Pure gas permeation results through MEM-FS200 and MEM-FL200 GO membranes (dashed straight lines showing Knudsen diffusion dominated permeance)

Table 2.1

Comparison of Ideal Selectivity and Binary Separation Factor of H_2/CO_2 for GO Membranes at Room Temperature

Membrane	Ideal pure gas data			Binary mixture data		
	Permeance (10^{-7}mol/m^2.s.Pa)		Ideal H_2/CO_2 selectivity	Permeance (10^{-7}mol/m^2.s.Pa)		H_2/CO_2 separation factor
	H_2	CO_2		H_2	CO_2	
MEM-FL200	1.33	0.038	35.3	1.14	0.046	22.5
MME-FS200	1.83	0.074	24.7	1.59	0.084	16.6

As shown in Table 2.1 and Figure 2.11, the binary mixture gives slightly (~15%) lower H_2 permeance but increased CO_2 permeance (and hence reduced H_2/CO_2 selectivity) as compared to the pure component data. These separation results are quite different from microporous zeolite membranes which show a reverse selectivity (H_2/CO_2 selectivity less than 1) for mixture feed as compared to ideal selectivity (H_2/CO_2 selectivity larger than 1) for pure gas feed (Kanezashi et al., 2008). Yu's group (2013) reported linear adsorption isotherm (constant slope or solubility) for H_2 and slightly non-linear adsorption isotherm (with slope or solubility decreases with increasing pressure) for CO_2 on GO membranes. As the permeance is proportional to the solubility, for H_2 the permeance is independent of pressure but for CO_2 it may increase slightly with decreasing CO_2 partial pressure. Therefore, the lower H_2/CO_2 selectivity for mixture is due to increased CO_2 permeance at lower CO_2 partial pressure in the mixture. However, the adsorption of CO_2 is not sufficiently strong to block permeation of H_2, which otherwise would cause reverse selectivity in the case of mixture separation.

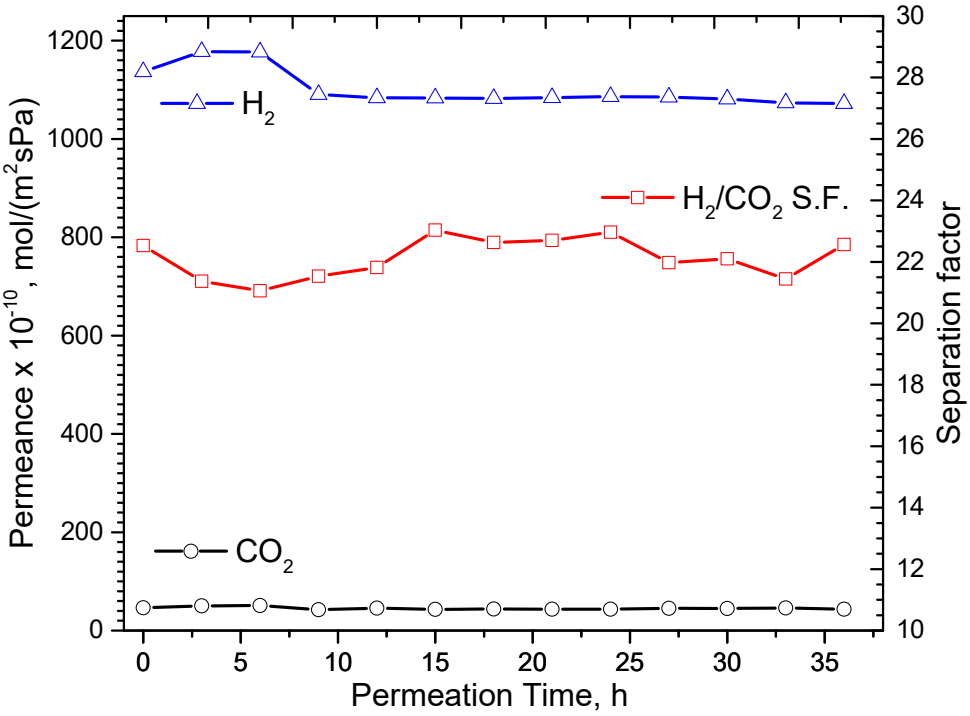

Figure 2.10 MEM-FL200 (200 nm thick) GO membrane performance for H_2/CO_2 equimolar mixture as a function of permeation time

2.3.3 Discussion on Gas Transport Mechanism of GO Membranes

As the prominent characteristic of GO laminates, interlayer spacing has been proven to play a significant role in molecular transport (Nair et al., 2012). For gas permeation, different transport models were proposed, and these models negate each other and cannot be used to explain our results. Jin's and Park's groups (2017; 2013) attributed the high H_2/CO_2 selectivity to the strong CO_2 adsorption specially at the carboxylic acid groups located at the edge of nanosheets, the adsorbed CO_2 molecules begin to act as barriers to hinder further penetration of CO_2 molecules through the boundaries between nanosheets. This contradicts with what is well accepted that in inorganic membranes gas that is adsorbed on the membrane pores usually has more perm-selective due to additional surface flow of the adsorbed molecules. Yu's group and Zhao's group (2016; 2013) attributed the

molecular-sieving separation of H_2 from CO_2 to the selective structural defects within GO flakes. This model, while suggesting that adsorption property does not have any effect on the permeation of pure gases and gas mixtures through the membrane, does not answer the question why the large CH_4 (3.8 Å) has permeance higher than smaller CO_2 (3.3 Å) and N_2 (3.6 Å)(Chi et al., 2016; Li et al., 2013) or why N_2 permeance is higher than that of CO_2 (Li et al., 2013).

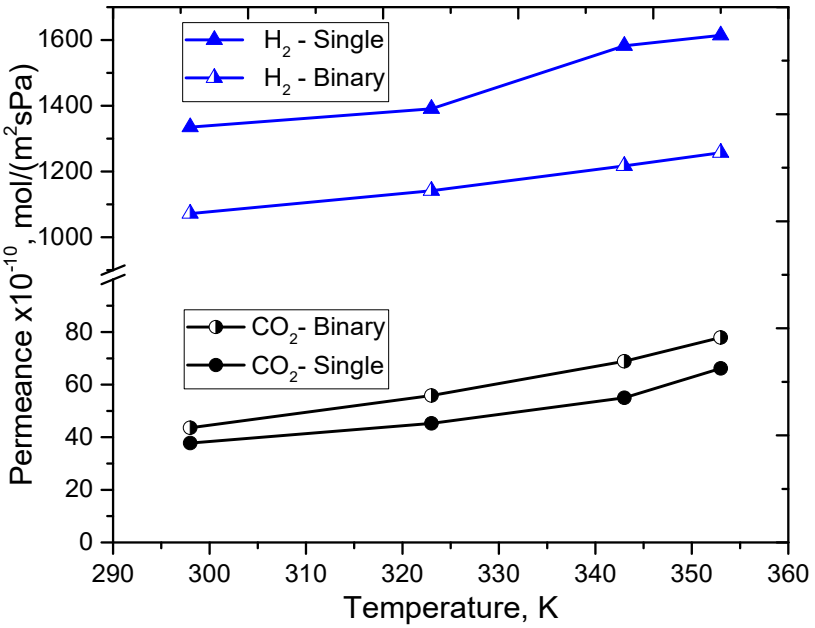

Figure 2.11 Pure and binary gas permeance for H_2 and CO_2 through MEM-FL200 as a function of temperature.

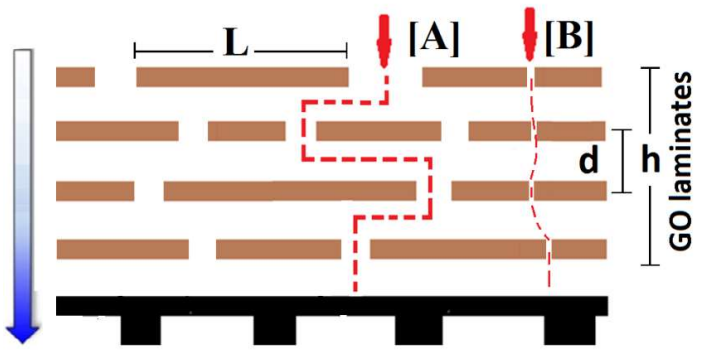

Figure 2.12 Proposed gas transport model through prepared GO membranes

According to the structure characteristics of GO sheets and our gas permeation/ separation results, we propose a 2-pathway transport model for GO membranes prepared in this study as schematically illustrated in Figure 2.12. Inter-sheet pathway A, and inner-sheet defect pathway B. The inter-sheet pathway A is composed primarily of randomly distributed channels formed at membrane wrinkles, lamellae spacing and free interspace height between stacked GO sheets. The inner-sheet pathway constitutes GO sheet structural defects as shown in Figure 2.12 since the tortuosity factor for pathway B is much smaller than the tortuosity for pathway A. Assuming linear adsorption isotherm (or non-adsorption) for all gases, the pure gas permeance can be described by:

$$F = \left(\frac{1}{h}\right)\left[\left(\frac{\varepsilon_A}{\tau_A}\right) D_A K_A + \left(\frac{\varepsilon_B}{\tau_B}\right) D_B K_B\right] \qquad \text{Equation 2.5}$$

where h is the GO membrane thickness, ε and τ are the porosity and tortuosity for pores of pathways A and B; D and K is gas diffusivity and adsorption equilibrium constant (solubility) in the pores of pathways A or B. As shown by Equation 2.6 the gas permeance is determined by the surface properties (affecting the solubility) and pore size (affecting diffusivity) as well as porosity and tortuosity of both pathways, which are controlled by

the synthesis of GO sheets and GO membrane. Compared to high quality microporous crystalline (such as zeolite or metal organic framework) membranes, GO membranes exhibit much more complex transport mechanism shown by Equation 2.5.

The effect of the solubility, K, on gas transport properties, is quite complex, depending on the surface properties of the pores in pathways A and B and properties of permeating molecules. However, at high temperatures, or for inert gas such as He or Ar, the solubility becomes K=1/RT, and its effects become negligible. Diffusion rate is mainly determined by the relative size of the gas to the pore size of the pathway. Gas diffusion through the micropores of pathway A or B can be described by the translational diffusion model(Kanezashi &Lin, 2009; Kanezashi et al., 2008).

$$D = \phi\left(\frac{8R}{\pi\, Mw}\right)^{0.5} \exp\left(\frac{-E_d}{RT}\right) \qquad \text{Equation 2.6}$$

where ϕ is pore channel structure, M_w is gas molecular weight, and E_d is the activation energy for diffusion. E_d is mainly determined by the size ratio (λ) of kinetic diameter of permeating gas, dm, to that of the pore diameter, d_p (λ=dm/dp). E_d is small (close to zero) with λ<0.6 and it increases exponentially with further increasing λ (Kanezashi &Lin, 2009). The porosity ε is difficult to be determined for pathway A and B, as ε_A is related to the inter-sheet structure and surface groups and ε_B to the size and concentration of the inner-sheet defects and alignment of the defects in each sheet with each other. Both ε_A and ε_B depend on synthesis of GO sheets and membranes. Although the defect density determined by Raman is low but the tortuosity for pathway B, τ_B, is extremely small compared to τ_A as one can assume straight gas flow through the defects of the GO sheets,

based on Raman results. The tortuosity for pathway A, τ_A, can be approximated as ratio of the GO sheet length to thickness:

$$\tau_A = \frac{L}{d} \qquad \text{Equation 2.7}$$

Then the large GO sheets would give a larger tortuosity for pathway A and hence, a smaller pathway A flow contribution to the total permeance measured. This model can be used to discuss semi-quantitatively the permeation and separation data obtained in this work.

XRD results for membranes MEM-L1 and MEM-S1 show that the 'empty' inter-space between the GO sheets (pathway A) is 5.25 and 5.09 Å respectively, larger than the kinetic diameter of CH_4 (3.8Å), N_2 (3.6Å) and CO_2 (3.3Å). The size of the defects (pores of pathway B) should be smaller than those for pathway A. With relatively small value for the ratio of the molecular size to the pore size for pathway A, E_d for pathway A for these three molecules is approximately zero. A much larger value for E_d for pathway B is expected for these three molecules due to the smaller pore size for pathway B. Thus, at room temperature, for CH_4, N_2 and CO_2, the first term in Equation 2.5 is significantly larger than the second term. The permeance for these gases is dominated by pathway A flow. Because the E_d is close to zero, the exponential term in eq. 4 is less significant than the pre-exponential term which is related to the molecular weight of the permeating gas and temperature in the same way as Knudsen diffusion. This explains the Knudsen-like diffusion permeation characteristics for these three gases at room temperature. Since pathway A flow dominates gas permeation, the ratio of gas permeance for the small sheet GO membrane to that of the large sheet GO membrane should be approximately equal to the ratio of large GO sheet size (33 μm) to the small one (17μm) (~2 in this study) due to

the difference in the tortuosity in first term in Equation 2.5. The results given in Figure 2.8 indeed show that small to large sheet GO membrane permeance ratio ($F_{MEM\text{-}FS200}/F_{MEM\text{-}FL200}$) in the range of 1.8-2.5 for these three large molecules.

The diffusion activation energy, E_d for the small molecules H_2 and He in pathway B is much smaller than that for the three larger molecules. Therefore, the second term in Equation 2.5 (transport through pathway B) for H_2 and He is significantly large, and at room temperature, both the first term (pathway A flow) and the second term (pathway B flow) contribute to the overall permeance measured. Since pathway B is not of Knudsen-like transport, both H_2 and He exhibit permeance above the Knudsen line shown in Figure 2.9. Because pathway B does not depend on the GO sheet size, the small GO sheet to large GO sheet permeance ratio ($F_{MEM\text{-}FS200}/F_{MEM\text{-}FL200}$) for H_2 and He should be closer to 1, depending on the contribution of the flow from pathway B. Indeed, the ratio is about 1.4 from the data given Figure 9 for these two smaller molecules.

On temperature dependence, the permeance contributed by pathway A may decrease slightly with increasing temperature due to Knudsen-like transport mechanism but that contributed by pathway B increases with increasing temperature. Thus, the temperature dependence of the measured permeance (contributed by both pathways A and B) can be quite complex, depending on the relative size of the permeating molecules, porosity/tortuosity for pathways A and B, temperature range, and heat of adsorption. The activation energy for diffusion for the larger molecule CO_2 in pathway B is larger than that for the smaller molecule H_2. Thus, the flow through pathway B and its contribution to the measured permeance for CO_2 increase more with temperature than that for H_2. This

explains the higher observed activation energy for CO_2 permeance than H_2, and decreasing H_2/CO_2 selectivity with increasing temperature as reported here.

2.4 Conclusions

High quality GO membranes can be deposited on the PETE substrate by vacuum filtration method using suspensions containing GO sheets with average sheet size of 33 and 17 μm. Gas permeation through the GO membranes can be explained by an inter-sheet and inner-sheet two-pathway model proposed here. At room temperature, the large molecules (CH_4, N_2 and CO_2) permeate through inter-sheet pathway of the GO membranes, exhibiting Knudsen-like diffusion characteristics, with the permeance for the small sheet GO membrane about twice that for the large sheet GO membrane. The smaller gases (H_2 and He) exhibit much higher permeance, showing significant flow through the inner-sheet pathway in addition to the flow through inter-sheet pathway. The GO membranes show good H_2/CO_2 selectivity for both pure gas and binary gas feeds, without CO_2 blockage effect for mixture separation found for crystalline microporous membranes. Gas permeation in GO membranes is more complex than in crystalline microporous membrane, with permeance determined by solubility (surface properties), diffusivity (relative molecular size to pore size), porosity and tortuosity of both inter-sheet pores and inner-sheet defect pores. These properties are strongly influenced by the synthesis method and conditions for preparation of GO sheets and membranes, which explain the inconsistent results reported in the literature.

CHAPTER 3

SYNTHESIS OF GRAPHENE OXIDE MEMBRANES ON POLYESTER SUBSTRATE BY SPRAY COATING FOR GAS SEPARATION

3.1 Introduction

Graphene oxide (GO) is a unique material that can be viewed as a single monomolecular layer of graphite with various oxygen containing groups spread on the sheet basal planes and edges (Lerf et al., 1998). Membranes prepared by stacking GO sheets have shown attractive gas separation characteristics specially for hydrogen (Chi et al., 2016; Li et al., 2013), that make them of interest for large-scale industrial applications. Filtration is the most commonly used method to prepare stacked GO membranes with good control over membrane thickness (Huang et al., 2014b). However, extrinsic wrinkles were observed in GO membranes made by filtration (Chi et al., 2016; Dikin et al., 2007; Ibrahim &Lin, 2018; Klechikov et al., 2015; Wei et al., 2016) and the method itself is difficult to scale up for large area membrane production.

Wrinkling is a common phenomenon in 2D films and membranes. Graphene sheets are not perfectly flat and TEM studies showed that graphene is microscopically corrugated (Meyer et al., 2007). Further atomistic simulation show that such ripples with an amplitude of about 1 Å were intrinsic (Fasolino et al., 2007). GO is more susceptible to intrinsic corrugations due thermal fluctuations and stresses during oxidation, attached functional groups (Zheng et al., 2010) and structural defects (Liu et al., 2011). Unlike the atomic or nanometer level wrinkles in monolayer graphene oxide sheets, the undulation seen in GO membranes normally has much higher amplitudes and seems to affect the GO membrane performance. Higher H_2 permeance and lower H_2/CO_2 separation factor (51 vs 240) of GO

membranes made by filtration compared to membranes made by spin coating using the same GO suspension, was attributed to the formation of extrinsic wrinkles in the membranes made by filtration (Chi et al., 2016). Wei et al.,(2016) showed that GO channels under wrinkles are larger than those under the flat area which reduce the resistance to water permeation in GO membranes. They also found that GO wrinkles became narrower and water flux decreases under the influence of hydraulic pressure during filtration.

Some efforts were done to analyze the reasons for the formation of wrinkles in graphene based membranes. Wrinkles were observed in large-area, few-layer graphene grown on a poly-nickel substrate under optimized CVD conditions (Chae et al., 2009). It was proposed that the wrinkles were formed by two processes: i) nucleation of defect lines on step edges between Ni terraces and ii) thermal-stress-induced formation of wrinkles around step edges and defect lines. Wei et al. (2016) showed that the formation of wrinkles on the surface of GO membranes originates with the formation of slender initial wrinkles that gradually grow with the deposition of GO sheets. Initial wrinkles could form due to GO sheet wrinkle, sheet folding or stacking. They also demonstrated that the formation of GO sheet wrinkles originates due to the water accumulating between the substrate and the soft GO sheets. The water drains gradually and a wrinkle is formed when the GO sheet contacts the substrate. Also, Kim and coworkers (2014), showed that GO sheets placed in the edge-to-edge arrangement tend to buckle due to hydrogen bonding between the edges. GO sheet interactions and water accumulation between the substrate and GO sheets cannot be avoided in membrane synthesis by filtration.

Jin and co-workers (2017) used spray coating to fabricate GO membranes on alpha-alumina substrates for gas separation offering promising results for scalable GO membrane

synthesis. Their study focused on the effect of evaporation rate on GO stacking during the whole assembly process by controlling the volume of ethanol to water in GO suspension. Although, alpha-alumina substrates are mechanically strong, they are expensive and difficult to scale up for production of membrane modules with high packing density.

To fully explore the scalability of spray coating method for GO membrane synthesis, GO membranes should be deposited on cost-effective, easily scalable polymer substrates. In this work, we combine GO membrane synthesis using scalable spray coating method on a scalable, planar polymer substrate. Since GO nanosheets can be cheaply produced in a large scale by oxidation and exfoliation of graphite (Sun &Fugetsu, 2013), this obtained results could demonstrate a cost-effective scalable approach for GO membrane synthesis for large area industrial gas separation applications. Furthermore, we expect spray coating method to produce GO membranes with less wrinkles and thus better separation characteristics due to the following reasons. Using dilute concentration GO suspensions in spray coating may decrease GO edge-to-edge interactions since each spray disperses a few number of GO sheets on the substrate at a larger distance between the sheets. Also, the solvent in spray coating evaporates as it reaches the substrate different from the drainage system of the solvent in filtration. The objective of this work is to evaluate the synthesis and gas separation properties of GO membranes by spray coating on scalable polyester track etch (PETE) substrates, compare the structure and properties of these GO membranes with those obtained by the filtration method with focus on analyzing the effect of extrinsic wrinkles on membrane performance.

3.2 Experimental

Modified Hummers' method (1958) was applied for the synthesis of GO sheets as reported in Chapter 2, Section 2.2.1. Typically, 100 ml of concentrated sulfuric acid, (H_2SO_4, EMD Millipore, SX1244, 95.0-98.0%) was charged into a flask equipped with a Teflon mechanical stirrer. The flask was cooled down to 0 °C using an ice bath. 2 g graphite flakes (Sigma-Aldrich, SKU: 332461, ~150 μm flakes) were added to the flask under stirring followed by 1g sodium nitrate ($NaNO_3$, Alfa Aesar, ACS, 99.0%). 5 min later, 12 g of potassium permanganate ($KMnO_4$, Alfa Aesar, ACS, 99.0%) was slowly added in small doses to the mixture under stirring. The whole mixture was then stirred for 30 min then the ice bath was replaced by tap water bath and heat was supplied to keep the temperature at 40 ºC while stirring continued for 5 h. After that, 100 ml of deionized water was slowly added to the flask raising the suspension temperature to 98°C. The mixture was further stirred at this temperature for 15 min with no external heat and subsequently diluted with 300 ml deionized water and 6 ml hydrogen peroxide (H_2O_2, Sigma Aldrich, 35 wt. %). The washed and vacuum dried GO powder was sonicated in ethanol for 30 min to achieve sheet exfoliation and prepare 2 mg/ml GO suspension.

Polyester track etch (PETE) membranes (Sterlitech, SKU: PET0125100) were used as the substrates for coating GO membranes. The substrates containing pores of 0.1μm in pore diameter were 10 μm in thickness and 25 mm in diameter. To investigate the effect of sheet stacking method on the quality of the membrane, GO membranes were synthesized in this study by vacuum filtration and spray coating method. For GO membrane fabrication by filtration, the prepared GO suspension (2 mg/ml in ethanol) was further diluted with water to a concentration of 0.002 mg/ml. A home made vacuum filtration system was used to

deposit the desired volume of GO suspension onto PETE substrate. Details in vacuum filtration synthesis of GO membraens was described elsewhere [6]. For spray coating, GO suspensions of concentrations 1, 0.5 and 0.1 mg/ml were used. Suspension dilution in spray coating was done using 50:50 vol % water-ethanol mixture. The desired amount of GO suspension was vertically sprayed onto PETE substrates using a gravity feed airbrush (Paasche Talon TG-SET/ USA), with a head size of 0.38 mm and assembled with air as a carrier gas, as shown in (Figure 3.1). The inlet pressure of air was regulated at 50 psi and the spraying rate was adjusted to 5 ml/ min. The airbrush tip was placed vertically at 15 cm from the substrate and thus the tiny droplets of the sprayed solution covers the entire cross section of the mounted substrate. Spraying is carried out for ~2 seconds, and time is given for the solvent to evaporate by the air continuously coming out of the airbrush. As spray deposition continues, the coating grows to form a continuous GO film covering the pores of the PETE substrate.

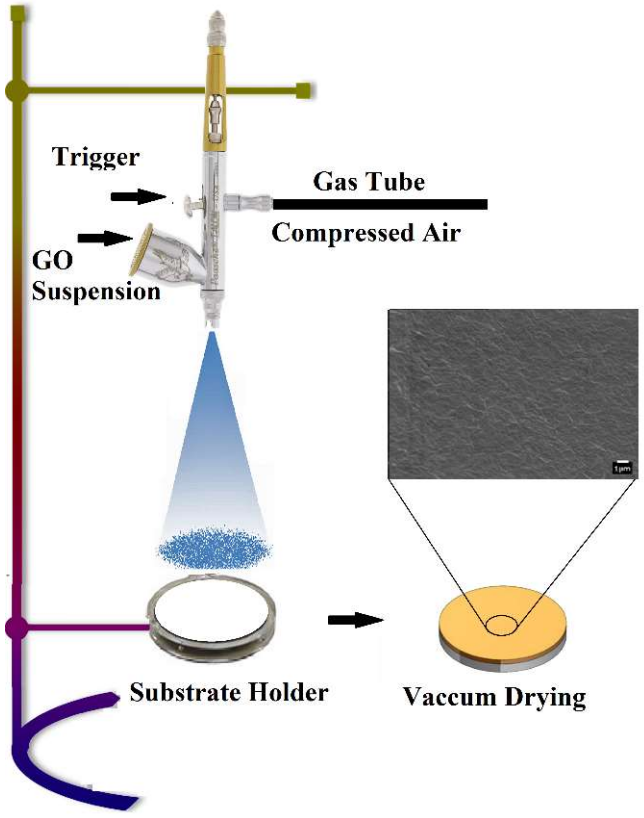

Figure 3.1 Schematic illustration for GO membrane synthesis by spray coating

Prepared membranes are named as MEM-xLy, where x represent the preparation method (F for filtration and S for spray coating), L represent the large size fraction as presented in chapter 2, while y represent the measured thickness of the membrane in nm. The produced GO membranes were dried under vacuum to remove the residue water before characterization and permeation tests. The XRD patterns for GO nanosheets and membranes prepared in this work were collected by a Bruker D8 ADVANCE powder diffractometer with Cu Kα radiation (λ = 1.542 Å) at 40 kV and 40 mA and scan step of 0.05°. The surface topology and cross-section of prepared GO membranes were imaged using scanning electron microscope (SEM, Philips FEI XL-30). Bruker Dimension atomic

force microscopy (AFM, D3000) was used to image GO membrane surface in a taping mode.

Gas permeation experiments of the prepared GO membranes were conducted on a steady state multicomponent gas permeation/separation system (Appendix A). A GO membrane on the polyester substrate was fixed in a stainless-steel membrane cell, with the GO layer facing the upstream side, and sealed by silicone O-rings. Pure gases and mixture experiments were performed in the Wicke Kallenbach configuration at atmospheric pressure. Single gases of H_2, He, CH_4, N_2, and CO_2 of industrial grade were fed at a flow rate of 25 ml/min using mass flow controllers in the cross-flow mode on the GO film surface. The downstream surface of the membrane was swept at 25 ml/min argon. In 50:50 vol% H_2/CO_2 mixture experiments, the feed was controlled at 50 ml/min. The flow rate of the retentate and permeate streams are measured using a bubble flowmeter and analyzed using gas chromatography (Agilent Technologies, 6890 N, Appendix B). Gas permeation experiments were carried out also as a function of operation temperature with 30 min allowed at each temperature step. The Gas permeation data is reported as a mean of three measurements and maximum 3% accuracy. The permeance and separation factor are calculated according to Equations 2.5 and 2.6.

3.3 Results and Discussion

3.3.1 GO Sheets and Membrane Characteristics

XRD patterns given in Figure 3.2 show obvious differences between the structure of the used graphite flakes and the produced GO powder. As shown, the graphite has an intensive peak at 2θ of 26.65°, whereas GO has its diffraction peak at 2θ of 10.4°, corresponding to interlayer distances, d_{002} of 3.34 and 8.5 Å for graphite and GO

respectively. Oxidation process opens the space between the graphitic layers and thus facilitates subsequent GO sheet exfoliation upon ultrasonication.

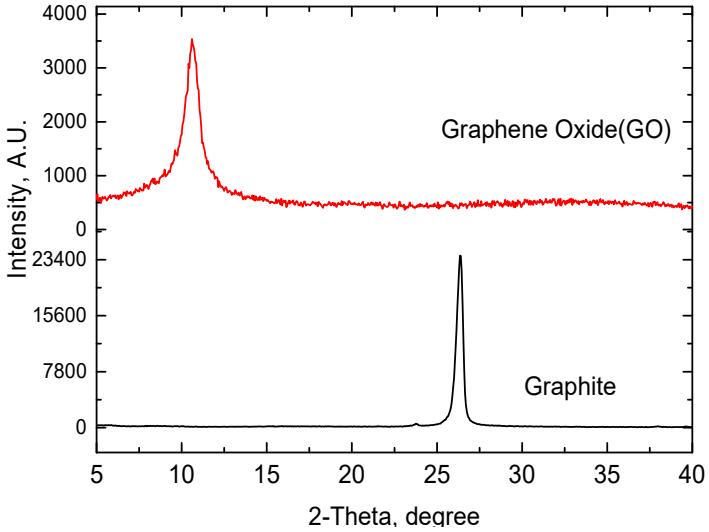

Figure 3.2 XRD patterns of used graphite flakes and produced GO powder.

SEM surface and cross section images of MEM-FL500 GO membrane prepared by vacuum filtration with more focus on membrane wrinkles are in Figure 3.3. The surface of the membrane is corrugated showing ripples and extrinsic wrinkles with different heights. The GO sheets are stacked parallel to the substrate very densely packed as shown in cross section images (Figure 3.3 B and C), however, this horizontal packing is interrupted at the wrinkles. Wrinkles form a fold like structure that start closer to the substrate and grow with increasing the membrane thickness. With the deposition of GO sheets, initial wrinkles grow and form surface wrinkles. AFM was applied to image MEM-FL500 GO membrane surface to get more details about the height of membrane wrinkles. The amplitude scan images in Figure 3.4-A for the membrane show the same wrinkles observed in SEM images. Section analysis of the height images in Figure 3.4-B show that the maximum wrinkle height over the membrane surface is about 350 nm. More section profiles are given

in Appendix E. The height of the surface wrinkle depends on the position of the nethermost wrinkle, and thus to some extent the thickness of surface wrinkle determines its altitude.

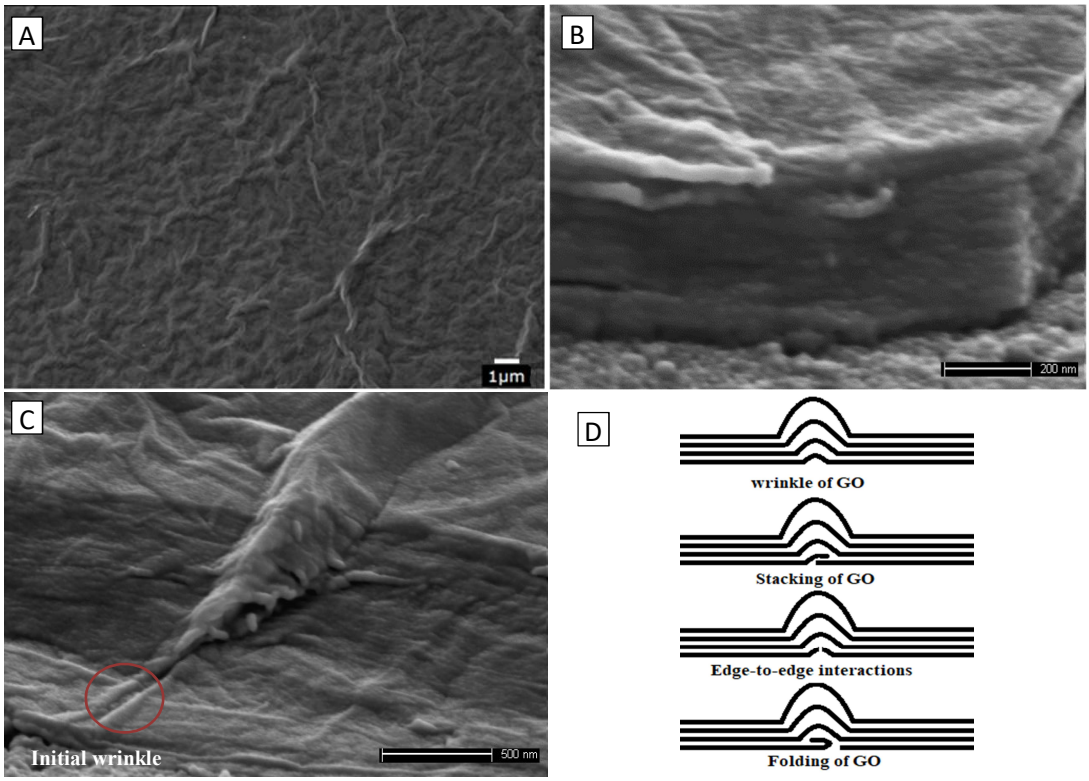

Figure 3.3 SEM surface (A) and cross-section images (B, C) of MEM-F500 GO membrane made by vacuum filtration with focus on membrane wrinkles and schematic diagram for wrinkle formation (D).

The SEM surface morphology images of GO membranes prepared by spray coating with different GO suspension concentrations are given in Figure 3.5. Extrinsic wrinkles are observed in the surface of GO membrane prepared using 1.0 and 0.5 mg/ml GO suspension. These wrinkles are more visible and densely distributed on membrane surface compared to those observed in GO membranes made by filtration. Decreasing GO suspension concentration to 0.1 mg/ml results in a notable decrease or disappearance of GO membrane surface wrinkles as shown in Figure 3.5-C and D. AFM amplitude and height images of

the membrane in Figure 3.6 also confirm the absence of surface wrinkles observed in the membranes prepared by filtration. The high magnification SEM cross-section images of the membrane prepared from 0.1 mg/ml GO suspension (Figure 3.5 E and F) show that the GO sheets are packed horizontally parallel to the substrate regardless of the synthesis method.

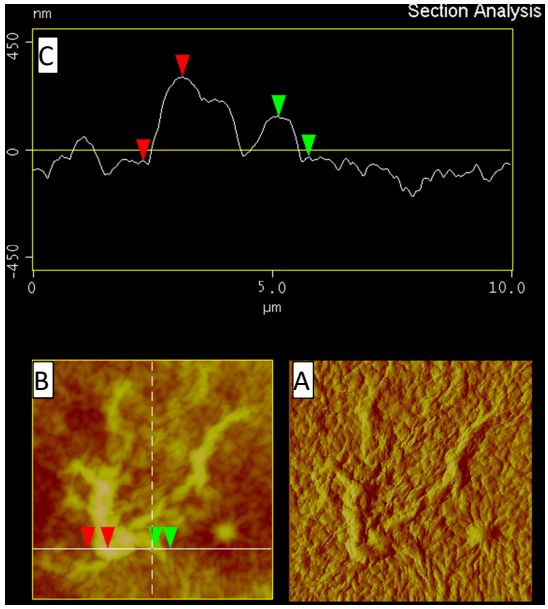

Figure 3.4 10 x 10 µm AFM images for MEM-FL500 GO membrane made by filtration. A: amplitude, B: height, C: section analysis.

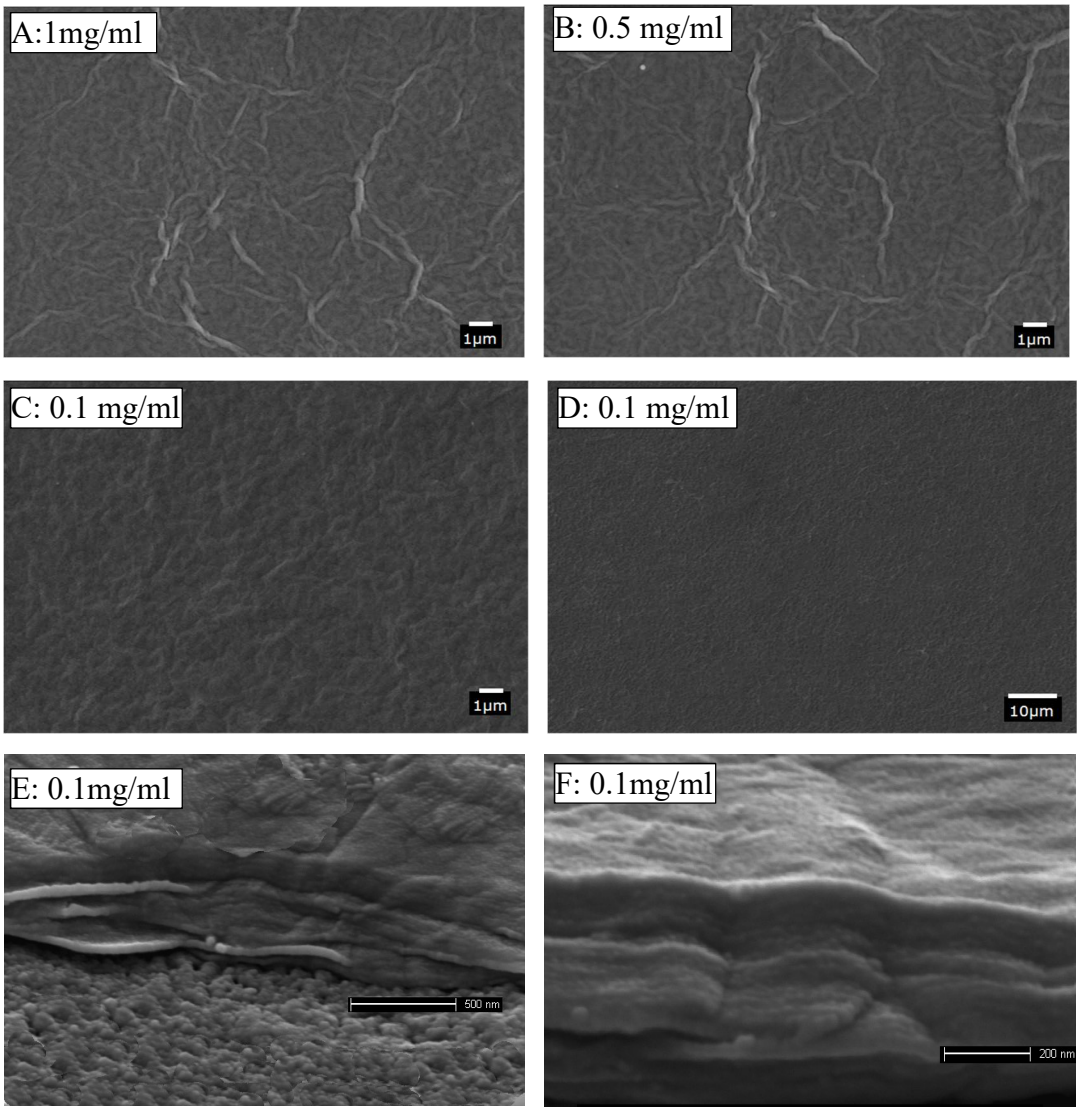

Figure 3.5 SEM images of 500 nm thick GO membranes prepared by spray coating on PETE substrate at different GO suspension concentrations: A-D surface images, E and F cross-section images of MEM-SL500 made using GO suspension of 0.1 mg/ml.

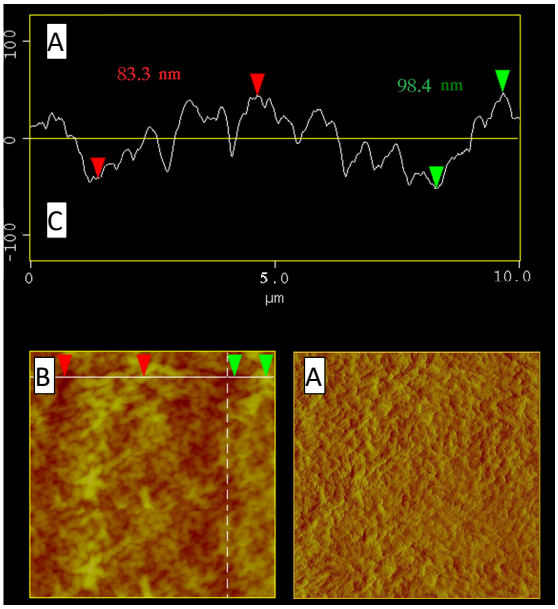

Figure 3.6 10 x 10 µm AFM images for MEM-SL500 GO membrane made by spray coating using GO suspension of 0.1 mg/ml. A: amplitude, B: height, C: section analysis.

XRD characterization was also carried out to study the stacking behavior of GO membranes prepared in this work as given in Figure 3.7. The peak at ~26° is a feature diffraction peak of PETE substrate. GO peaks are recorded at 2θ of 10.1, 10.1, 10.6 and 10.35° for spray coated GO membranes at suspension concentrations 1.0, 0.5 0.1 mg/ml and GO membrane made by vacuum filtration respectively. The corresponding calculated interlayer free space heights are 5.42, 5.42, 5.0 and 5.21 Å (Nair et al., 2012). The SEM and AFM data shows that the wrinkle are fold structures of a max height of 350 nm above the membrane surface, which suggest that the space between GO sheets at the wrinkles ranges from 1~2 times the interspace height detected by XRD and increases gradually from the substrate towards the top GO layers of the membrane. Increasing the concentration of spray coating suspension and the formation of the wrinkles, result in lower intensity GO peak slightly shifted to lower diffraction angles as shown in Figure 3.7.

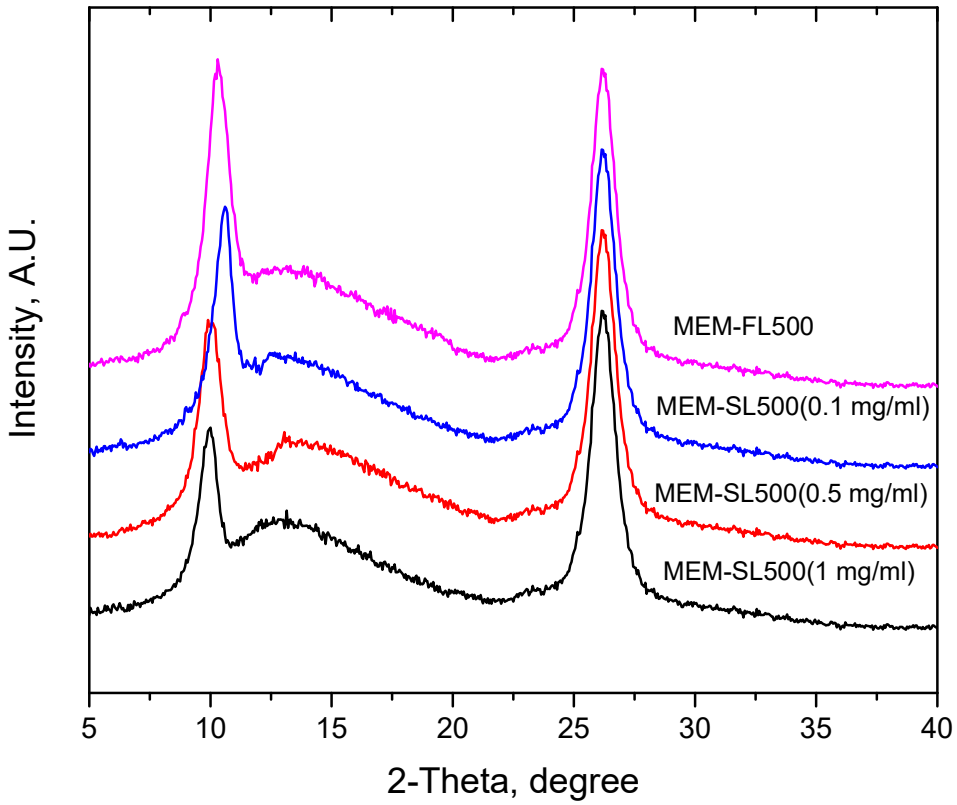

Figure 3.7 XRD patterns of MEM-FL500 GO membrane prepared by vacuum filtration and membranes prepared by spray coating technique using GO suspension of concentrations 1.0, 0.5 and 0.1 mg/ml.

The membranes presented in this work are made using the same GO suspension, with an average sheet size of 33 µm which confirm that the absence/existence of extrinsic wrinkles is due to the membrane stacking method and synthesis conditions. As indicated from the SEM images and through literature (Shen et al., 2014; Wei et al., 2016), surface wrinkles originates from a small initial wrinkle that grow with the deposition of GO sheets. Initial wrinkles could form due to one or more of conditions given in Figure 3.3-D, typically: sheet buckling up and down due to edge-to-edge hydrogen bonding, GO sheet wrinkles, sheet stacking and/or folding. We believe that two key factors control the formation of the initial wrinkle: 1) the concentration of GO suspension and the drainage or

evaporation of water/solvent between the sheets and substrate and/or stacked sheets. Very dilute concentrations are used in filtration, however, concentration polarization phenomena during the dead-end filtration of the suspension may lead to a gradual build-up in the concentration of GO at the boundary layer between the substrate surface and the liquid phase. Thus, increasing the possibility for GO flakes to interact when found in the conditions of the boundary layer. Also, the gradual drainage of water between the substrate and the first deposited GO layers could lead to formation of initial wrinkles as pointed out by Wei et al.,(2016).

Extrinsic wrinkles were also observed in case of spray coating with high concentration GO suspensions. Higher GO concentrations mean large number of GO sheets per spray. One spray for even 2 second, could lead to stacking few layers on the substrate, which result in sheet interactions and water accumulation between stacked sheets, that form wrinkles when gradually drained through the substrate or through the sides of the substrate. In the case of using dilute GO concentration (0.1 mg/ml), each spray will disperse a few number of GO sheets on the substrate, possibly forming single layers for each spray and the distance between the sheets probably larger. As a result, the sheets' edge to edge interactions are minimized and the water drains to a shorter distance (sheet dimension) if sufficient time is allowed between sprays to insure evaporation of the solvent and semi-drying of the deposited GO layers.

3.3.2 Gas Permeation and Separation Properties

Permeability results of five pure gases at room temperature H_2, (kinetic diameter of 2.9Å), He (2.6), CH_4 (3.8Å), N_2 (3.6Å) and CO_2 (3.3Å) through MEM-SL250 and MEM-SL270 GO membranes synthesized by spray coating using suspension concentrations of

0.5 and 0.1 mg/ml are given in Table 3.1. To compare the changes in the structure and permeability of the membranes made by spray coating and vacuum filtration, the permeability of MEM-FL200 made by filtration (Chapter 2) using the same GO suspension is also presented in Table 3.1. Generally, the permeability of pure gases decreases as the molecular weight of propping gas increases regardless of the GO sheet stacking method. MEM-SL270 show larger ideal selectivity of H_2 over large gas molecules (CH_4, N_2 and CO_2) compared to MEM-SL250 and MEM-FL-200 as presented in Table 3.2. The apparent difference in the structure of the three membranes is the formation of extrinsic wrinkles in the assembled membranes using vacuum filtration or high concentration GO suspension in spray coating as observed in SEM and AFM images.

Table 3.1

Permeability of MEM-SL250 and MEM-SL270 GO Membranes Prepared by Spray Coating and MEM-FL200 Made using Same GO Suspension by Vacuum Filtration

Gas type	Mw. [g/mol]	Permeability [Barrer] 1 Barrer = 1×10^{-10} cm^3 $cm/cm^2 \cdot sec \cdot cm$ Hg at STP		
		MEM-SL250 [0.5mg/ml]	MEM-SL270 [0.1mg/ml]	MEM-FL200 [0.002mg/ml]
H_2	02	84.63	78.41	79.71
He	04	65.10	60.00	61.50
CH_4	16	06.70	04.20	05.07
N_2	28	03.54	02.10	02.53
CO_2	44	03.13	01.83	02.26

Table 3.2

Ideal Selectivity of MEM-SL250 and MEM-SL270 GO Membranes Prepared by Spray Coating and MEM-FL200 Made by Vacuum Filtration

H_2/Gas	Knudsen selectivity	Perm-selectivity		
		MEM-SL250	MEM-SL270	MEM -FL200
H_2/He	1.41	01.30	01.31	01.30
H_2/CH_4	2.83	12.63	18.67	15.71
H_2/N_2	3.74	23.88	37.34	31.46
H_2/CO_2	4.69	27.00	42.85	35.32

The inter-sheet and inner-sheet gas transport model proposed in Chapter 2, Section 2.3.3 can be used to discuss semi quantitively the obtained permeation and separation data given in Table 3.1 and 3.2. The inter-sheet pathway A is composed of randomly distributed channels at wrinkles and interlayer space between stacked GO sheets. The inner-sheet pathway, B constitutes GO sheet structural defects as shown in Chapter 2, Figure 2.12. Normalizing Equation 2.5 by the membrane thickness, permeability can be expressed as:

$$P = \left[\left(\frac{\varepsilon_A}{\tau_A}\right) D_A K_A + \left(\frac{\varepsilon_B}{\tau_B}\right) D_B K_B\right] \quad \text{Equation 3.1}$$

where ε and τ are the porosity and tortuosity for pores of pathways A and B; D and K are gas diffusivity and adsorption equilibrium constant in the pores of pathways A or B.

Gas diffusion through the micropores of pathway A or B can be described by the translational diffusion model(Kanezashi &Lin, 2009; Kanezashi et al., 2008) as expressed in Equation 2.5. The activation energy of diffusion, E_d is mainly determined by the size ratio (λ) of kinetic diameter of permeating gas molecule, dm, to that of the pore diameter, dp (λ=dm/dp). E_d is close to zero with λ<0.6 and increases exponentially with further increasing λ (Kanezashi &Lin, 2009). XRD results showed that the empty interlayer space

heights for MEM-SL250, MEM-SL270, and MEM-FL200 are 5.42, 5.0 and 5.21 Å respectively, larger than the kinetic diameter of all tested gas molecules. If extrinsic wrinkles exist as observed in MEM-SL250, and MEM-FL200, the channel formed at membrane wrinkle is ~1-2 times the free interlayer space height detected by XRD and thus, E_d is zero. Because of this, the exponential term in Equation 2.5 is less significant than the pre-exponential term which is determined by the molecular weight of the permeating gas. The minimization of extrinsic wrinkles in MEM-SL270 will lead to slightly larger E_d as compared to MEM-FL200 and MEM-SL250. However, the order of the permeability of the large gas molecules does not change CH_4>N_2>CO_2 which indicates that the activation energy for diffusion is still close to zero and the pre-exponential term remains more significant.

Using the same GO suspension implies no changes in diffusivity, D_B in pathway B, since defect size and concentration does not change and differences in the free interspace height as detected by XRD are insignificant. Also, no changes in sorption properties, K_A, K_B and tortuosity factors, τ_B, τ_A and ε_B are expected. Therefore, the flow of small gas molecules in membrane defects should not be affected by wrinkle formation. Large gas molecules, (CH_4, N_2, and CO_2), according to our proposed model (Ibrahim &Lin, 2018) permeate dominantly in the inter-sheet pathways, while small gas molecules (H_2 and He) permeate mostly in the inner-sheet pathway. The formation of extrinsic wrinkles in GO membrane will affect the porosity in inter-sheet pathway, ε_A, while it does not have any effect on the inner-sheet pathway. The larger the wrinkle height, the more porous is the inter sheet pathways of GO membranes and thus the more the contribution of inter-sheet

pathway in the measured permeability of large gas molecules. As a result, the selectivity of large gas molecule over small gas molecules will decrease.

The permeability ratio $P_{MEM\text{-}SL250}/P_{MEM\text{-}FL200}$ is 1.06, 1.06, 1.32, 1.40, and 1.39 for H_2, He, CH_4, N_2, and CO_2 respectively. The noticeable increase in the permeability of large gas molecules is attributed to the visible wrinkles observed for MEM-SL250 compared to MEM-FL200. The ratio $P_{MEM\text{-}FL200}/P_{MEM\text{-}SL270}$ is 1.02, 1.03, 1.21, 1.21, 1.23 for H_2, He, CH_4, N_2, and CO_2 respectively. Similarly, the decrease in the permeability of large gas molecules for MEM-SL270 is due to minimizing extrinsic wrinkles compared to MEM-FL200. These results clearly show that the permeability of small gas molecules is not affected by the wrinkle formation since they flow dominantly in GO sheet defects.

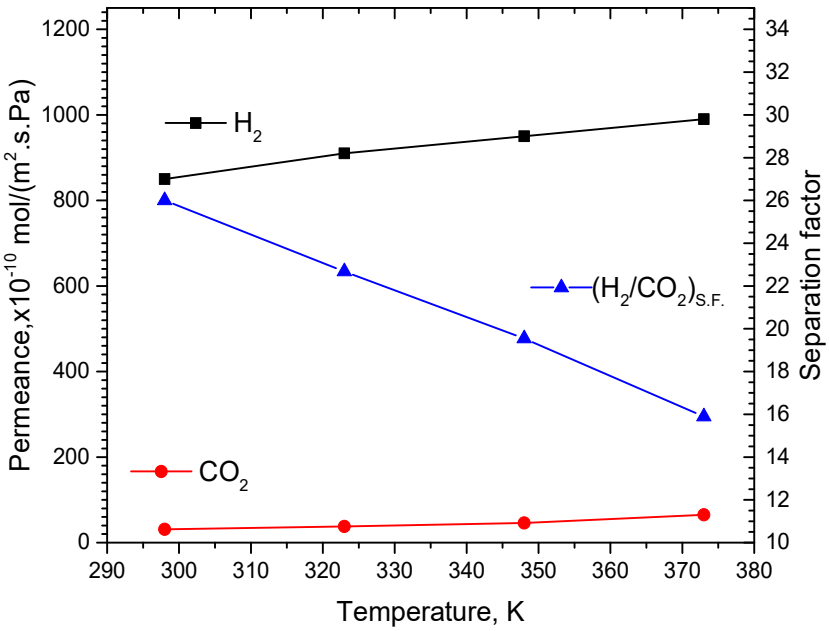

Figure 3.8 The performance of MEM-SL270 membrane in equimolar (H_2/ CO_2) binary mixture as a function of temperature.

MEM-SL270 made by spray coating using 0.1mg/ml GO suspension is H_2 selective in both pure and binary H_2/CO_2 mixture similar to MEM-FL-200 made by filtration with a

separation factor of 26 compared to 22.5 for MEM-FL-200 at room temperature. Gas permeance for equimolar H_2/CO_2 binary mixture feed for MEM-SL270 membrane at different temperatures is presented in Figure 3.8. CO_2 permeance increases faster than H_2 with temperature, due to a more activated CO_2 diffusion than that of H_2 through pathway B. The apparent activation energy for permeation for H_2 and CO_2 respectively in the binary mixture are 1.8, 8.82 kJ/mol for MEM-SL270 slightly higher compared to 1.60 and 8.13 kJ/mol for MEM-FL200.

3.4 Conclusions

High quality GO membranes can be readily coated on porous polymer substrate by the scalable spray coating method. GO membranes prepared by spray coating method offer gas characteristics similar to those made by filtration, however using dilute GO suspension in spray coating will help reduce the formation of extrinsic wrinkles. Wrinkles are fold like structures composed of layers of wrinkles, and initiate from a small slender wrinkle and grow with the deposition of the GO sheets, which makes the spacing between the sheets at the wrinkles ~1-2 times the interlayer free space detected by XRD. Minimizing wrinkles formation results in reduction in the porosity of the inter-sheet pathway where the transport of large gas molecules dominates. The flow of small gas molecules dominates through sheet defects which is not affected by formation of the wrinkles. Therefore, GO membranes prepared with spray coating using dilute GO suspension show enhanced separation characteristics of small gas molecules (H_2 and He) over large gas molecules (CH_4, N_2 and CO_2,) compared to GO membranes made with high concentration GO suspension and membranes made by filtration.

CHAPTER 4

BRODIE'S DERIVED GRAPHENE OXIDE MEMBRANES WITH FINE-TUNED INTERLAYER GALLERIES FOR ENHANCED HYDROGEN SEPARATION

4.1 Introduction

Graphene oxide (GO) sheets are the oxidative exfoliation product of graphite with atomic layer thickness and oxygen-containing functional groups attached to their edges and basal planes (Lerf et al., 1998). GO nanosheets offer an encouraging opportunity to assemble membranes with distinct laminar structure for gas separation (Huang et al., 2014b). However, the synthesis of GO membranes with enhanced separation property for hydrogen based on understanding of the gas transport mechanism of these membranes is still challenging.

In Chapter 2, we proposed a two-pathway transport model to explain the gas permeation and separation characteristics for GO membranes. We found that large gas molecules (CH_4, N_2 and CO_2) flow with Knudsen like permeation characteristics, dominantly through an inter-sheet pathway composed primarily of randomly distributed interlayer spacing between stacked GO sheets and channels formed at membrane wrinkles. While small gas molecules (H_2 and He) permeate through inner-sheet pathway that constitutes GO sheets structural defects in addition to their flow in the inter-sheet pathway. The defect size and concentration on a GO sheet is very difficult to control and depend on the GO synthesis method and extent of oxidation (Botas et al., 2013; Krishnamoorthy et al., 2013). Therefore, producing GO membranes for enhanced hydrogen molecular sieving property requires fine-tuning of the interlayer spacing height of GO sheets to add more restriction to the flow of large gas molecules through GO membranes.

Some efforts were done to produce GO membranes with controlled free spacing for enhanced gas separation property of the membrane. Jin and coworkers (2016) applied centrifugal force during vacuum filtration of GO suspension with alternative deposition of polyethyleneimine/GO layers. The high H_2/CO_2 selectivity of 30 was attributed to achieving small interlayer free spacing height of 0.4 nm. The slow rate vacuum filtration synthesized GO membranes, were almost impermeable to m-xylene vapor and exhibited a good separation performance for several gas pairs (H_2/N_2, H_2/CO, H_2/CH_4, H_2/C_2H_6, H_2/C_4H_{10} and H_2/SF_6) exceeding nearly twice those corresponding to Knudsen type of diffusion (Romanos et al., 2015). Hung and coworkers (2015) also showed that the microstructure of GO membranes prepared by pressure and vacuum filtration greatly varies. XRD results indicated that the GO layer d-spacing varied from 8.3 Å to 9.7 Å for pressure and vacuum filtration methods respectively. Researchers also developed physical or chemical approaches to modulate the intergalleries to improve water flux and/or selectivity (Huang et al., 2013; Hung et al., 2014; Qiu et al., 2011; Tang et al., 2014; Xi et al., 2016) or produce impermeable GO films (Su et al., 2014).

Those early reported studies to modulate the interlayer galleries are difficult to finely regulate the GO inter-sheet channels of staked sheets to smaller < 0.4 nm size that is necessary for precise separation of hydrogen in gas separation applications. Here we report a new method to prepare GO membranes with narrow interlayer spacing height using GO powder prepared by modified Brodie's method (1859). Brodie's method provides GO with smaller interlayer distance compared to Hummers' method (1958) and the sheets are free of not-easy to remove contaminants such as sulfur (Petit et al., 2009). Thin films prepared from Brodie's GO are flexible: they can be folded several times without breaking (Talyzin

et al., 2014) and show superior mechanical properties compared to those prepared using Hummers' GO (Talyzin et al., 2017). Therefore, there is a strong interest in testing Brodie's GO sheets for the preparation of GO membranes and in comparing their properties with Hummers' GO membranes. In the present work, we investigated the gas permeation and separation characteristics of GO membranes made from Brodie's GO sheets on polyester track etch substrates using vacuum and pressure filtration deposition methods. The objective of the work is to produce GO membranes using Brodie's derived GO sheets with narrow interlayer spacing height to improve the hydrogen molecular sieving properties of GO membranes.

4.2 Experimental

The GO powder was produced by a slightly modified version of Brodie's method (1859). 10 ml of fuming nitric acid was charged into a flask equipped with a Teflon mechanical stirrer. The flask was cooled down to 0 °C using an ice bath. 1g graphite flakes (Sigma-Aldrich, SKU: 332461, ~150 μm flakes) was added to the flask under stirring. 5 min later 10 g potassium chlorate ($KClO_3$, Alfa Aesar, +99.0%), was slowly added in small doses to the mixture under stirring in a period of 30 min to avoid temperature increase and prevent strong reaction at local points. The whole mixture was then stirred for 30 min, then the obtained dark green thick slurry was left unstirred at ambient temperature for 24 h. The loss of nitric acid due to evaporation was retrieved by adding another 10 ml of nitric acid. The slurry was then heated to 60 °C using tab water bath and kept at this temperature for 8 h while stirring. The reaction was terminated by transferring the pasty mixture into 500 ml of distilled water.

The resulting solid material was separated from the solution by centrifugation at a speed of 6000 rpm and washed with 2x 200 ml of 10% HCl solution to remove metal ions and then with at least 5x 200 ml of distilled water to remove remnant acid and later dried under vacuum. The GO suspension at a concentration of 0.2 mg/ml was prepared using water as the solvent, and ultrasonicated for 30 min to achieve exfoliation of the sheets using Cole-Parmer ultrasonic cleaner (model 8890-21-USA,70W, 42 kHz). This type of GO does not get dispersed in water even after prolonged sonication until the solvent is made slightly basic using 0.01 M NaOH.

Hydrophilic macroporous polyester track etch (PETE) membranes obtained from commercial resources (Sterlitech, SKU: PET0125100) were used as the substrates for coating GO membranes. The substrates are 10 μm in thickness and 25 mm in diameter, contain cylindrical pores with pore diameter of 0.1μm. For membrane fabrication, the prepared GO suspension 0.2 mg/ml was further diluted with water to a concentration of 0.006 mg/ml. Vacuum and pressure filtration systems were used to deposit 30 ml of the prepared GO suspension with different sheet packing density on the PETE substrate. The resultant GO membranes were accordingly named MEM-xF-y, where x represents the type of the filtration system used (V for vacuum and P for pressurized), and y represent the applied pressure to filtrate the liquid in bars.

The produced GO membranes were dried under vacuum to remove the residue water before characterization and permeation tests. GO nanosheets and membranes were characterized by XRD for phase structure and crystallinity (Bruker D8ADVANCE X-ray diffractometer; Cu Kα radiation λ = 1.542 Å at 40 kV and 40 mA, scan step of 0.05º). Scanning electron microscope (SEM, Amray 1910) was used for imaging membrane

surface topology and cross-section as well as the lateral dimension of the GO sheets. Fourier transform infrared (FT-IR, Thermo Nicolet 6700) was used for identifying surface functional groups of GO nanosheets. Raman spectroscopy measurements were performed on a Renishaw InVia Raman microscope with a 488-nm laser for excitation to quantify the defects of GO powder.

Gas permeation experiments of the prepared GO membranes were conducted on a multicomponent gas permeation/separation system [Appendix A]. A PETE supported GO membrane was mounted in a stainless-steel membrane cell, with the GO layer facing the feed side, and sealed by silicone O-rings. Pure gases and gas mixture experiments were performed in the Wicke Kallenbach configuration with atmospheric feed at room temperature, with zero transmembrane pressure difference. The total flow rate of the feed side was controlled using mass flow controllers at 25 ml/min in single gas experiments and at 50 ml/min in 50/50 vol.% binary (H_2/CO_2) gas mixtures. The permeate side was swept by 25 ml/min argon. The prepared GO membranes were further tested for separation of equimolar H_2/CO_2 mixture in humid atmosphere by bubbling the gas feed into water. The membrane was kept at 60 ^oC during experiments and the effect of two different water partial pressures was studied as a function of permeation time. Cold traps were used to collected the water condensate before compositional analysis. Gas permeation data is reported as a mean of three measurements and a maximum error of 5%. Compositional analysis of permeate and retentate gases was determined using gas chromatography (Agilent Technologies, 6890 N, Appendix B) and permeance was calculated using bubble flowmeter using Equation 2.1.

4.3 Results and Discussion

4.3.1 GO Powder and Sheets Characteristics

The FT-IR spectrum for GO powder produced using Brodie's method (GO-B) is given in Figure 4.1 presented along with the FT-IR spectrum of GO powder produced by Hummers' method (GO-H) synthesized according to procedure reported in section 2.2.1. The two spectra are very similar in general exhibiting the same peaks. However, the relative intensity of some peaks is remarkably different, which shows that Hummers' and Brodie's synthesis methods indeed result in different chemical functionalities of GO. The spectrum exhibits overlapping bands in the 3650 cm^{-1} to 3000 cm^{-1} range that indicates the presence of hydroxyl groups (O-H stretching vibration of free hydroxyl groups of physiosorbed water and C-OH, stretching vibration of structural hydroxyl groups of GO). No clear distinction seems possible between C-OH and H_2O peaks (Cerveny et al., 2010; Szabó et al., 2006). However, The GO-B sample has stronger spectral features for 3650 cm^{-1} to 3000 cm^{-1} range and also for the adsorption band at 1369 cm^{-1} assigned for (C–OH) bending vibrations (You et al., 2013). On the other hand, the GO-B powder shows a less pronounced signals from the (C=O) stretching vibration assigned to carboxyl groups at1725 cm^{-1} and (C-O) epoxy stretching vibration at 1222 cm^{-1} (You et al., 2013). Other prominent signals in the GO's spectrum such as those at 1620 cm^{-1} and 1036 cm^{-1} originate from the stretching of unoxidized graphitic sp^2 (C=C) and the (C-O) alkoxy stretching, respectively (Zhang et al., 2010). The higher relative amount of (C=O) groups in GO-H, in contrast to the increased number of C–OH groups in GO-B, is likely the main reason for the strong difference in hydration and exfoliation behavior of both GO samples (You et al., 2013).

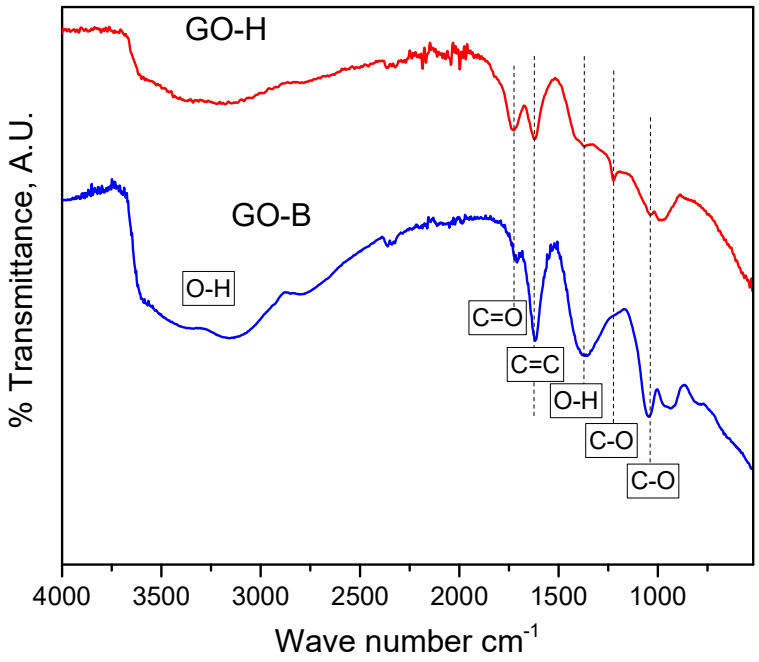

Figure 4.1 FT-IR spectra of synthesized GO powder produced using Brodie's and Hummers' methods.

XRD patterns for the produced GO powder using Brodie's and Hummers' methods and the graphite used as a starting material are given in Figure 4.2. XRD provides conclusive proof for the completion of the oxidation reaction as the interlayer distances of the starting graphite and the end products are highly different. As shown, the graphite has an intensive peak at 2θ of 26.65°, whereas GO samples have their diffraction peaks at 2θ of 14.7° and 10.4° for GO-B and GO-H. Because of oxidation process and the accommodation of various oxygen species, the interlayer distance increases from 3.34 Å for graphite to 6.02 and 8.5 Å for GO-B and GO-H respectively. GO-B sample show better crystallinity evidenced by higher intensity and less broad GO peak which indicates better sheet ordering (You et al., 2013).

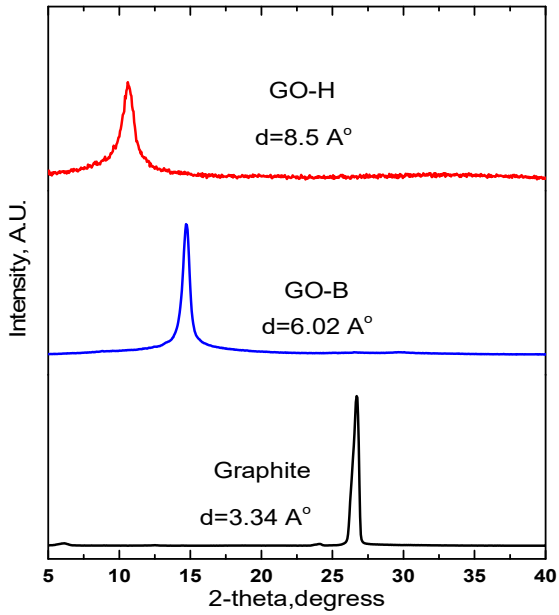

Figure 4.2 XRD patterns of used graphite flakes and GO powder produced by Brodie's and Hummers' methods.

The Raman spectrum for Brodie's GO is shown in Figure 4.3 compared with the Raman spectrum for the Hummers' sheets previously reported in chapter 2. The G band was noticed at at 1584 cm^{-1} and the D band at 1348 cm^{-1}. The value of the (I_D/I_G) ratio was also obtained and presented in Figure 4.3. The FWHM of the D and G peaks are 140 and 163 cm^{-1} respectively, and thus typical of stage 2 region based on the discussion provided in chapter 2. Based on equation 2.4, L_D is about 1.39 nm and the defect density $n_D(\mu m^{-2}) = 10^8/\pi L_D^2$ (Cançado et al., 2011) is 162780. These calculations suggest a sheet porosity of GO-B slightly larger than GO-H.

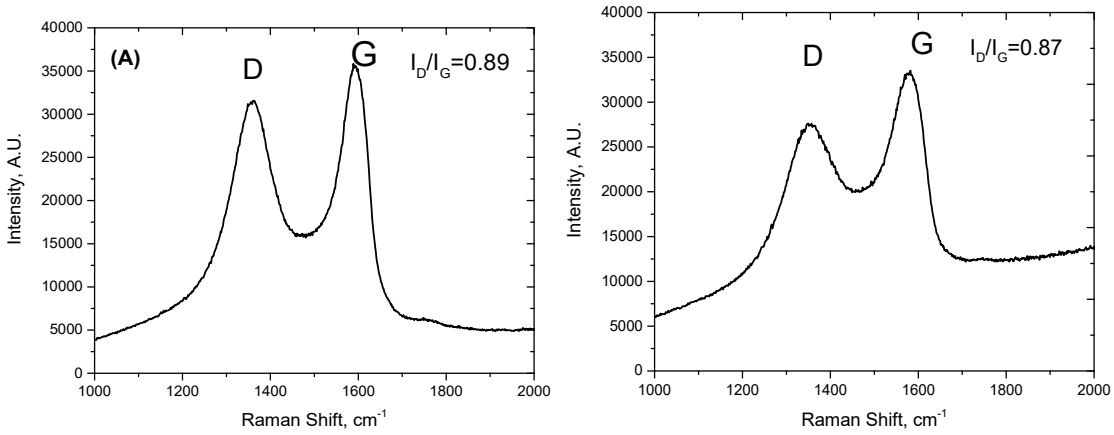

Figure 4.3 Raman spectra of GO powder samples prepared by Hummers' (A) and Brodie's (B) methods.

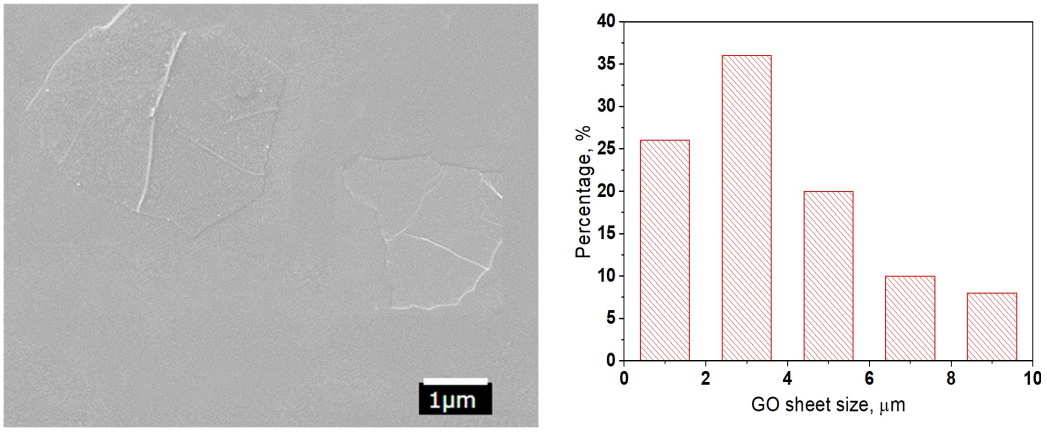

Figure 4.4 SEM images and corresponding histogram of produced GO sheets.

SEM images of GO sheets used for membrane fabrication as well as the corresponding histogram for the sheet size distributions obtained by measuring the longest lateral dimension of 100 sheets in GO-B sample are indicated in Figure 4.4. Ultrasonication of GO-B for 30 min produced GO sheets with average size of 3.5 µm.

4.3.2 GO Membrane Structure and Separation Performance

XRD characterization was carried out to study the stacking behavior and interlayer spacing height of GO membranes prepared by vacuum and pressure filtration systems as given in Figure 4.5. After subtraction of PETE diffraction peaks, the GO membranes on PETE sample clearly show one diffraction peak at 2θ of 13.64 °, 13.9°, 14.2° and 14.2° for MEM-VF-1, MEM-PF-1, MEM-PF-2 and MEM-PF-3 respectively. The corresponding interlayer distances using Bragg's law are 6.5, 6.37, 6.23 and 6.23 Å. The GO peak shifts to a larger angle when pressure is applied in the filtration system and increases from 1 to 3 bar which indicates an enhancement of the packing density as a function in pressure filtration compared to the broad, low intensity peak of MEM-VF-1 made by vacuum filtration. Considering that the electronic clouds around graphene sheets extend over a distance of ~3.34 Å, the interlayer spacing heights for MEM-VF-1, MEM-PF-1, MEM-PF-2 and MEM-PF-3 are 3.15, 3.03, 2.9 and 2.9 Å (Nair et al., 2012). This spacing is just between the size of H_2 (kinetic diameter of 2.9Å) and CO_2 (3.3Å) which suggests enhanced separation potential of these GO membranes.

The SEM images of the surface and cross sections of the synthesized GO membranes using vacuum and pressure filtration are given in Figure 4.5. Overall, the surface is relatively corrugated, showing sheet edges and extrinsic wrinkles with no obvious defects (pores or cracks). Similar wrinkles on the surface of GO membranes made by pressurized filtration were reported (Wei et al., 2016). The height of wrinkles was noticed to decrease with increasing the applied pressure in pressure filtration system.

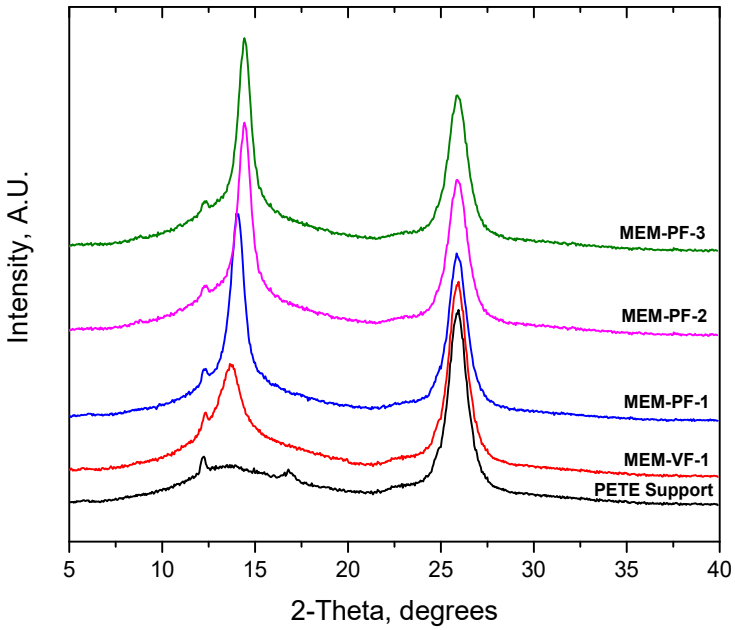

Figure 4.5 XRD spectra of GO membranes prepared by vacuum and pressurized filtration deposition on PETE substrate using GO-B.

The gas permselectivity and transport behavior of the GO membranes were investigated by measuring the permeability of single gases: H_2 (kinetic diameter of 2.9Å), He (2.6 Å), CH_4 (3.8Å), N_2 (3.6Å) and CO_2 (3.3Å). Pure gas permeability results for the GO-B membranes made by vacuum and pressure filtration are given in Table 4.1. The permeability results for MEM-FL200 made by vacuum filtration using GO-H (Chapter 2) is also given in Table 4.1. A notable reduction in the permeability of the MEM-VF-1 membrane prepared by vacuum filtration using GO-B was noticed compared to MEM-FL200 made using GO-H. The permeability ratio for different gases for MEM-FL200 to other membranes synthesized using GO-B sheets are given in Table 4.2. The reduction of the permeability of large gas molecules for MEM-VF-1 was found to be twice the reduction in the permeability of small gas molecules.

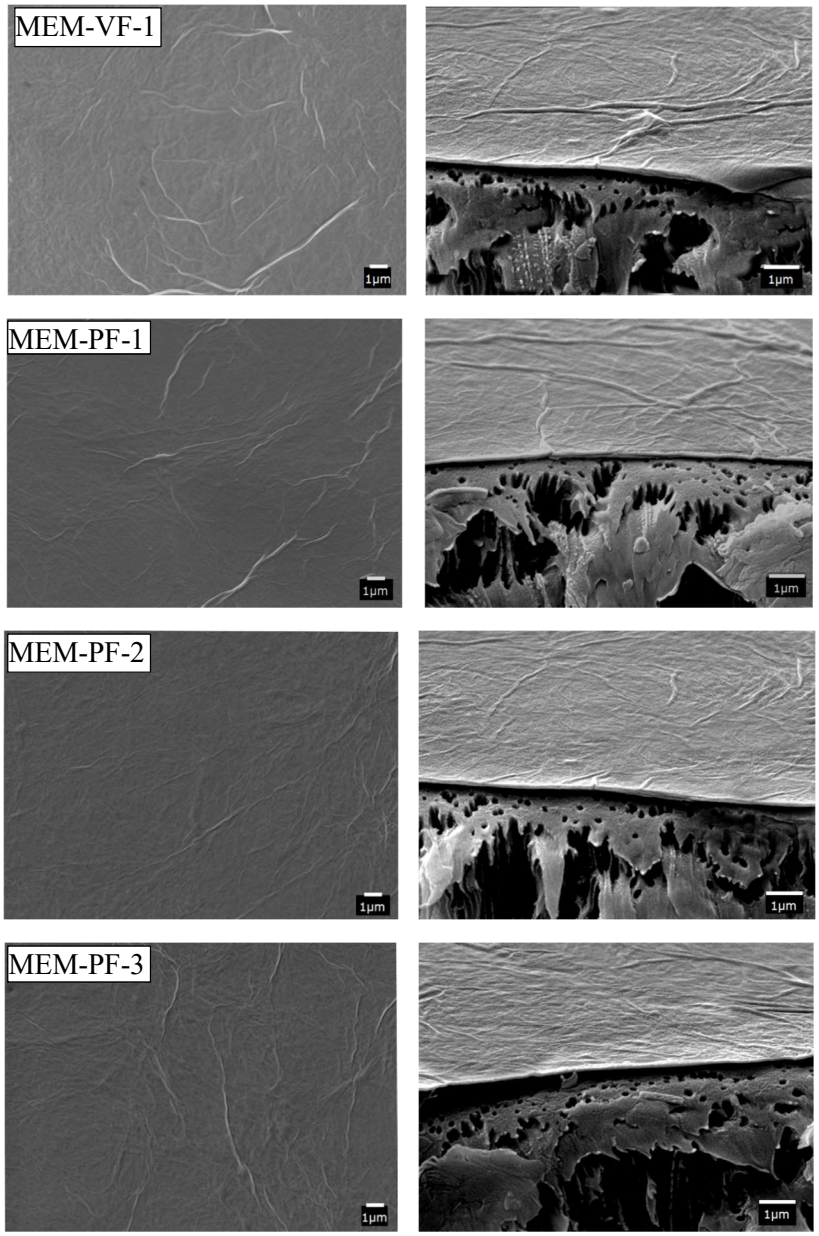

Figure 4.6 SEM surface and cross-section images of GO membranes prepared by vacuum and pressure filtration using GO-B.

MEM-PF-1 made using GO-B in a pressure filtration system of 1 bar show more reduction in the permeability of all gases. However, the reduction of the permeability of large gas molecules was more significant compared to MEM-VF-1 made by vacuum filtration. The driving force applied to filtrate the liquid in both membranes is the same

(1bar). These results suggest that the packing density of the sheets is enhanced in pressure filtration system. The reduction in the rate of applied vacuum due to the growth of the GO film during vacuum filtration may cause the sheets far from the support surface to be loosely packed and less ordered compared to the sheets directly on the support surface.

Table 4.1

Pure Gas Permeability of GO Membranes Prepared by Pressure Filtration and MEM-VF-1 and MEM-FL200 Made by Vacuum Filtration

Gas type	Mw. [g/mol]	Permeability [Barrer]		
		MEM-FL200 Vacuum filtration (GO-H)	MEM-VF-1 Vacuum filtration (GO-B)	MEM-PF-1bar Pressure filtration (GO-B)
H_2	02	79.71	28.26	22.50
He	04	61.50	21.74	16.90
CH_4	16	05.07	01.02	0.560
N_2	28	02.53	0.470	0.290
CO_2	44	02.26	0.350	0.150

Table 4.2

Pure Gas Permeability Ratio of MEM-FL200 Membrane Made by Vacuum Filtration using GO-H over GO Membranes Made using GO-B

Gas type	Mw. [g/mol]	Permeability ratio of MEM-FL200 and	
		MEM-VF-1 Vacuum filtration	MEM-PF-1bar Pressure filtration
H_2	02	2.82	03.54
He	04	2.83	03.64
CH_4	16	4.97	09.07
N_2	28	5.38	08.62
CO_2	44	6.40	15.38

Membrane fabrication by pressure filtration was further extended by increasing the filtration pressure from 1 to 2 and 3 bars. Increasing the filtration pressure resulted in little changes in permeability of small gas molecules but more significant reduction in the permeability of large gas molecules as given in Tables 4.3.

Table 4.3

Pure Gas Permeability of GO Membranes Prepared by Pressure Filtration using GO-B as a Function of the Applied Filtration Pressure

Gas type	Mw. [g/mol]	Permeability [Barrer] 1 Barrer = 1×10^{-10} cm^3 $cm/cm^2 \cdot sec \cdot cm$ Hg at STP		
		MEM-PF-1bar	MEM-PF-2bar	MEM -B200-3bar
H_2	02	22.50	21.49	21.80
He	04	16.90	15.92	16.30
CH_4	16	0.560	0.230	0.310
N_2	28	0.290	0.070	0.110
CO_2	44	0.150	0.040	0.050

The two-pathway gas transport model proposed in this work in section 2.3.3 can be used to explain the permeation and separation data obtained in Tables 4.1, 4.2 and 4.3. The quality of the GO membrane depends on the type of GO sheets used for membrane synthesis. XRD results for MEM-VF-1 membrane show that the 'empty' inter-space height between the GO sheets (pathway A) is 3.15 Å, while for MEM-FL200 is 5.25 Å. The reduction in the height of the free space between the stacked GO sheets will result in increasing, the activation energy for diffusion, E_d for large gas molecules and add more restriction to their flow in inter-sheet pathways. The space width is now smaller than the size of the propping large gas molecules (CH_4 (3.8Å), N_2 (3.6Å) and CO_2 (3.3Å)) and thus no permeance for these molecules should be expected in the free interspace height of stacked sheets. However, if we consider the channels formed at the extrinsic wrinkles, these channels could allow the flow of large gas molecules.

The porosity ε is difficult to be determined for pathway A and B, as ε_A is related to the inter-sheet structure and surface groups and ε_B to the size and concentration of the inner-sheet defects and alignment of the defects in each sheet with each other. Both ε_A and

ε_B depend on synthesis of GO sheets and membranes. Although the defect density determined by Raman is low but the tortuosity for pathway B, τ_B, is extremely small compared to τ_A as one can assume straight gas flow through the defects of the GO sheets, based on Raman results. The defect concentration on GO-B is slightly larger than GO-H as given by Raman characterization. However, the permeability of small gases (H_2 and He) of GO membranes made from Brodie's sheets was significantly lower compared to membranes based on Hummers' GO sheets. The interspace height in GO-H derived membranes is larger than the interspace of GO-B derived membranes, which make the diffusion of small gas molecules from one defect to another between stacked GO sheets in case of GO-H based membranes easier.

The quality of GO membranes also depends on the stacking method, using the same GO sheets. The XRD patterns in Figure 4.5 shows that MEM-VF-1 made by vacuum filtration has lower intensity and broad GO peak compared to MEM-PF-1made by pressure filtration. Also, the interlayer spacing height of MEM-VF-1 is larger than MEM-PF-1. Using pressure filtration enhances the packing density of GO sheets adding more restriction to the flow of large gas molecules in the inter-sheet pathways. Increasing the filtration pressure from 1 to 2 bar, resulted in little decrease in permeability of small gas molecules but more significant reduction in the permeability of large gas molecules and thus a notable enhancement in perm-selectivity of small H_2 over large gas molecules as given in Tables 4.3. XRD results show that MEM-PF-2 has a shorter interlayer height compared to MEM-PF-1, and SEM images in Figure 4.6 show that the extrinsic wrinkle height has been suppressed. These observations explain the increased restriction to gas flow through inter-sheet pathways and demonstrate that packing the GO structure and the interlayer spacing

are sensitively affected by the filtration pressure applied during film formation. Further increase in the filtration pressure will probably cause rapid filtration and random stacking of the GO sheets and defect formation which explains the little increase of small gas and large gas permeability of MEM-PF-3.

Table 4.4 compares binary mixture H_2 and CO_2 permeance and separation data for the GO membranes prepared in this study at different filtration pressures with the pure component data. The GO membranes are perm-selective to H_2 with pure and mixture gas feeds. The binary mixture gives slightly lower, ~20% H_2 permeance but increased CO_2 permeance and thus reduced H_2/CO_2 selectivity as compared to the pure component data. The decreased H_2 permeance in the binary mixture is attributed to the partially hindered transport of H_2 molecules by the strongly adsorbed CO_2 molecules. However, the adsorption of CO_2 is not sufficiently strong to block permeation of H_2.

Moreover, the desirable sufficiently long gas permeation and H_2/CO_2 separation stability of the MEM-PF-1 GO membrane is confirmed a function of time for 36 h as shown in Figure 4.7. This separation performance has exceeded the upper bound of reported polymeric membranes (Robeson, 2008) as presented in Figure 4.8. The GO membranes prepared in this study are also competitive with silica and zeolite membranes (De Vos &Verweij, 1998; Tang et al., 2009), MOFs (Huang et al., 2014a; Li et al., 2010; Wang et al., 2015b), membranes of intrinsic microporosity, PIMs (Carta et al., 2013) and laminar GO membranes (Chi et al., 2016; Guan et al., 2017; Shen et al., 2016).

Table 4.4

Comparison of Ideal Selectivity and Binary Separation Factor of H_2/CO_2 at Room Temperature for GO Membranes Synthesized in this Work Using GO-B

Membrane	Ideal pure gas data			Binary mixture data		
	Permeance (10^{-8}mol/m^2.s.Pa)		Ideal H_2/CO_2 selectivity	Permeance (10^{-8}mol/m^2.s.Pa)		Mixture H_2/CO_2 separation factor
	H_2	CO_2		H_2	CO_2	
MEM-PF-1	3.77	0.025	168.4	3.15	0.033	100.1
MEM-PF-2	3.53	0.007	504.3	2.90	0.010	214.2
MEM-PF-3	3.65	0.008	457.5	2.93	0.012	190.4

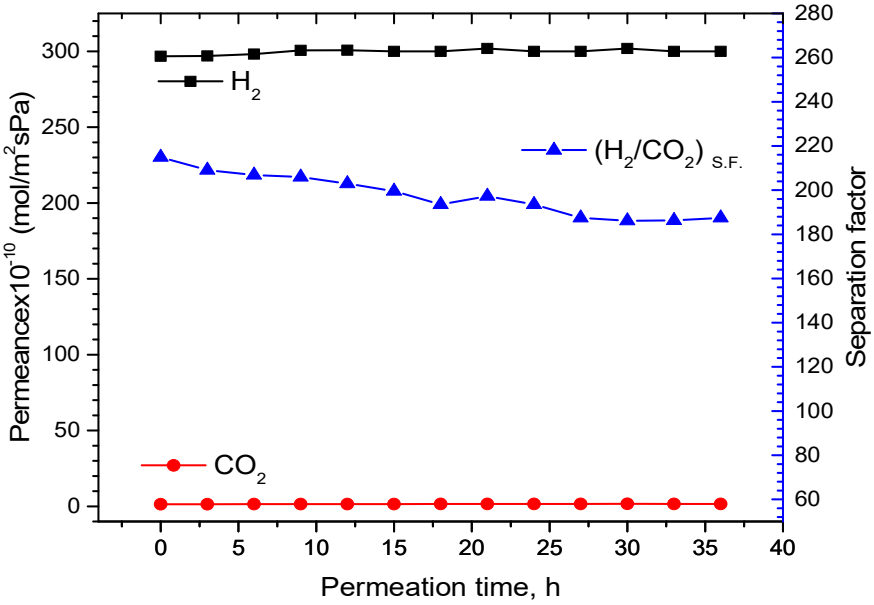

Figure 4.7 MEM-PF-2 GO membrane performance for H_2/CO_2 equimolar mixture as a function of permeation time.

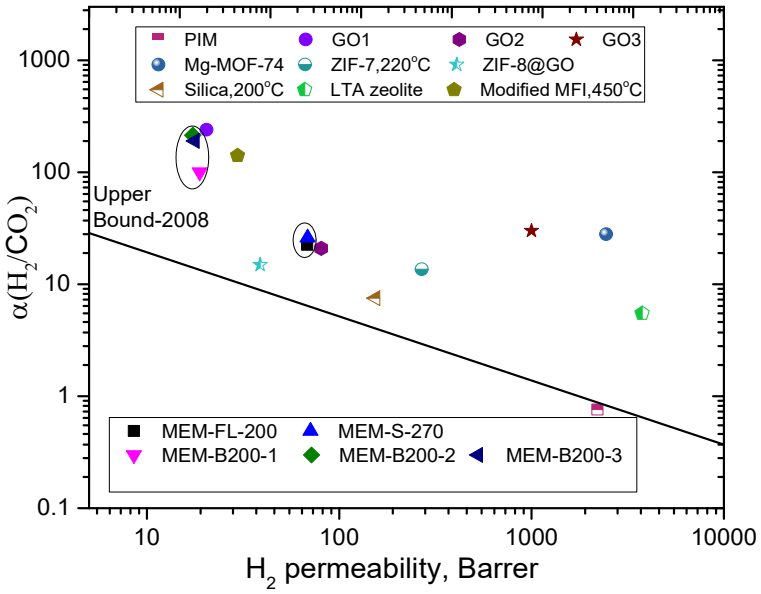

Figure 4.8 Comparison of GO membranes in this work with the 2008 upper bound of polymeric membrane for H_2/CO_2 (Robeson, 2008) and some other typical microporous and GO membranes.

The effect of water vapor in the feed stream on the gas transport and separation performance of GO membranes for binary H_2/CO_2 mixture was investigated by changing the relative humidity of the feed. The H_2/CO_2 separation performance of MEM-PF-1 as a function of permeation time using humid gas feed for two water vapor partial pressures is given in Figure 4.9. Because GO is hydrophilic, a strong affinity between water molecules and GO sheets was expected. The adsorbed water molecules between GO sheets can hinder the diffusion of gases through the GO membranes. The CO_2 permeance has slightly increased at low water vapor partial pressure; however, at high water vapor partial pressure, the CO_2 permeance has significantly increased compared to its performance for dry feed conditions. H_2 gas permeance has significantly decreases at high water vapor partial

pressure and thus, the presence of water vapor led to a significant decrease of H_2/ CO_2 selectivity.

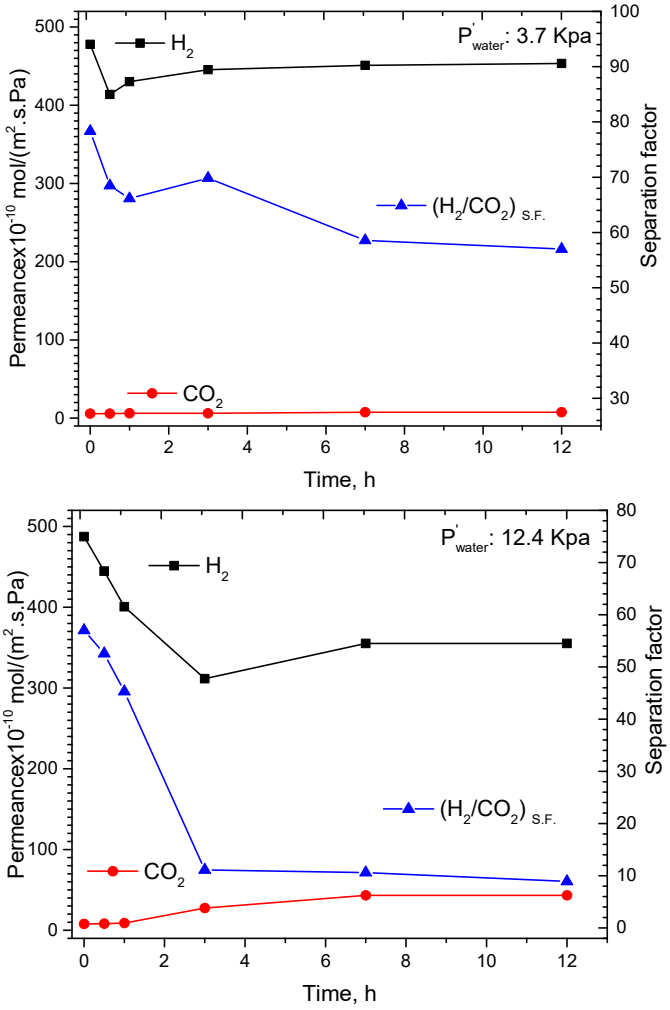

Figure 4.9 MEM-PF-1 performance for H_2/CO_2 binary mixture separation in humid feed.

Hydrogen has a higher gas diffusivity coefficient and lower solubility coefficient in water compared to CO_2(Dodds et al., 1956). In general, the presence of water in GO membranes reduce gas permeabilities due to reduced gas diffusivities and solubilities (Kim et al., 2014). Condensed water molecules in the pores or between GO layers hinder the transport of noncondensable small H_2 molecules due to reduced gas diffusivities and solubilities, while CO_2 sorption in water overwhelms the reduced CO_2 diffusivity specially

at high water vapor partial pressure resulting in reduced H_2/CO_2 selectivity. In addition, water vapor can lead to swelling of GO layers, resulting in the expansion of interlayer distance between stacked sheets which can explain the little increase of the permeance of hydrogen after about 3 h of operation.

4.4 Conclusions

A series of GO membranes synthesized using vacuum and pressurized filtration of GO sheets prepared by Brodie's method have been evaluated using pure and binary H_2/CO_2 gas mixtures experiments. Synthesized membranes showed overall low permeability compared to GO membranes made using Hummers' derived GO sheets due to smaller interlayer space height of Brodie's sheets (~3 Å). The reduction in permeability of large gas molecules (CH_4, N_2 and CO_2) was more significant than the reduction of the permeability of small gas molecules (H_2 and He) and therefore, more improved selectivity for H_2 over large gas molecules was achieved. The well packed sheet structure of Brodie's sheets was further improved using pressure filtration and is found sensitively affected by the applied filtration pressure. The packing density might be expected to increase as the filtration pressure increases; however, higher pressures lead to a faster filtration process, and this may lead to defects in the GO film. The produced Brodie's derived GO membranes are hydrogen selective in pure and binary H_2/CO_2 mixture feeds as well as in slightly humid gas mixture with reduction in the H_2 separation property of the membrane. The enhanced CO_2 sorption capability in GO membranes in relatively humid gas feeds leads to higher CO_2 permeability resulting in significant reduction in H_2/CO_2 selectivity.

CHAPTER 5

SUMMARY AND RECOMMENDATIONS

5.1 Summary

This dissertation presented the synthesis, characterization and gas permeation and separation characteristics of GO membranes synthesized on polyester track etch substrates using different film deposition techniques such as vacuum filtration, spray coating and pressurized filtration. The graphene oxide sheets are prepared by modified Hummers' and Brodie's methods. Prepared GO powder and membranes were characterized using conventional characterization techniques such as XRD, FT-IR, Raman AFM, and SEM. Single gas permeation and equimolar binary H_2/CO_2 mixture separation experiments were conducted both at room temperature and as a function of permeation temperature and obtained results are correlated with XRD and SEM characteristics of the membranes. In chapter 1 we introduced membrane gas separation basics and detailed review on GO membrane synthesis, gas permeation and separation characteristics and proposed transport models.

In chapter 2, we introduced the first objective of this dissertation, that is to provide clear understanding of the gas permeation and separation characteristics of GO membranes and explain their transport mechanism. To achieve our target, GO membranes are synthesized using GO suspensions with large GO sheets of different sizes (33 and 17 μm) to provide better stacking order of GO sheets and thus, reliable gas permeation and separation data can be obtained. An inter-sheet and inner-sheet two-pathway model is proposed in this work to explain the permeation and separation results of GO membranes synthesized in this study. At room temperature, the large molecules (CH_4, CO_2, and N_2)

permeate through inter-sheet pathway of GO membranes, with Knudsen diffusion characteristics. The permeance for the small sheet GO membrane is about twice that for the large sheet GO membrane. The small gases (H_2 and He) exhibit much higher permeance, showing significant flow through the inner-sheet pathway in addition to the flow through inter-sheet pathway. Gas permeation in GO membranes, more complex than in crystalline microporous membranes, is determined by solubility (surface properties), diffusivity (relative molecular size to pore size), porosity and tortuosity of both the inter-sheet pores and inner-sheet defect pores. These properties are strongly influenced by synthesis method and conditions for GO sheets and membranes.

GO membranes are hydrogen selective in both pure and binary H_2/CO_2 mixture gas feeds. At room temperature, the binary mixture gives slightly lower, ~10-20% H_2 permeance but increased CO_2 permeance (and hence reduced H_2/CO_2 selectivity) as compared to the pure component data. The decreased H_2 permeance in mixture experiments is attributed to the partially hindered transport of H_2 molecules by the strongly adsorbed CO_2 molecules. However, the adsorption of CO_2 is not sufficiently strong to block permeation of H_2, which otherwise would cause reverse selectivity in the case of mixture separation found for crystalline microporous membranes. Gas permeance for equimolar H_2/CO_2 binary mixture feed for produced GO membranes at different temperatures was also investigated. Permeance for CO_2 increases faster than H_2 with temperature, due to a more activated CO_2 diffusion than that of H_2 through inner sheet pathway. The apparent activation energy for permeation of H_2 in pure and binary mixture experiments is lower than the apparent activation energy for CO_2.

Chapter 3 presented the second objective in this contribution that is to produce high quality efficient GO membranes on the scalable polyester polymer substrate using scalable deposition techniques such as spray coating while controlling the formation of extrinsic wrinkles. Extrinsic wrinkles found in GO membranes made by vacuum filtration affect gas permeation and separation characteristics of GO membranes. Therefore, the fabrication of membranes with less extrinsic wrinkles on GO membranes is important. In this regard, we focused on minimizing GO sheet's edge-to-edge interactions using GO suspension of average large size (33μm) and dilute concentration in spray coating. High quality GO membranes can be readily coated on porous polymer substrate by the scalable spray coating method. GO membranes prepared by spray coating method offer gas characteristics similar to those made by filtration, however using dilute GO suspension in spray coating will help reduce the formation of extrinsic wrinkles. Wrinkles are fold like structures composed of layers of wrinkles, and initiate from a small slender wrinkle and grow with the deposition of the GO sheets, which makes the spacing between the sheets at the wrinkles ~1-2 times the interlayer free space detected by XRD. Minimizing wrinkles formation results in reduction in the porosity of the inter-sheet pathway where the transport of large gas molecules dominates. The flow of small gas molecules dominates through sheet defects which is not affected by formation of the wrinkles. Therefore, GO membranes prepared with spray coating using dilute GO suspension show enhanced separation characteristics of small gas molecules (H_2 and He) over large gas molecules (CH_4, N_2 and CO_2) compared to GO membranes made with high concentration GO suspension and membranes made by filtration.

Chapter 4 addresses the third objective of this research work, that is to produce GO membranes with narrow controlled interlayer free space height between stacked GO sheets to improve the molecular sieving characteristics of GO membranes. GO membrane studies showed that the interlayer galleries play an important role in selective molecular gas transport in addition to the flow through GO sheet defects. The defect size and concentration on GO sheets depend on the GO synthesis conditions and thus will be difficult to control. Therefore, producing GO membranes with improved hydrogen molecular sieving property requires fine-tuning of the interlayer spacing to add more restriction to the flow of large gas molecules.

To address this objective, a series of GO membranes prepared using GO sheets synthesized by Brodie's method were evaluated for separation of pure and binary H_2/CO_2 gas mixtures. Synthesized membranes showed overall low permeability compared to GO membranes made using GO sheets prepared by Hummers' method. The reduction in permeability of large gas molecules (CH_4, N_2 and CO_2) due to smaller inter sheet space of Brodie's sheets, is more significant than the reduction in permeability of small gas molecules (H_2 and He). As a result, more enhanced selectivity for small gas molecules over large gas molecules was achieved using Brodie's derived GO sheets. The morphology of the GO film reveals a well-packed structure with an interlayer spacing of ~3 Å which is found sensitively affected by the applied filtration pressure. Packing density might be expected to increase as the applied filtration pressure increases; however, higher pressures lead to a faster filtration process, and this may lead to defects in the film. The produced Brodie's derived GO membranes are hydrogen selective in pure and binary H_2/CO_2 mixture feeds as well as in slightly humid gas mixture with reduction in the H_2 separation property

of the membrane. The enhanced CO_2 sorption capability in GO membranes in relatively humid gas feeds leads to higher CO_2 permeability resulting in significant reduction in H_2/CO_2 selectivity.

5.2 Recommendations

Our work has demonstrated that excellent separation quality of GO membranes can be achieved using Brodie's method derived GO sheets with narrow interlayer spacing of ~3 Å. However, the prepared 200 nm membranes show relatively low permeance. Further decrease in membrane thickness is suggested to increase the membrane permeance without compromising the H_2/CO_2 selectivity. Controlling the membrane thickness can be achieved through using smaller volumes of same concentration used in this study. However, at the same filtration pressure and smaller amount of GO suspension, the rapid filtration rate may cause random stacking of GO sheets and decreases the quality of the GO film and thus using more dilute suspension is highly recommended.

The correlation between the gas separation capacity of the GO membranes and the pore size of the used support was never studied. All the GO membranes synthesized in this work were prepared on polyester track etch substrates with pore diameter of 100 nm. Using substrates with smaller pore size is suggested to enhance the molecular sieving quality of GO membranes. Moreover, using small pore diameter substrate, will help prepare thinner GO membranes down to few nanometers as suggested in our first recommendation.

High quality GO membranes are produced using spray coating deposition on polyester substrates using Hummers' method derived GO sheets. Spray coating with dilute concentration help minimize the formation of extrinsic wrinkles. However, the interlayer spacing will depend on the spacing of the parent GO suspension. Brodie's derived GO

show smaller interlayer space height compared to Hummers' prepared GO sheets and thus using Brodie's derived GO for membrane synthesis is expected to achieve efficient membranes for large area applications.

REFERENCES

Achari, A., S, S., & Eswaramoorthy, M. (2016). High performance MoS2 membranes: effects of thermally driven phase transition on CO2 separation efficiency. *Energy & Environmental Science, 9*(4), 1224-1228. doi:10.1039/C5EE03856A

Air-Products. (2017). Air products engineered membrane systems Retrieved from http://www.airproducts.com/products/Gases/supply-options/prism-membranes/prism-membrane-engineered-systems.aspx

Akbari, A., Sheath, P., Martin, S. T., Shinde, D. B., Shaibani, M., Banerjee, P. C., Tkacz, R., Bhattacharyya, D., & Majumder, M. (2016). Large-area graphene-based nanofiltration membranes by shear alignment of discotic nematic liquid crystals of graphene oxide. *Nature Communications, 7*, 10891. doi:10.1038/ncomms10891

Al-Mufachi, N. A., Rees, N. V., & Steinberger-Wilkens, R. (2015). Hydrogen selective membranes: a review of palladium-based dense metal membranes. *Renewable and Sustainable Energy Reviews, 47*(Supplement C), 540-551. doi:10.1016/j.rser.2015.03.026

Araujo, P. T., Terrones, M., & Dresselhaus, M. S. (2012). Defects and impurities in graphene-like materials. *Materials Today, 15*(3), 98-109. doi:10.1016/S1369-7021(12)70045-7

Athanasekou, C., Pedrosa, M., Tsoufis, T., Pastrana-Martínez, L. M., Romanos, G., Favvas, E., Katsaros, F., Mitropoulos, A., Psycharis, V., & Silva, A. M. T. (2017). Comparison of self-standing and supported graphene oxide membranes prepared by simple filtration: gas and vapor separation, pore structure and stability. *Journal of Membrane Science, 522*, 303-315. doi:10.1016/j.memsci.2016.09.031

Bae, S., Kim, H., Lee, Y., Xu, X., Park, J.-S., Zheng, Y., Balakrishnan, J., Lei, T., Ri Kim, H., Song, Y. I., Kim, Y.-J., Kim, K. S., Ozyilmaz, B., Ahn, J.-H., Hong, B. H., & Iijima, S. (2010). Roll-to-roll production of 30-inch graphene films for transparent electrodes. *Nat Nano, 5*(8), 574-578. doi:10.1038/nnano.2010.132

Baker, R. W. (2002). Future directions of membrane gas separation technology. *Industrial & Engineering Chemistry Research, 41*(6), 1393-1411. doi:10.1021/ie0108088

Baker, R. W., & Lokhandwala, K. (2008). Natural gas processing with membranes: an overview. *Industrial & Engineering Chemistry Research, 47*(7), 2109-2121. doi:10.1021/ie071083w

Bernardo, P., Drioli, E., & Golemme, G. (2009). Membrane gas separation: a review/state of the art. *Industrial & Engineering Chemistry Research, 48*(10), 4638-4663. doi:10.1021/ie8019032

Berry, V. (2013). Impermeability of graphene and its applications. *Carbon, 62*, 1-10. doi:10.1016/j.carbon.2013.05.052

Botas, C., Álvarez, P., Blanco, P., Granda, M., Blanco, C., Santamaría, R., Romasanta, L. J., Verdejo, R., López-Manchado, M. A., & Menéndez, R. (2013). Graphene materials with different structures prepared from the same graphite by the Hummers and Brodie methods. *Carbon, 65*, 156-164. doi:10.1016/j.carbon.2013.08.009

Brodie, B. C. (1859). On the atomic weight of graphite. *Philosophical Transactions of the Royal Society of London, 149*, 249-259. doi:10.2307/108699

Bunch, J. S., Verbridge, S. S., Alden, J. S., van der Zande, A. M., Parpia, J. M., Craighead, H. G., & McEuen, P. L. (2008). Impermeable Atomic Membranes from Graphene Sheets. *Nano Letters, 8*(8), 2458-2462. doi:10.1021/nl801457b

Cançado, L. G., Jorio, A., Ferreira, E. H. M., Stavale, F., Achete, C. A., Capaz, R. B., Moutinho, M. V. O., Lombardo, A., Kulmala, T. S., & Ferrari, A. C. (2011). Quantifying defects in graphene via Raman spectroscopy at different excitation energies. *Nano Letters, 11*(8), 3190-3196. doi:10.1021/nl201432g

Carta, M., Malpass-Evans, R., Croad, M., Rogan, Y., Jansen, J. C., Bernardo, P., Bazzarelli, F., & McKeown, N. B. (2013). An efficient polymer molecular sieve for membrane gas separations. *Science, 339*(6117), 303-307. doi:10.1126/science.1228032

Cerveny, S., Barroso-Bujans, F., Alegría, Á., & Colmenero, J. (2010). Dynamics of water intercalated in graphite oxide. *The Journal of Physical Chemistry C, 114*(6), 2604-2612. doi:10.1021/jp907979v

Chae, S. J., Güneş, F., Kim, K. K., Kim, E. S., Han, G. H., Kim, S. M., Shin, H.-J., Yoon, S.-M., Choi, J.-Y., Park, M. H., Yang, C. W., Pribat, D., & Lee, Y. H. (2009). Synthesis of large-area graphene layers on poly-nickel substrate by chemical vapor deposition: wrinkle formation. *Advanced Materials, 21*(22), 2328-2333. doi:10.1002/adma.200803016

Chi, C., Wang, X., Peng, Y., Qian, Y., Hu, Z., Dong, J., & Zhao, D. (2016). Facile preparation of graphene oxide membranes for gas separation. *Chemistry of Materials, 28*(9), 2921-2927. doi:10.1021/acs.chemmater.5b04475

Cohen-Tanugi, D., & Grossman, J. C. (2012). Water desalination across nanoporous graphene. *Nano Letters, 12*(7), 3602-3608. doi:10.1021/nl3012853

Compton, O. C., & Nguyen, S. T. (2010). Graphene oxide, highly reduced graphene oxide, and graphene: versatile building blocks for carbon-based materials. *Small, 6*(6), 711-723. doi:10.1002/smll.200901934

Darvish Ganji, M., & Dodangeh, R. (2017). Hydrogen purification performance of a nanoporous hexagonal boron nitride membrane: molecular dynamics and first-principle simulations. *Physical Chemistry Chemical Physics, 19*(19), 12032-12044. doi:10.1039/C7CP01665D

Dave, S. H., Gong, C., Robertson, A. W., Warner, J. H., & Grossman, J. C. (2016). Chemistry and Structure of Graphene Oxide via Direct Imaging. *ACS Nano, 10*(8), 7515-7522. doi:10.1021/acsnano.6b02391

De Vos, R. M., & Verweij, H. (1998). Improved performance of silica membranes for gas separation. *Journal of Membrane Science, 143*(1), 37-51. doi:10.1016/S0376-7388(97)00334-7

Dikin, D. A., Stankovich, S., Zimney, E. J., Piner, R. D., Dommett, G. H. B., Evmenenko, G., Nguyen, S. T., & Ruoff, R. S. (2007). Preparation and characterization of graphene oxide paper. *Nature, 448*(7152), 457-460. doi:10.1038/nature06016

Dodds, W. S., Stutzman, L. F., & Sollami, B. J. (1956). Carbon Dioxide Solubility in Water. *Industrial & Engineering Chemistry Chemical & Engineering Data Series, 1*(1), 92-95. doi:10.1021/i460001a018

Dreyer, D. R., Park, S., Bielawski, C. W., & Ruoff, R. S. (2010). The chemistry of graphene oxide. *Chemical Society Reviews, 39*(1), 228-240. doi:10.1039/B917103G

Du, H., Li, J., Zhang, J., Su, G., Li, X., & Zhao, Y. (2011). Separation of hydrogen and nitrogen gases with porous graphene membrane. *The Journal of Physical Chemistry C, 115*(47), 23261-23266. doi:10.1021/jp206258u

Eigler, S., Dotzer, C., & Hirsch, A. (2012). Visualization of defect densities in reduced graphene oxide. *Carbon, 50*(10), 3666-3673. doi:10.1016/j.carbon.2012.03.039

Erickson, K., Erni, R., Lee, Z., Alem, N., Gannett, W., & Zettl, A. (2010). Determination of the local chemical structure of graphene oxide and reduced graphene oxide. *Advanced Materials, 22*(40), 4467-4472. doi:10.1002/adma.201000732

Evans, R. B., Watson, G. M., & Mason, E. A. (1961). Gaseous diffusion in porous media at uniform pressure. *The Journal of Chemical Physics, 35*(6), 2076-2083. doi:10.1063/1.1732211

Fasolino, A., Los, J. H., & Katsnelson, M. I. (2007). Intrinsic ripples in graphene. *Nat Mater, 6*(11), 858-861. doi:10.1038/nmat2011

Ferrari, A. C., & Robertson, J. (2000). Interpretation of Raman spectra of disordered and amorphous carbon. *Physical Review B, 61*(20), 14095-14107.

Gilje, S., Han, S., Wang, M., Wang, K. L., & Kaner, R. B. (2007). A Chemical route to graphene for device applications. *Nano Letters, 7*(11), 3394-3398. doi:10.1021/nl0717715

Guan, K., Shen, J., Liu, G., Zhao, J., Zhou, H., & Jin, W. (2017). Spray-evaporation assembled graphene oxide membranes for selective hydrogen transport. *Separation and Purification Technology, 174*, 126-135. doi:10.1016/j.seppur.2016.10.012

Hegab, H. M., & Zou, L. (2015). Graphene oxide-assisted membranes: fabrication and potential applications in desalination and water purification. *Journal of Membrane Science, 484*, 95-106. doi:10.1016/j.memsci.2015.03.011

Hofmann, U., & Holst, R. (1939). Über die säurenatur und die methylierung von graphitoxyd. *Berichte der deutschen chemischen Gesellschaft (A and B Series), 72*(4), 754-771. doi:10.1002/cber.19390720417

Hu, M., & Mi, B. (2013). Enabling Graphene Oxide Nanosheets as Water Separation Membranes. *Environmental Science & Technology, 47*(8), 3715-3723. doi:10.1021/es400571g

Huang, A., Liu, Q., Wang, N., Zhu, Y., & Caro, J. (2014a). Bicontinuous zeolitic imidazolate framework ZIF-8@GO membrane with enhanced hydrogen selectivity. *Journal of the American Chemical Society, 136*(42), 14686-14689. doi:10.1021/ja5083602

Huang, H., Song, Z., Wei, N., Shi, L., Mao, Y., Ying, Y., Sun, L., Xu, Z., & Peng, X. (2013). Ultrafast viscous water flow through nanostrand-channelled graphene oxide membranes. *4*, 2979. doi:10.1038/ncomms3979

Huang, H., Ying, Y., & Peng, X. (2014b). Graphene oxide nanosheet: an emerging star material for novel separation membranes. *Journal of Materials Chemistry A, 2*(34), 13772-13782. doi:10.1039/C4TA02359E

Huang, L., Zhang, M., Li, C., & Shi, G. (2015). Graphene-based membranes for molecular separation. *The Journal of Physical Chemistry Letters, 6*(14), 2806-2815. doi:10.1021/acs.jpclett.5b00914

Hummers, W. S., & Offeman, R. E. (1958). Preparation of graphitic oxide. *Journal of the American Chemical Society, 80*(6), 1339-1339. doi:10.1021/ja01539a017

Hung, W.-S., Tsou, C.-H., De Guzman, M., An, Q.-F., Liu, Y.-L., Zhang, Y.-M., Hu, C.-C., Lee, K.-R., & Lai, J.-Y. (2014). Cross-linking with diamine monomers to prepare composite graphene oxide-framework membranes with varying d-spacing. *Chemistry of Materials, 26*(9), 2983-2990. doi:10.1021/cm5007873

Ibrahim, A., & Lin, Y. S. (2018). Gas permeation and separation properties of large-sheet stacked graphene oxide membranes. *Journal of Membrane Science, 550*, 238-245. doi:10.1016/j.memsci.2017.12.081

Joshi, R. K., Carbone, P., Wang, F. C., Kravets, V. G., Su, Y., Grigorieva, I. V., Wu, H. A., Geim, A. K., & Nair, R. R. (2014). Precise and ultrafast molecular sieving through graphene oxide membranes. *Science, 343*(6172), 752-754. doi:10.1126/science.1245711

Kanezashi, M., & Lin, Y. S. (2009). Gas permeation and diffusion characteristics of MFI-type zeolite membranes at high temperatures. *The Journal of Physical Chemistry C, 113*(9), 3767-3774. doi:10.1021/jp804586q

Kanezashi, M., O'Brien-Abraham, J., Lin, Y. S., & Suzuki, K. (2008). Gas permeation through DDR-type zeolite membranes at high temperatures. *AIChE Journal, 54*(6), 1478-1486. doi:10.1002/aic.11457

Kharton, V. V., Yaremchenko, A. A., Kovalevsky, A. V., Viskup, A. P., Naumovich, E. N., & Kerko, P. F. (1999). Perovskite-type oxides for high-temperature oxygen separation membranes. *Journal of Membrane Science, 163*(2), 307-317. doi:10.1016/S0376-7388(99)00172-6

Kim, H. W., Yoon, H. W., Yoo, B. M., Park, J. S., Gleason, K. L., Freeman, B. D., & Park, H. B. (2014). High-performance CO2-philic graphene oxide membranes under wet-conditions. *Chemical Communications, 50*(88), 13563-13566. doi:10.1039/C4CC06207H

Kim, H. W., Yoon, H. W., Yoon, S.-M., Yoo, B. M., Ahn, B. K., Cho, Y. H., Shin, H. J., Yang, H., Paik, U., Kwon, S., Choi, J.-Y., & Park, H. B. (2013). Selective gas transport through few-layered graphene and graphene oxide membranes. *Science, 342*(6154), 91-95. doi:10.1126/science.1236098

Klechikov, A., Yu, J., Thomas, D., Sharifi, T., & Talyzin, A. V. (2015). Structure of graphene oxide membranes in solvents and solutions. *Nanoscale, 7*(37), 15374-15384. doi:10.1039/C5NR04096E

Kovtyukhova, N. I., Ollivier, P. J., Martin, B. R., Mallouk, T. E., Chizhik, S. A., Buzaneva, E. V., & Gorchinskiy, A. D. (1999). Layer-by-layer assembly of ultrathin composite films from micron-sized graphite oxide sheets and polycations. *Chemistry of Materials, 11*(3), 771-778. doi:10.1021/cm981085u

Krishnamoorthy, K., Veerapandian, M., Yun, K., & Kim, S. J. (2013). The chemical and structural analysis of graphene oxide with different degrees of oxidation. *Carbon, 53*(Supplement C), 38-49. doi:10.1016/j.carbon.2012.10.013

Kumar, P. V., Bardhan, N. M., Tongay, S., Wu, J., Belcher, A. M., & Grossman, J. C. (2014). Scalable enhancement of graphene oxide properties by thermally driven phase transformation. *Nat Chem, 6*(2), 151-158. doi:10.1038/nchem.1820

Lee, J., & Aluru, N. R. (2013). Water-solubility-driven separation of gases using graphene membrane. *Journal of Membrane Science, 428*, 546-553. doi:10.1016/j.memsci.2012.11.006

Lei, W., Mochalin, V. N., Liu, D., Qin, S., Gogotsi, Y., & Chen, Y. (2015). Boron nitride colloidal solutions, ultralight aerogels and freestanding membranes through one-step exfoliation and functionalization. *6*, 8849. doi:10.1038/ncomms9849

Lerf, A., He, H., Forster, M., & Klinowski, J. (1998). Structure of graphite oxide revisited. *The Journal of Physical Chemistry B, 102*(23), 4477-4482. doi:10.1021/jp9731821

Li, D., Muller, M. B., Gilje, S., Kaner, R. B., & Wallace, G. G. (2008). Processable aqueous dispersions of graphene nanosheets. *Nat Nano, 3*(2), 101-105. doi:10.1038/nnano.2007.451

Li, H., Song, Z., Zhang, X., Huang, Y., Li, S., Mao, Y., Ploehn, H. J., Bao, Y., & Yu, M. (2013). Ultrathin,molecular-sieving graphene oxide membranes for selective hydrogen separation. *Science, 342*(6154), 95-98. doi:10.1126/science.1236686

Li, L. H., Cervenka, J., Watanabe, K., Taniguchi, T., & Chen, Y. (2014). Strong oxidation resistance of atomically thin boron nitride nanosheets. *ACS Nano, 8*(2), 1457-1462. doi:10.1021/nn500059s

Li, X., Cai, W., An, J., Kim, S., Nah, J., Yang, D., Piner, R., Velamakanni, A., Jung, I., Tutuc, E., Banerjee, S. K., Colombo, L., & Ruoff, R. S. (2009). Large-area synthesis of high-quality and uniform graphene films on copper foils. *Science, 324*(5932), 1312-1314. doi:10.1126/science.1171245

Li, Y., Liang, F., Bux, H., Yang, W., & Caro, J. (2010). Zeolitic imidazolate framework ZIF-7 based molecular sieve membrane for hydrogen separation. *Journal of Membrane Science, 354*(1), 48-54. doi:10.1016/j.memsci.2010.02.074

Lin, Y. S. (2001). Microporous and dense inorganic membranes: current status and prospective. *Separation and Purification Technology, 25*(1–3), 39-55. doi:10.1016/S1383-5866(01)00089-2

Lin, Y. S., & Burggraaf, A. J. (1993). Experimental studies on pore size change of porous ceramic membranes after modification. *Journal of Membrane Science, 79*(1), 65-82. doi:10.1016/0376-7388(93)85018-R

Lin, Y. S., & Duke, M. C. (2013). Recent progress in polycrystalline zeolite membrane research. *Current Opinion in Chemical Engineering, 2*(2), 209-216. doi:10.1016/j.coche.2013.03.002

Liu, T.-H., Gajewski, G., Pao, C.-W., & Chang, C.-C. (2011). Structure, energy, and structural transformations of graphene grain boundaries from atomistic simulations. *Carbon, 49*(7), 2306-2317. doi:10.1016/j.carbon.2011.01.063

Marcano, D. C., Kosynkin, D. V., Berlin, J. M., Sinitskii, A., Sun, Z., Slesarev, A., Alemany, L. B., Lu, W., & Tour, J. M. (2010). Improved synthesis of graphene oxide. *ACS Nano, 4*(8), 4806-4814. doi:10.1021/nn1006368

Masuda, T., Fukumoto, N., Kitamura, M., Mukai, S. R., Hashimoto, K., Tanaka, T., & Funabiki, T. (2001). Modification of pore size of MFI-type zeolite by catalytic cracking of silane and application to preparation of H2-separating zeolite membrane. *Microporous and Mesoporous Materials, 48*(1), 239-245. doi:10.1016/S1387-1811(01)00358-4

Meyer, J. C., Geim, A. K., Katsnelson, M. I., Novoselov, K. S., Booth, T. J., & Roth, S. (2007). The structure of suspended graphene sheets. *Nature, 446*(7131), 60-63. doi:10.1038/nature05545

Morigami, Y., Kondo, M., Abe, J., Kita, H., & Okamoto, K. (2001). The first large-scale pervaporation plant using tubular-type module with zeolite NaA membrane. *Separation and Purification Technology, 25*(1), 251-260. doi:10.1016/S1383-5866(01)00109-5

Nair, R. R., Wu, H. A., Jayaram, P. N., Grigorieva, I. V., & Geim, A. K. (2012). Unimpeded permeation of water through helium-leak–tight graphene-based membranes. *Science, 335*(6067), 442-444. doi:10.1126/science.1211694

Novoselov, K. S., Geim, A. K., Morozov, S. V., Jiang, D., Zhang, Y., Dubonos, S. V., Grigorieva, I. V., & Firsov, A. A. (2004). Electric field effect in atomically thin carbon films. *Science, 306*(5696), 666-669. doi:10.1126/science.1102896

Ockwig, N. W., & Nenoff, T. M. (2007). Membranes for hydrogen separation. *Chemical Reviews, 107*(10), 4078-4110. doi:10.1021/cr0501792

Ogino, I., Yokoyama, Y., Iwamura, S., & Mukai, S. R. (2014). Exfoliation of graphite oxide in water without sonication: bridging length scales from nanosheets to macroscopic materials. *Chemistry of Materials, 26*(10), 3334-3339. doi:10.1021/cm501305c

Oyama, S. T., Yamada, M., Sugawara, T., Takagaki, A., & Kikuchi, R. (2011). Review on mechanisms of gas permeation through inorganic membranes. *Journal of the Japan Petroleum Institute, 54*(5), 298-309. doi:10.1627/jpi.54.298

Paci, J. T., Belytschko, T., & Schatz, G. C. (2007). Computational studies of the structure, behavior upon heating, and mechanical properties of graphite oxide. *The Journal of Physical Chemistry C, 111*(49), 18099-18111. doi:10.1021/jp075799g

Pacilé, D., Meyer, J. C., Fraile Rodríguez, A., Papagno, M., Gómez-Navarro, C., Sundaram, R. S., Burghard, M., Kern, K., Carbone, C., & Kaiser, U. (2011). Electronic properties and atomic structure of graphene oxide membranes. *Carbon, 49*(3), 966-972. doi:10.1016/j.carbon.2010.09.063

Pakdel, A., Bando, Y., & Golberg, D. (2014). Nano boron nitride flatland. *Chemical Society Reviews, 43*(3), 934-959. doi:10.1039/C3CS60260E

Pantelic, R. S., Meyer, J. C., Kaiser, U., Baumeister, W., & Plitzko, J. M. (2010). Graphene oxide: A substrate for optimizing preparations of frozen-hydrated samples. *Journal of Structural Biology, 170*(1), 152-156. doi:10.1016/j.jsb.2009.12.020

Peng, Y., Li, Y., Ban, Y., Jin, H., Jiao, W., Liu, X., & Yang, W. (2014). Metal-organic framework nanosheets as building blocks for molecular sieving membranes. *Science, 346*(6215), 1356-1359. doi:10.1126/science.1254227

Perreault, F., Fonseca de Faria, A., & Elimelech, M. (2015). Environmental applications of graphene-based nanomaterials. *Chemical Society Reviews, 44*(16), 5861-5896. doi:10.1039/C5CS00021A

Petit, C., Seredych, M., & Bandosz, T. J. (2009). Revisiting the chemistry of graphite oxides and its effect on ammonia adsorption. *Journal of Materials Chemistry, 19*(48), 9176-9185. doi:10.1039/B916672F

Pham, V. H., Cuong, T. V., Hur, S. H., Shin, E. W., Kim, J. S., Chung, J. S., & Kim, E. J. (2010). Fast and simple fabrication of a large transparent chemically-converted graphene film by spray-coating. *Carbon, 48*(7), 1945-1951. doi:10.1016/j.carbon.2010.01.062

Qiu, L., Zhang, X., Yang, W., Wang, Y., Simon, G. P., & Li, D. (2011). Controllable corrugation of chemically converted graphene sheets in water and potential application for nanofiltration. *Chemical Communications, 47*(20), 5810-5812. doi:10.1039/C1CC10720H

Robeson, L. M. (1991). Correlation of separation factor versus permeability for polymeric membranes. *Journal of Membrane Science, 62*(2), 165-185. doi:10.1016/0376-7388(91)80060-J

Robeson, L. M. (1999). Polymer membranes for gas separation. *Current Opinion in Solid State and Materials Science, 4*(6), 549-552. doi:10.1016/S1359-0286(00)00014-0

Robeson, L. M. (2008). The upper bound revisited. *Journal of Membrane Science, 320*(1), 390-400. doi:10.1016/j.memsci.2008.04.030

Romanos, G., Pastrana-Martínez, L. M., Tsoufis, T., Athanasekou, C., Galata, E., Katsaros, F., Favvas, E., Beltsios, K. G., Siranidi, E., Falaras, P., Psycharis, V., & Silva, A. M. T. (2015). A facile approach for the development of fine-tuned self-standing graphene oxide membranes and their gas and vapor separation performance. *Journal of Membrane Science, 493*, 734-747. doi:10.1016/j.memsci.2015.07.034

Ruess, G. (1947). Über das graphitoxyhydroxyd (graphitoxyd). *Monatshefte für Chemie und verwandte Teile anderer Wissenschaften, 76*(3), 381-417. doi:10.1007/BF00898987

Sanders, D. F., Smith, Z. P., Guo, R., Robeson, L. M., McGrath, J. E., Paul, D. R., & Freeman, B. D. (2013). Energy-efficient polymeric gas separation membranes for a sustainable future: A review. *Polymer, 54*(18), 4729-4761. doi:10.1016/j.polymer.2013.05.075

Saufi, S. M., & Ismail, A. F. (2004). Fabrication of carbon membranes for gas separation—a review. *Carbon, 42*(2), 241-259. doi:10.1016/j.carbon.2003.10.022

Scholz, W., & Boehm, H. P. (1969). Untersuchungen am graphitoxid. vi. betrachtungen zur struktur des graphitoxids. *Zeitschrift für anorganische und allgemeine Chemie, 369*(3-6), 327-340. doi:10.1002/zaac.19693690322

Shelekhin, A. B., Dixon, A. G., & Ma, Y. H. (1995). Theory of gas diffusion and permeation in inorganic molecular-sieve membranes. *AIChE Journal, 41*(1), 58-67. doi:10.1002/aic.690410107

Shen, J., Liu, G., Huang, K., Chu, Z., Jin, W., & Xu, N. (2016). Subnanometer two-dimensional graphene oxide channels for ultrafast gas sieving. *ACS Nano, 10*(3), 3398-3409. doi:10.1021/acsnano.5b07304

Shen, X., Lin, X., Yousefi, N., Jia, J., & Kim, J.-K. (2014). Wrinkling in graphene sheets and graphene oxide papers. *Carbon, 66*(Supplement C), 84-92. doi:10.1016/j.carbon.2013.08.046

Sint, K., Wang, B., & Král, P. (2008). Selective ion passage through functionalized graphene nanopores. *Journal of the American Chemical Society, 130*(49), 16448-16449. doi:10.1021/ja804409f

Sk, M. A., Huang, L., Chen, P., & Lim, K. H. (2016). Controlling armchair and zigzag edges in oxidative cutting of graphene. *Journal of Materials Chemistry C, 4*(27), 6539-6545. doi:10.1039/C6TC01947A

Sotirchos, S. V., & Burganos, V. N. (1999). Transport of gases in porous membranes. *MRS Bulletin, 24*(3), 41-45. doi:10.1557/S0883769400051903

Spillman, R. W. (1989). *Economics of gas separation membranes* (Vol. 85). Chemical engineering progress.: American Institute of Chemical Engineers.

Staudenmaier, L. (1898). Verfahren zur darstellung der graphitsäure. *Berichte der deutschen chemischen Gesellschaft, 31*(2), 1481-1487. doi:10.1002/cber.18980310237

Strathmann, H. (2001). Membrane separation processes: current relevance and future opportunities. *AIChE Journal, 47*(5), 1077-1087. doi:10.1002/aic.690470514

Su, Y., Kravets, V. G., Wong, S. L., Waters, J., Geim, A. K., & Nair, R. R. (2014). Impermeable barrier films and protective coatings based on reduced graphene oxide. *Nat Commun, 5*. doi:10.1038/ncomms5843

Sun, L., & Fugetsu, B. (2013). Mass production of graphene oxide from expanded graphite. *Materials Letters, 109*, 207-210. doi:10.1016/j.matlet.2013.07.072

Szabó, T., Berkesi, O., Forgó, P., Josepovits, K., Sanakis, Y., Petridis, D., & Dékány, I. (2006). Evolution of surface functional groups in a series of progressively oxidized graphite Oxides. *Chemistry of Materials, 18*(11), 2740-2749. doi:10.1021/cm060258+

Talyzin, A. V., Hausmaninger, T., You, S., & Szabo, T. (2014). The structure of graphene oxide membranes in liquid water, ethanol and water-ethanol mixtures. *Nanoscale, 6*(1), 272-281. doi:10.1039/C3NR04631A

Talyzin, A. V., Mercier, G., Klechikov, A., Hedenström, M., Johnels, D., Wei, D., Cotton, D., Opitz, A., & Moons, E. (2017). Brodie vs Hummers graphite oxides for preparation of multi-layered materials. *Carbon, 115*, 430-440. doi:10.1016/j.carbon.2016.12.097

Tan, X., & Li, K. (2014). porous membrane reactors *Inorganic Membrane Reactors* (pp. 27-73): John Wiley & Sons, Ltd.

Tang, Y. P., Paul, D. R., & Chung, T. S. (2014). Free-standing graphene oxide thin films assembled by a pressurized ultrafiltration method for dehydration of ethanol. *Journal of Membrane Science, 458*, 199-208. doi:10.1016/j.memsci.2014.01.062

Tang, Z., Dong, J., & Nenoff, T. M. (2009). Internal surface modification of MFI-type zeolite membranes for high selectivity and high flux for hydrogen. *Langmuir, 25*(9), 4848-4852. doi:10.1021/la900474y

Tsou, C.-H., An, Q.-F., Lo, S.-C., De Guzman, M., Hung, W.-S., Hu, C.-C., Lee, K.-R., & Lai, J.-Y. (2015). Effect of microstructure of graphene oxide fabricated through different self-assembly techniques on 1-butanol dehydration. *Journal of Membrane Science, 477*, 93-100. doi:10.1016/j.memsci.2014.12.039

Uhlhorn, R. J. R., & Burggraaf, A. J. (1991). Gas separations with inorganic membranes. In R. R. Bhave (Ed.), *Inorganic Membranes Synthesis, Characteristics and Applications* (pp. 155-176). Dordrecht: Springer Netherlands.

Varoon, K., Zhang, X., Elyassi, B., Brewer, D. D., Gettel, M., Kumar, S., Lee, J. A., Maheshwari, S., Mittal, A., Sung, C.-Y., Cococcioni, M., Francis, L. F., McCormick, A. V., Mkhoyan, K. A., & Tsapatsis, M. (2011). Dispersible exfoliated zeolite nanosheets and their application as a selective membrane. *Science, 334*(6052), 72-75. doi:10.1126/science.1208891

Veldsink, J. W., van Damme, R. M. J., Versteeg, G. F., & van Swaaij, W. P. M. (1995). The use of the dusty-gas model for the description of mass transport with chemical reaction in porous media. *The Chemical Engineering Journal and the Biochemical Engineering Journal, 57*(2), 115-125. doi:10.1016/0923-0467(94)02929-6

Vidano, R., & Fischbach, D. B. (1978). New lines in the Raman spectra of carbons and graphite. *Journal of the American Ceramic Society, 61*(1-2), 13-17. doi:10.1111/j.1151-2916.1978.tb09219.x

Wang, D., Wang, Z., Wang, L., Hu, L., & Jin, J. (2015a). Ultrathin membranes of single-layered MoS2 nanosheets for high-permeance hydrogen separation. *Nanoscale, 7*(42), 17649-17652. doi:10.1039/C5NR06321C

Wang, N., Mundstock, A., Liu, Y., Huang, A., & Caro, J. (2015b). Amine-modified Mg-MOF-74/CPO-27-Mg membrane with enhanced H2/CO2 separation. *Chemical Engineering Science, 124*(Supplement C), 27-36. doi:10.1016/j.ces.2014.10.037

Wei, Y., Zhang, Y., Gao, X., Yuan, Y., Su, B., & Gao, C. (2016). Declining flux and narrowing nanochannels under wrinkles of compacted graphene oxide nanofiltration membranes. *Carbon, 108*, 568-575. doi:10.1016/j.carbon.2016.07.056

Xi, Y.-H., Hu, J.-Q., Liu, Z., Xie, R., Ju, X.-J., Wang, W., & Chu, L.-Y. (2016). Graphene oxide membranes with strong stability in aqueous solutions and controllable lamellar spacing. *ACS Applied Materials & Interfaces, 8*(24), 15557-15566. doi:10.1021/acsami.6b00928

Xiao, J., & Wei, J. (1992). Diffusion mechanism of hydrocarbons in zeolites—I. Theory. *Chemical Engineering Science, 47*(5), 1123-1141. doi:10.1016/0009-2509(92)80236-6

Xu, Q., Xu, H., Chen, J., Lv, Y., Dong, C., & Sreeprasad, T. S. (2015). Graphene and graphene oxide: advanced membranes for gas separation and water purification. *Inorganic Chemistry Frontiers, 2*(5), 417-424. doi:10.1039/C4QI00230J

Xu, X., Yang, W., Liu, J., Chen, X., Lin, L., Stroh, N., & Brunner, H. (2000). Synthesis and gas permeation properties of an NaA zeolite membrane. *Chemical Communications*(7), 603-604. doi:10.1039/B000478M

Yampolskii, Y. (2012). Polymeric gas separation membranes. *Macromolecules, 45*(8), 3298-3311. doi:10.1021/ma300213b

You, S., Luzan, S. M., Szabó, T., & Talyzin, A. V. (2013). Effect of synthesis method on solvation and exfoliation of graphite oxide. *Carbon, 52*, 171-180. doi:10.1016/j.carbon.2012.09.018

Yu, M., Noble, R. D., & Falconer, J. L. (2011). Zeolite membranes: microstructure characterization and permeation Mechanisms. *Accounts of Chemical Research, 44*(11), 1196-1206. doi:10.1021/ar200083e

Zhang, J., Yang, H., Shen, G., Cheng, P., Zhang, J., & Guo, S. (2010). Reduction of graphene oxide via l-ascorbic acid. *Chemical Communications, 46*(7), 1112-1114. doi:10.1039/B917705A

Zhang, W., Zou, X., Li, H., Hou, J., Zhao, J., Lan, J., Feng, B., & Liu, S. (2015a). Size fractionation of graphene oxide sheets by the polar solvent-selective natural deposition method. *RSC Advances, 5*(1), 146-152. doi:10.1039/C4RA08516G

Zhang, X., Zhang, H., Li, C., Wang, K., Sun, X., & Ma, Y. (2014). Recent advances in porous graphene materials for supercapacitor applications. *RSC Advances, 4*(86), 45862-45884. doi:10.1039/C4RA07869A

Zhang, Y., Shi, Q., Liu, Y., Wang, Y., Meng, Z., Xiao, C., Deng, K., Rao, D., & Lu, R. (2015b). Hexagonal boron nitride with designed nanopores as a high-efficiency membrane for separating gaseous hydrogen from methane. *The Journal of Physical Chemistry C, 119*(34), 19826-19831. doi:10.1021/acs.jpcc.5b04918

Zhao, J., Zhu, Y., Pan, F., He, G., Fang, C., Cao, K., Xing, R., & Jiang, Z. (2015). Fabricating graphene oxide-based ultrathin hybrid membrane for pervaporation dehydration via layer-by-layer self-assembly driven by multiple interactions. *Journal of Membrane Science, 487*, 162-172. doi:10.1016/j.memsci.2015.03.073

Zheng, Q., Geng, Y., Wang, S., Li, Z., & Kim, J.-K. (2010). Effects of functional groups on the mechanical and wrinkling properties of graphene sheets. *Carbon, 48*(15), 4315-4322. doi:10.1016/j.carbon.2010.07.044

Zhou, S., & Bongiorno, A. (2013). Origin of the chemical and kinetic stability of graphene oxide. *Scientific Reports, 3*, 2484. doi:10.1038/srep02484

Zhu, Y., Murali, S., Cai, W., Li, X., Suk, J. W., Potts, J. R., & Ruoff, R. S. (2010). Graphene and graphene oxide: synthesis, properties, and applications. *Advanced Materials, 22*(35), 3906-3924. doi:10.1002/adma.201001068

APPENDIX A

PROCEDURE FOR TESTING SINGLE AND BINARY GAS SEPARATION

1- Gas permeation experiments of the prepared GO membranes are conducted on a multicomponent gas permeation/separation system with the schematic shown in Figure A.1.

2- A PETE supported GO membrane is mounted in a stainless-steel membrane cell, with the GO layer facing the feed side, and sealed by silicone O-rings.

3- Membrane cell is placed in the oven and gas feed and sweep gas tubes are connected.

4- Experiments are performed in the Wicke Kallenbach configuration with atmospheric feed with zero transmembrane pressure difference.

5- The flow rate of the sweep gas (argon) is set at 25 ml/min using mass flow controllers. The flow rate of the feed gas was controlled at 25 ml/min in single gas experiments (H_2, He, CH_4, N_2, and CO_2) and 50 ml/min in 50/50 vol.% binary (H_2/CO_2) gas mixtures.

6- Once testing is ready to begin, after setting the appropriate flow of sweep gas and feed gas (pure /mixture), allow steady state to be reached. Usually an hour or so is necessary for the first point.

7- When steady state is reached, measure and record the flow rates on the permeate and retentate side with the attached bubble flow meters.

8- Gas samples, 1ml is then inject into the gas chromatography, Agilent 6890N (Appendix B) for composition analysis of the permeate and retentate sides.

9- Pure and equimolar (H_2/CO_2) mixture permeation experiments were conducted as a function of feed temperature. 30 min are allowed at each temperature step before injecting samples to GC for composition analysis.

10- Gas permeation data is reported as a mean of three measurements and errors represent the standard deviations from the mean value.

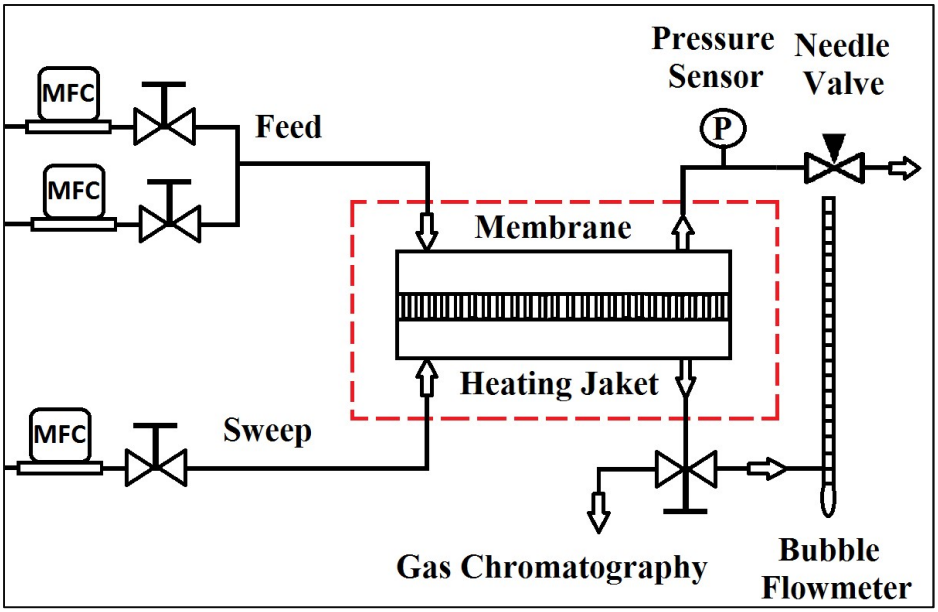

Figure A.1 Schematic diagram of cross- flow membrane gas permeation and separation setup

APPENDIX B

PROCEDURE FOR GAS CHROMATOGRAPHY ANALYSIS

1. Agilent Technologies, 6890 N gas chromatograph (GC) was used for measuring gas compositional analysis. This GC has thermal conductivity detector (TCD) and a 30 feet stainless-steel column (OD: 1/8 inch) packed with HayeSep DB 100/120 mesh porous polymer.
2. Ultra-high purity argon with a flowrate of 30 ml/min was used as the carrier gas for the GC.
3. Column temperature was adjusted at 100°C while injection amount was 1ml.
4. The GC calibration curves for pure gases: H_2, He, CH_4, N_2 and CO_2 are prepared by injection of different volumes to GC and calibration curves are shown in Figure B.1.

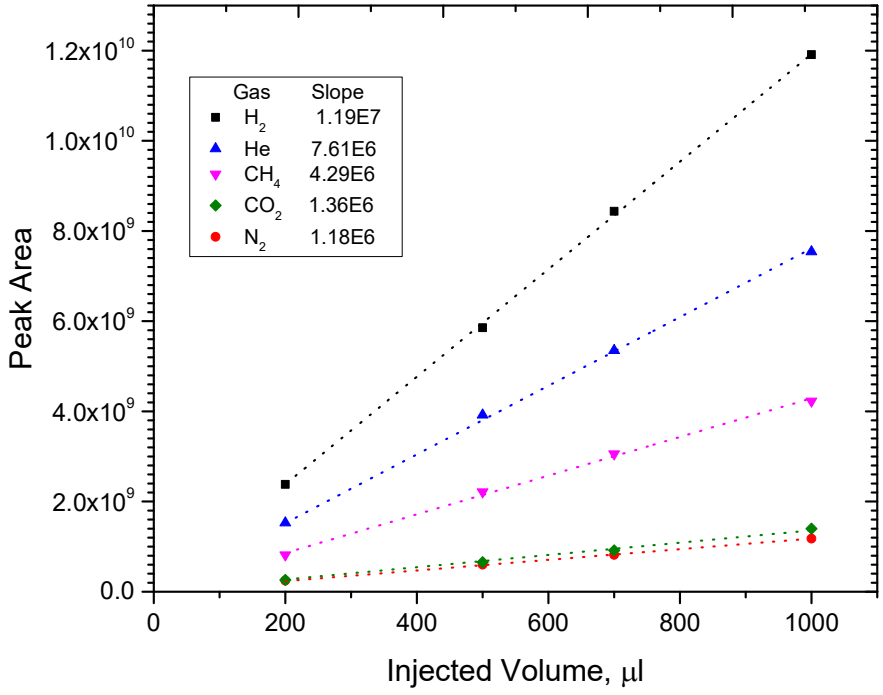

Figure B.1 Gas chromatograph calibration curves for H_2, He, CH_4, CO_2 and N_2, and corresponding calibration constant.

APPENDIX C

PROCEDURE FOR GRAPHENE OXIDE SYNTHESIS BY HUMMERS' METHOD

1. Modified Hummers' method was applied, using graphite fakes (Sigma-Aldrich, SKU: 332461, ~150 μm).
2. Add 100 ml of concentrated sulfuric acid (H_2SO_4, EMD Millipore, SX1244, 95.0-98.0%) to a flask equipped with a Teflon mechanical stirrer.
3. Place the flask in an ice bath to cool down to 0 °C.
4. After 10 min, while stirring add 2 g graphite flakes.
5. Add 1g sodium nitrate ($NaNO_3$, Alfa Aesar, ACS, 99.0%) to the mixture.
6. 5 min later, start adding 12 g of potassium permanganate ($KMnO_4$, Alfa Aesar, ACS, 99.0%) very slowly, while watching the mixture temperature. Temperature should not exceed 5 °C to prevent strong reaction at local points.
7. The addition of potassium permanganate could take like 30 min under stirring. Then the whole mixture is then stirred for 30 min. The suspension changes in color from black to dark green.
8. Then replace the ice bath by tap water bath and start heating, to keep the bath temperature at 40 ^oC for 5 h while stirring. The dark green suspension gradually became a grey viscous fluid and finally turned into dark brown.
9. After that, add 100 ml of deionized water in dropwise manner to the flask, in ~10 min, and as result of the hydration heat the temperature increases to 98°C.
10. Stir the mixture further at this temperature for 15 min with no external heat.
11. dilute the mixture with 300 ml of deionized water and 6 ml of hydrogen peroxide (H_2O_2, Sigma Aldrich, 35 wt. %) to reduce residual permanganate to soluble manganese ions and end the oxidation process. The color of the solution changes from dark brown to yellow.

12. Use the centrifugation at a speed of 6000 rpm to separate the solids.
13. Wash the solids with 2x 200 ml 10% HCl solution to remove metal ions and use centrifuge to get rid of the solvent.
14. Wash the solids with 5x 200 ml deionized water to remove the remnant acid.
15. Finally, wash the solids with ethanol
16. Dry the solids (GO powder) under vacuum at room temperature for 24 h.

APPENDIX D

PROCEDURE FOR GRAPHENE OXIDE SYNTHESIS BY BRODIE'S METHOD

1. Modified Brodie's method was applied, using graphite fakes (Sigma-Aldrich, SKU: 332461, ~150 μm).
2. Add 10 ml of fuming nitric acid to a flask equipped with a Teflon mechanical stirrer.
3. Place the flask in an ice bath to cool down to 0 °C.
4. After 10 min, while stirring add 1 g graphite flakes.
5. 5 min later, add 10 g potassium chlorate ($KClO_3$, Alfa Aesar, +99.0%), slowly in small doses to the mixture under stirring in a period of 30 min.
6. Stir the whole mixture for 30 min.
7. Leave the obtained dark green thick slurry unstirred at ambient temperature in the fume hood for 24 h.
8. Add 10 ml nitric acid to the mixture to retrieve the loss of nitric acid due to evaporation.
9. The flask is then placed in a water bath, control the temperature of the water bath at 60 °C for 8 h while stirring.
10. Terminate the reaction by transferring the pasty mixture into 500 ml of distilled water.
11. Use the centrifugation at a speed of 6000 rpm to separate the solids.
12. Wash the solids with 2x 200 ml 10% HCl solution to remove metal ions and use centrifuge to get rid of the solvent.
13. Wash the solids with 5x 200 ml deionized water to remove the remnant acid.
14. Dry the solids (GO powder) under vacuum at room temperature for 24 h.

APPENDIX E

AFM IMAGES OF MEM-FL200 GO MEMBRANE MADE BY VACUUM FILTRATION

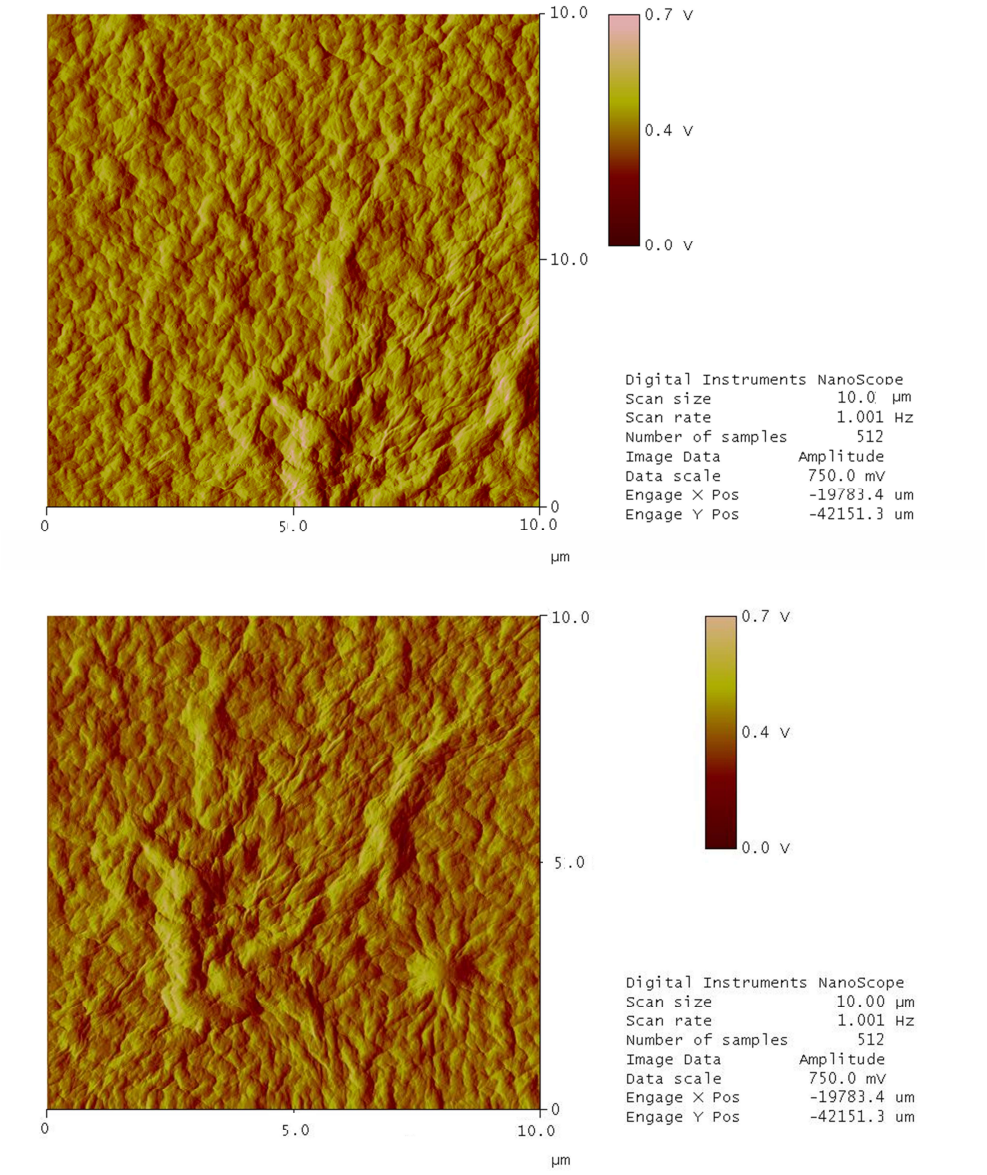

Figure F.1 AFM amplitude images of MEM-FL200.

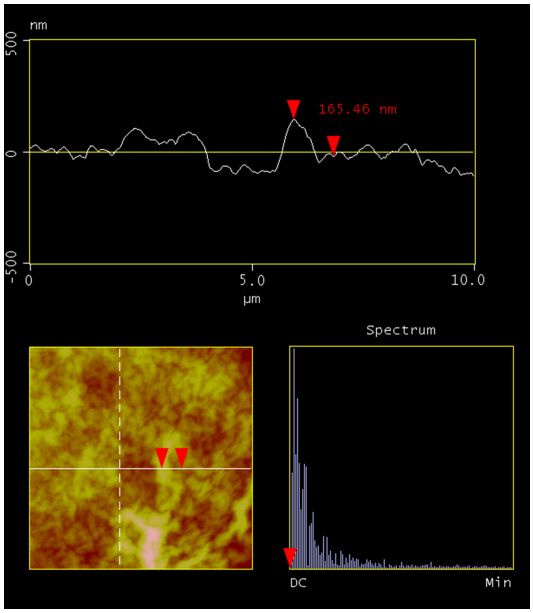
nm
500
0
-500
165.46 nm
0
5.0
10.0
µm
Spectrum
DC
Min

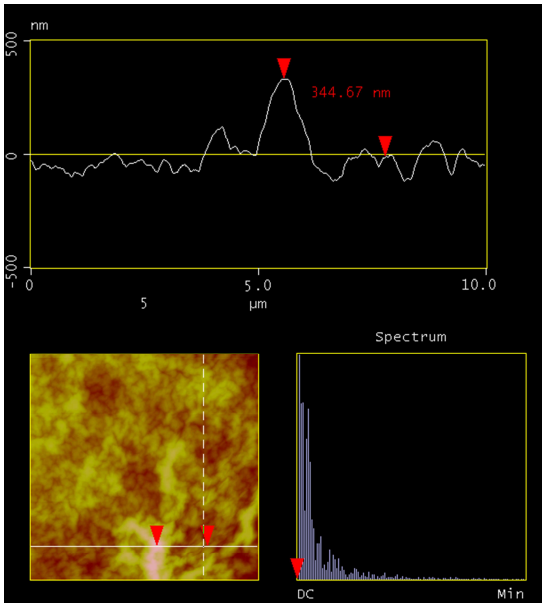
nm
500
0
-500
344.67 nm
0
5.0
10.0
µm
Spectrum
DC
Min

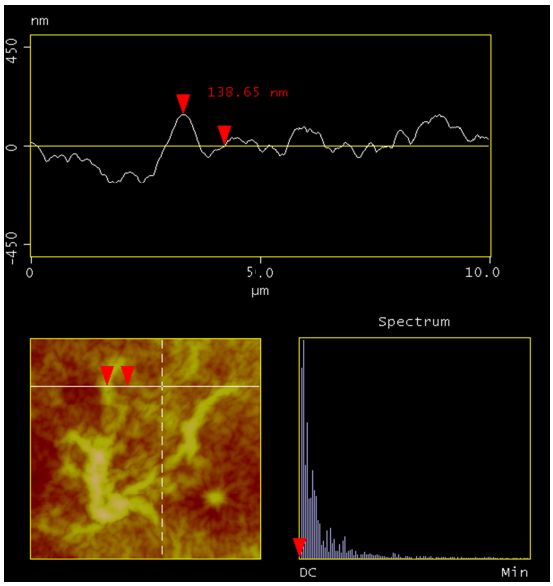
nm
450
0
-450
138.65 nm
0
5.0
10.0
µm
Spectrum
DC
Min

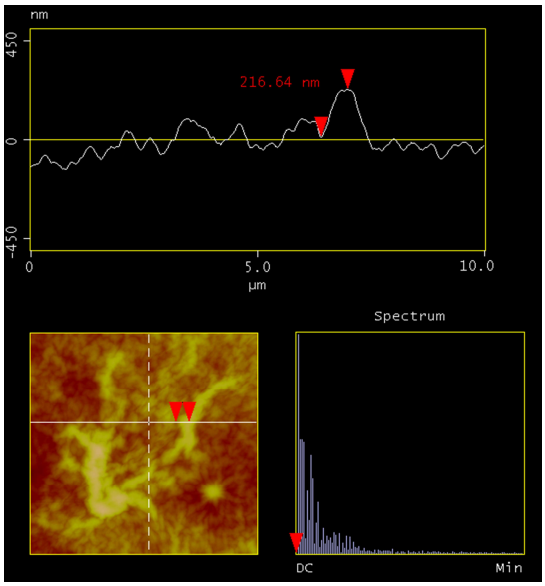
nm
450
0
-450
216.64 nm
0
5.0
10.0
µm
Spectrum
DC
Min

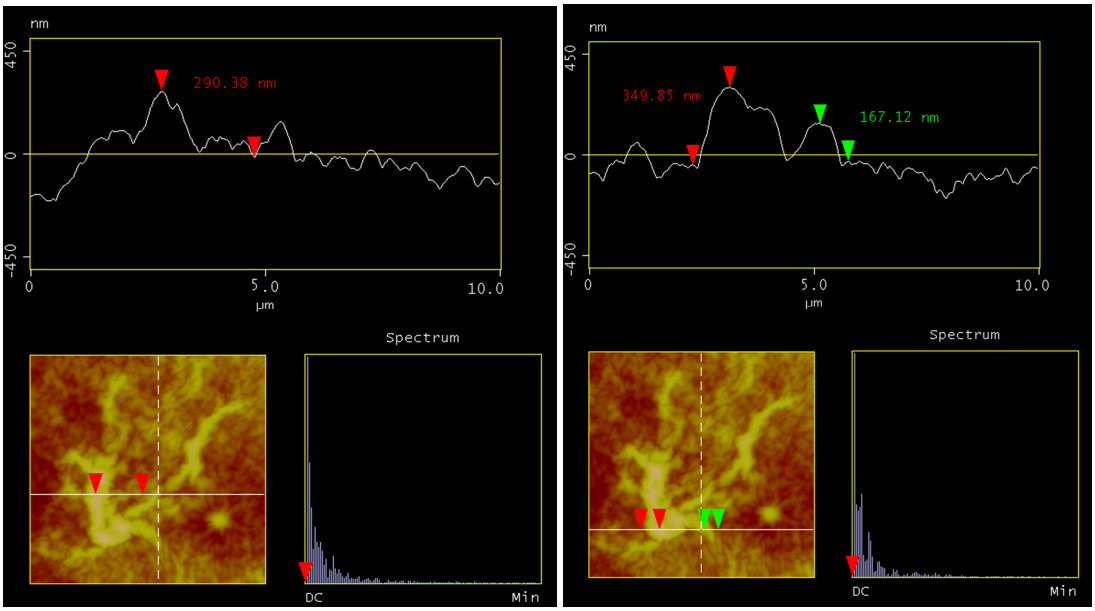

Figure F.2 AFM height images and section analysis for MEM-FL200 GO membrane.

APPENDIX G

AFM IMAGES OF MEM-SL270 GO MEMBRANE MADE BY SPRAY COATING

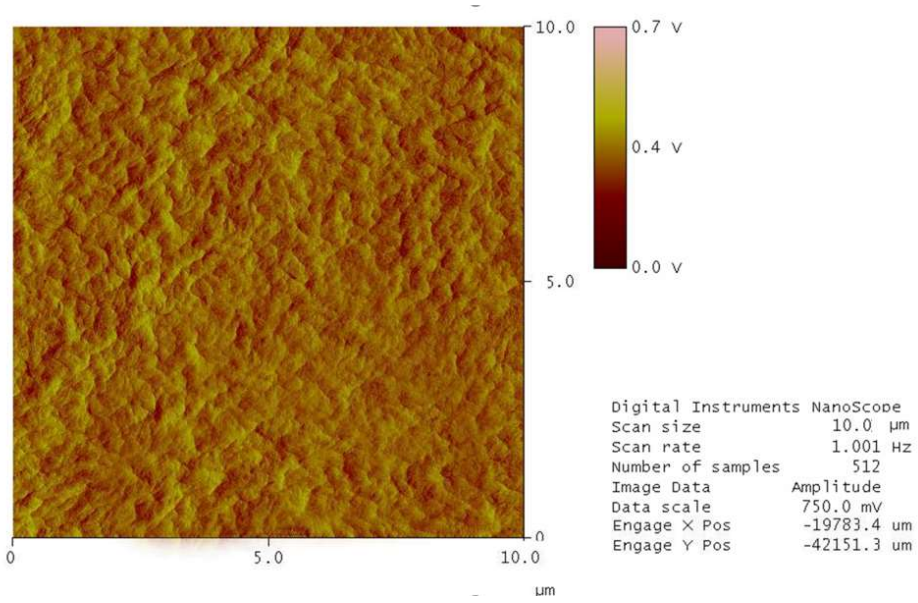

Figure G.1 AFM amplitude images of MEM-SL270.

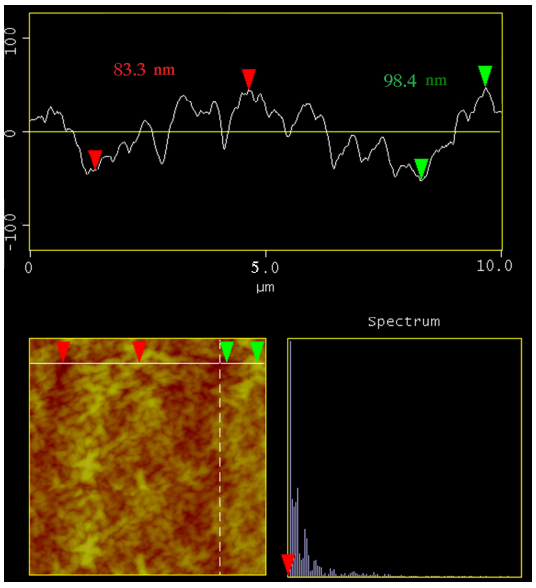

Figure G.2 AFM height image and section analysis for MEM-SL270 GO membrane.

APPENDIX H

PUBLICATIONS

The followings papers will be published in referred journals on the work summarized in the dissertation:

Ibrahim, A., & Lin, Y. S. (2018). Gas permeation and separation properties of large-sheet stacked graphene oxide membranes. *Journal of Membrane Science, 550*, 238-245.

Ibrahim, A., & Lin, Y. S. (2018). Synthesis of graphene oxide membranes on polyester substrate by spray coating for gas separation. *Chemical Engineering science.* Submitted

Ibrahim, A., & Lin, Y. S. (2018). Brodie's derived graphene oxide membranes with fine-tuned interlayer galleries for enhanced hydrogen separation. (In preparation)

The following paper has been published by the author of the dissertation, but the work is not included in the dissertation:

Ibrahim, A., & Lin, Y. S. (2016). Pervaporation separation of organic mixtures by MOF-5 membranes. *Industrial & Engineering Chemistry Research, 55*(31), 8652-8658. doi:10.1021/acs.iecr.6b01965